INFLUENCE OF CRITICAL MOHO REFLECTIONS ON STRONG GROUND MOTION ATTENUATION IN CALIFORNIA

by

Paul Somerville and Nancy Smith

Woodward-Clyde Consultants
566 El Dorado Street
Pasadena, California 91101

and

Douglas Dreger

Seismological Laboratory
California Institute of Technology
Pasadena, California 91125

Data Utilization Report CSMIP/93-01

California Strong Motion Instrumentation Program

December 1993

This study was conducted at the Woodward-Clyde Consultants and was supported by the Department of Conservation under Contract No. 1090-514.

California Department of Conservation
Division of Mines and Geology
Office of Strong Motion Studies
801 K Street, MS 13-35
Sacramento, California 95814-3531

DIVISION OF MINES AND GEOLOGY
JAMES F. DAVIS
STATE GEOLOGIST

DISCLAIMER

The content of this report was developed under Contract No. 1090-514 from the Strong Motion Instrumentation Program in the Division of Mines and Geology of the California Department of Conservation. This report has not been edited to the standards of a formal publication. Any opinions, findings, conclusions or recommendations contained in this report are those of the authors, and should not be interpreted as representing the official policies, either expressed or implied, of the State of California.

PREFACE

The California Strong Motion Instrumentation Program (CSMIP) in the Division of Mines and Geology of the California Department of Conservation promotes and facilitates the improvement of seismic codes through the Data Interpretation Project. The objective of the this project is to increase the understanding of earthquake strong ground shaking and its effects on structures through interpretation and analysis studies of CSMIP and other applicable strong motion data. The ultimate goal is to accelerate the process by which lessons learned from earthquake data are incorporated into seismic code provisions and seismic design practices.

The specific objectives of the CSMIP Data Interpretation Project are to:

1. Understand the spatial variation and magnitude dependence of earthquake strong ground motion.

2. Understand the effects of earthquake motions on the response of geologic formations, buildings and lifeline structures.

3. Expedite the incorporation of knowledge of earthquake shaking into revision of seismic codes and practices.

4. Increase awareness within the seismological and earthquake engineering community about the effective usage of strong motion data.

5. Improve instrumentation methods and data processing techniques to maximize the usefulness of SMIP data. Develop data representations to increase the usefulness and the applicability to design engineers.

This report is the third in a series of CSMIP data utilization reports designed to transfer recent research findings on strong-motion data to practicing seismic design professionals and earth scientists. CSMIP extends its appreciation to the members of the Strong Motion Instrumentation Advisory Committee and its subcommittees for their recommendations regarding the Data Interpretation Research Project.

Moh J. Huang
CSMIP Data Interpretation
Project Manager

Anthony F. Shakal
CSMIP Program Manager

ABSTRACT

A search has been made for the influence of critical reflections from the lower crust on the attenuation of peak acceleration with distance in individual California earthquakes. At close distances, the direct upgoing shear wave generates the largest ground motion amplitude. However, shear waves reflected from the lower crust become large in amplitude once the distance (and the angle of incidence) are large enough to become critical, that is, when all of the incident energy is reflected back to the surface. Strong ground motion amplitudes remained approximately uniform in the distance range of about 50 to 80 km during the 1989 Loma Prieta earthquake, and strong ground motion levels on rock and alluvium in the central San Francisco Bay area exceeded those of empirical attenuation relations. It has been suggested that these large ground motions were critical Moho reflections (S_mS), and contributed about equally with impedance contrast amplification effects in generating destructive ground motions at soft soil sites in the central San Francisco Bay area.

The approach used in this study is to construct profiles of accelerograms having absolute times for each of several major California earthquakes. Evidence for the presence of critical reflections consists of large phases that arrive near the time predicted for critical reflections from lower crustal layers such as the Conrad and Moho, and have a horizontal phase velocity appropriate for critical reflections from the lower crust. For selected events, the interpretation of these profiles of recorded accelerograms is facilitated by synthetic seismograms that represent the effects of wave propagation in horizontally layered models of the earth's crust. The effect of these reflected phases on the attenuation of peak acceleration with distance is then assessed.

We have analyzed profiles of accelerograms from seven large California earthquakes and several aftershocks. For the older events, the strong motion recordings did not have absolute time, and so it was difficult to identify critical reflections in these recordings. Also, for the larger events, the source duration was sufficiently long that it obscured the individual phases that we would like to identify. Nevertheless, we generally found evidence of critical reflections in large, late wave arrivals that may be S_mS, and these arrivals were associated with a flattening of the empirical attenuation curve. Analysis of aftershock recordings, which have briefer source functions, provided clear evidence of the presence of these reflected phases.

These results suggest that critical reflections influence the attenuation of strong ground motion throughout California, and are already included to an extent in standard attenuation relations. However, the smoothly decaying functional form of most attenuation relations, while fitting observed strong motion data when averaged over many events, may not accurately describe the attenuation that is observed in a single event. The attenuation relation of the Loma Prieta earthquake is the most prominent demonstration of this. Since we do not expect crustal earthquakes in California to occur much deeper than 18 km, or the crustal thickness to be much less than 25 km, the Loma Prieta case may approximately represent an upper bound on the departure of the attenuation relation of an individual event from that of the larger strong motion data set in California. As a rule of thumb, the distance at which the attenuation curve

for an individual earthquake begins to flatten can be estimated from the critical distance of the S_mS phase, which is easily calculated from the crustal structure and the source depth.

Table of Contents

INTRODUCTION

This study was motivated by the hypothesis based on analysis of strong motion recordings of the 1989 Loma Prieta earthquake that critical reflections from the Moho caused peak ground motion amplitudes to remain approximately uniform in the distance range of about 50 to 100 km (Somerville and Smith, 1991). Strong ground motion levels on rock and alluvium in the central San Francisco Bay area exceeded those of empirical attenuation relations. According to the hypothesis, these large ground motions were critical Moho reflections, and contributed about equally with impedance-contrast amplification effects in generating destructive ground motions at soft soil sites in the central San Francisco Bay area. The objective of this project is to look for the effects of critical Moho reflections in the strong motion recordings of other large California earthquakes. The results of the study are summarized in Table 1.

Table 1. Summary of the effect of crustal reflections on ground motion attenuation from California earthquakes.

Event	Absolute Time on Records	Source Duration (sec)	Number of Stations	Distance Range of Stations	Reflected Phases Identified	Range of Flattening
1952 Kern Co.	No	14	4	40-125	No	None
1968 Borrego Mountain	No	5	5	70-230	Yes	Suggestion (100-200)
1971 San Fernando						
Profile 1:	No	6	9	30-140	Yes	Pronounced (80-120)
Profile 2:	No	6	6	40-180	Yes	Pronounced (70-180+)
1983 Coalinga	6/11	5	11	53-69	Yes	None
1986 North Palm Springs	Yes	5	9	30-75	Yes (Wood-Anderson)	None
1987 Whittier Narrows	Yes	0.4	10	10-90	Yes	Clear (50-90)
1989 Loma Prieta	Yes	6	18	20-110	Yes (aftershocks)	Clear (50-80)

APPROACH

The approach used in this study has been described by Burger *et al.* (1987) and Somerville *et al.* (1990). The propagation of seismic waves in a horizontally layered crust is illustrated schematically in Figure 1. In addition to the direct S arrival, there are arrivals that are initially downgoing but then reflected from lower crustal interfaces such as the Conrad and Moho layers (S_cS and S_mS respectively), and arrivals that are initially upgoing but are reflected from the surface and then back to the surface (phases such as sS, sS_cS and sS_mS). At close distances, the direct ray has the largest amplitude. However, the phases reflected from the lower crust become large in amplitude once the distance (and the angle of incidence) are large enough to become critical, that is, when all of the incident energy is reflected back to the surface.

The contribution of direct, downgoing, and upgoing arrivals to the overall seismogram as a function of distance is shown in Figure 2 for a strike-slip earthquake at a depth of 10 km in a southern California crustal model (Helmberger *et al.*, 1992, Model D). The individual contributions are calculated by the method of generalized rays. At 50 km, the largest arrival is the direct S wave. However, at 100 km, the surface reflected phase sS and the critical reflection from the Moho S_mS have become large and make an important contribution to the total seismogram. At 150 km, the direct arrival has become small and the largest motions are those due to reflected phases. The depth dependence of the sS phase is opposite that of critical reflections from the lower crust: the sS phase becomes larger and occurs closer to the source with decreasing depth, while the S_mS phase becomes larger and occurs closer to the source with increasing source depth. Figure 2 illustrates the diminishing role of the direct arrival and the increasing role of reflected phases in controlling the attenuation of strong ground motion as the distance from the source increases.

The effect of the distance-dependent evolution of these different seismic arrivals on the attenuation of ground motion is shown schematically in Figure 3. While the direct S arrival dominates the peak motion at close distances, the

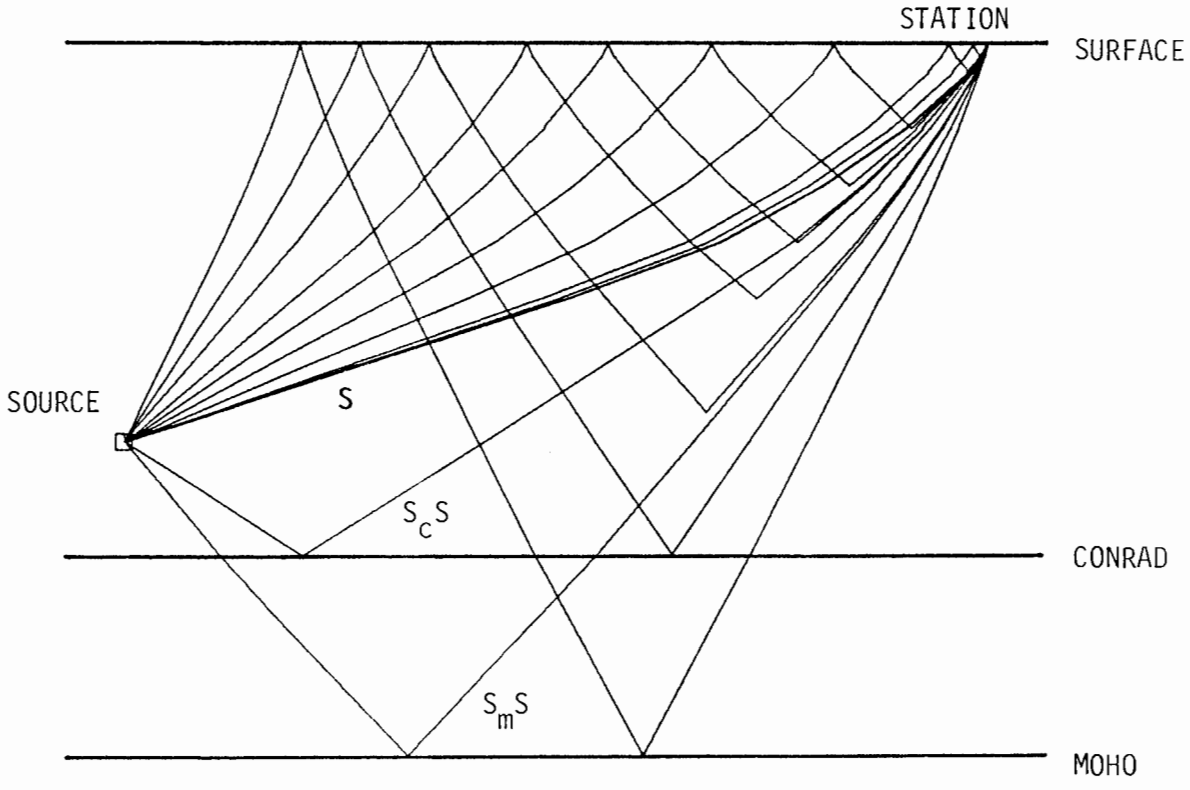

Figure 1. Simplified model of wave propagation in a layered crust.

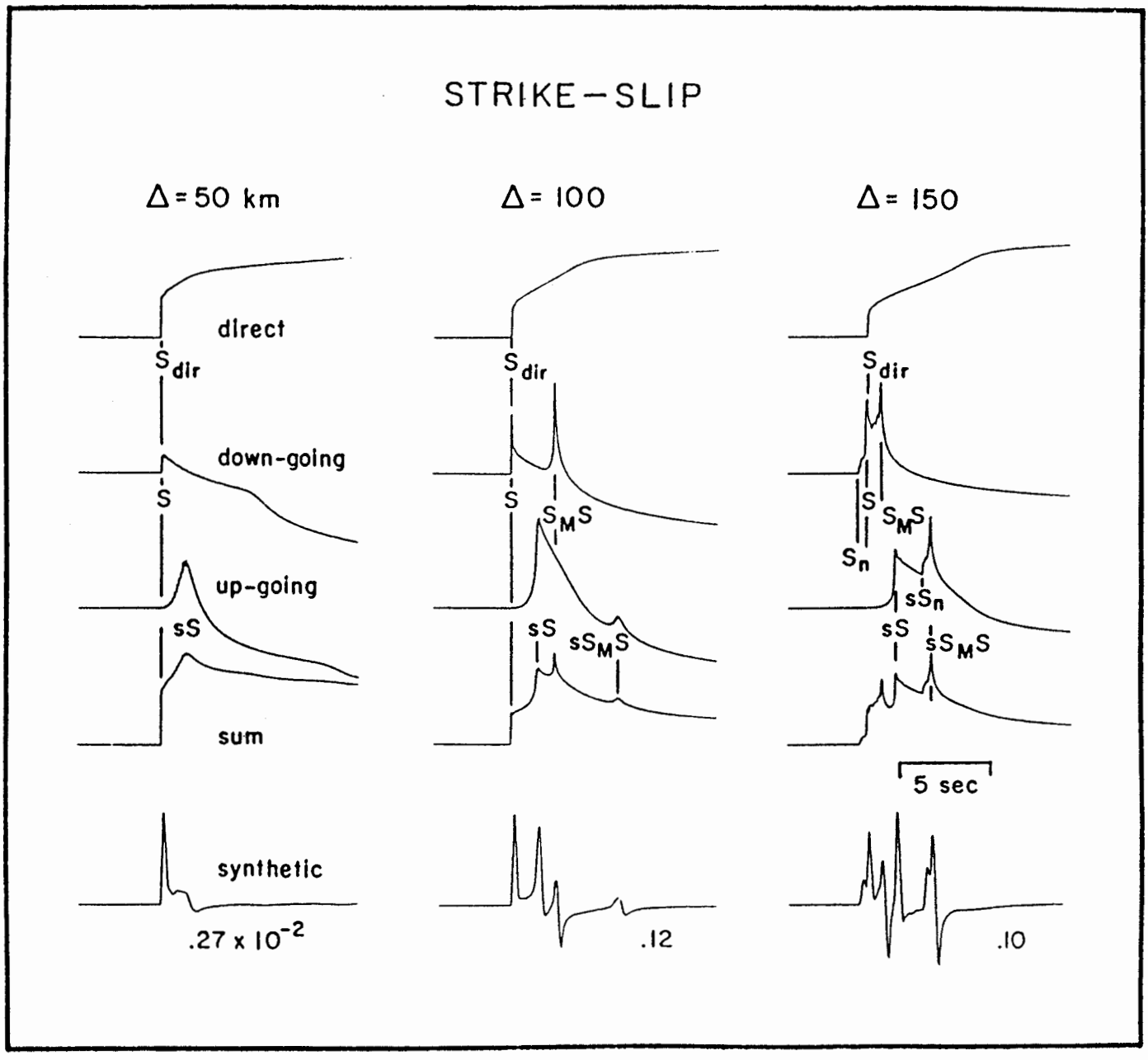

Figure 2. Decomposition of the wavefield into direct, downgoing, and upgoing paths for a strike-slip source at a depth of 10 km in the southern California crustal model of Hadley and Kanamori (1979). The phase sS becomes large between 50 and 100 km, and the critical reflection S_mS dominates beyond 100 km

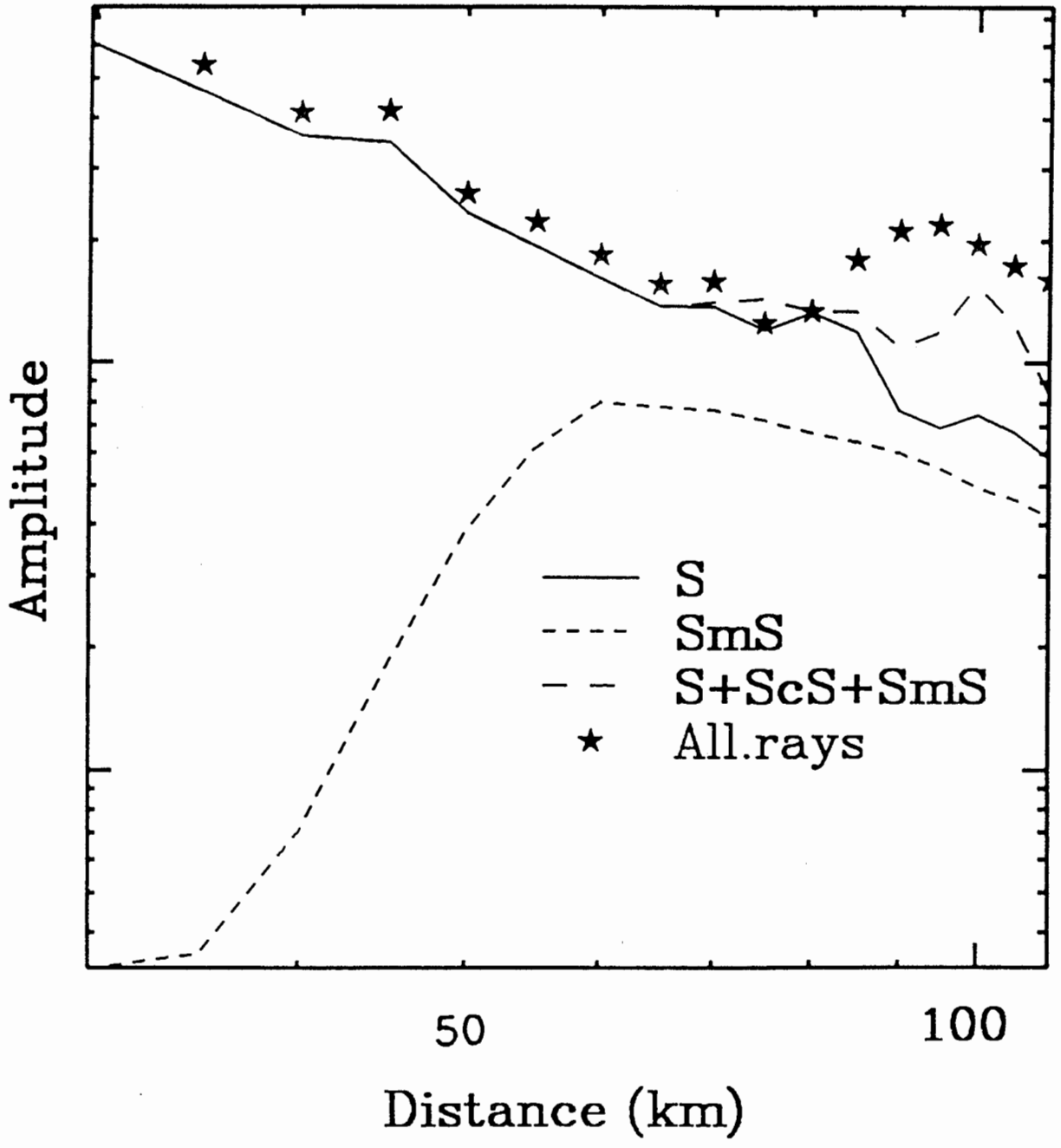

Figure 3. Schematic diagram showing the contribution of direct and critically reflected energy to the overall attenuation of peak ground motion amplitude.

critically reflected arrivals begin to dominate at larger distances, and the effect of surface reflections (included in overall attenuation shown by stars) is also important.

It is widely recognized that recorded strong ground motions can be strongly influenced by site effects. If there is a correlation between site conditions and the distance of recording stations from a given earthquake, then there is the potential for site effects to influence the shape of the ground motion attenuation pattern of that event. For some events, such as the 1987 Whittier Narrows and 1989 Loma Prieta earthquakes, there are enough recordings to allow subsets of stations having similar categories of site conditions to be analyzed, thereby reducing the potential influence of site effects on the pattern of attenuation. However, for the other events the data are too sparse to define the attenuation pattern for a given site category, and so the potential influence of site effects on the attenuation pattern may be larger. Modification of the recorded data to take account of site effects is beyond the scope of this study.

In Figure 4, we demonstrate two methods that we have used to generate synthetic seismograms for this project. The seismogram on the left was generated by the method of generalized rays using the 8 rays shown below. The seismogram in the middle was generated using 24 rays. This seismogram closely resembles the seismogram on the right, generated by the reflectivity method, which includes all arrivals. These seismograms were generated in the course of modeling the data from the 1986 and 1988 North Palm Springs earthquakes, discussed further below.

A contour map of crustal thickness in California is shown in Figure 5 (Mooney and Weaver, 1990). In the region of the San Andreas fault system extending from north of the Transverse Ranges to north of the San Francisco Bay area, the depth to the Moho is 25 ± 1 km. In the region south of the Transverse Ranges, including almost all of southern California, the crustal thickness is 30 ± 2 km. The relatively uniform crustal thickness in each of these regions, and the significant contrast in crustal thickness between them, suggests that there could be

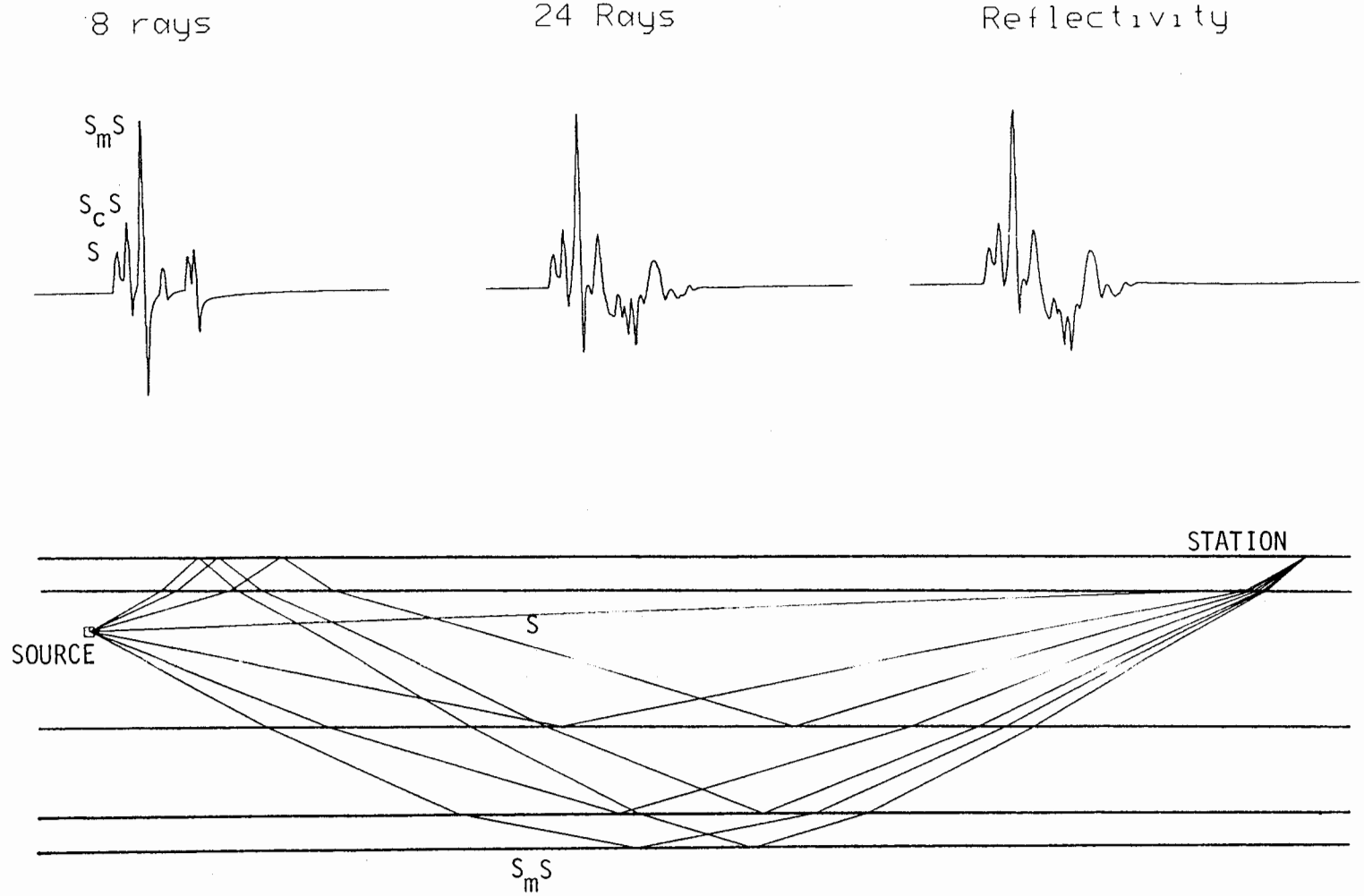

Figure 4. Comparison of synthetic seismograms generated by generalized rays and by the reflectivity method. The seismogram on the left was generated using the 8 generalized rays shown below. The seismogram in the center, generated with 24 rays, closely resembles the reflectivity seismogram shown on the right.

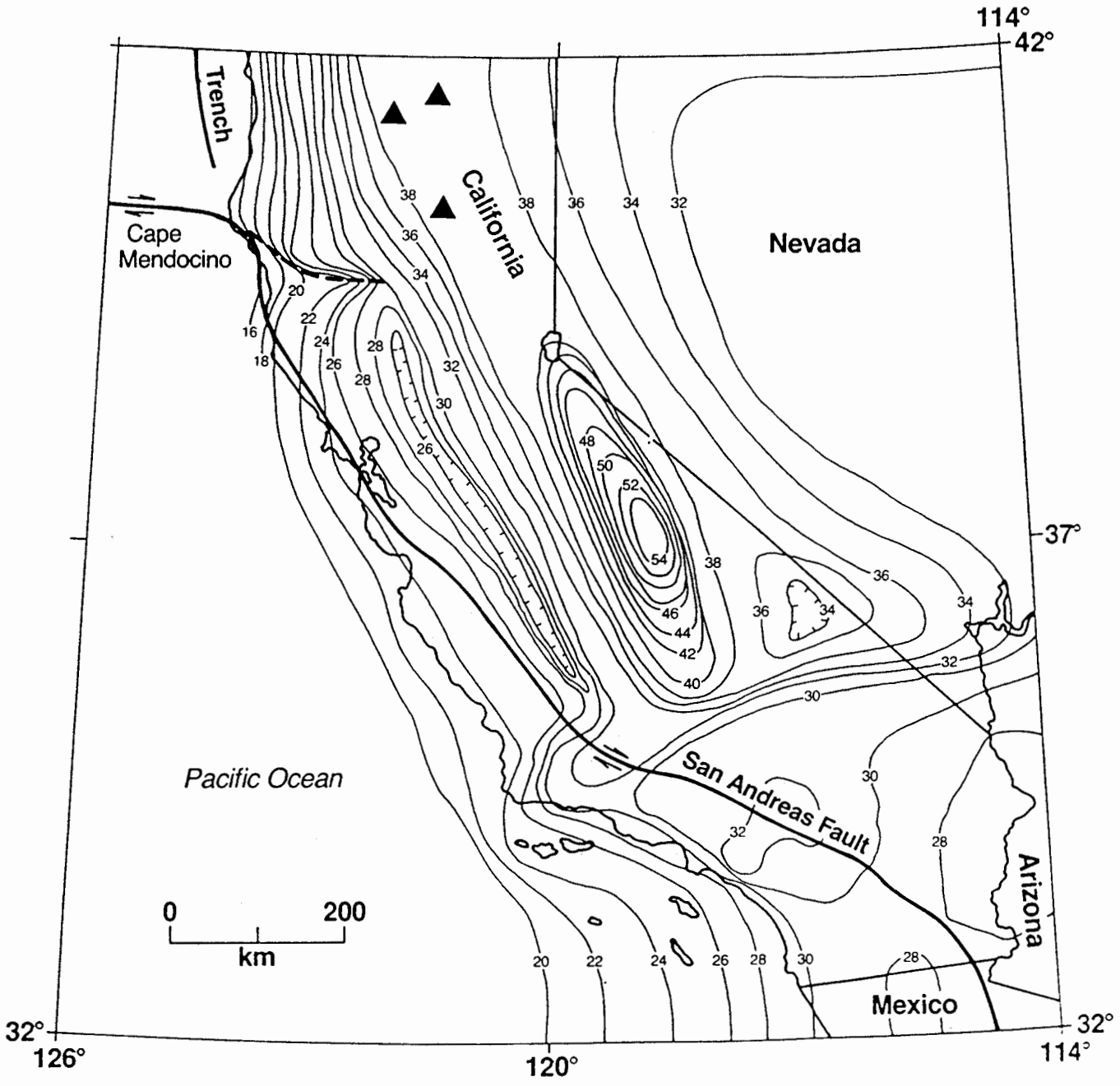

Figure 5. Contour map of crustal thickness in California, showing 25 ± 1 km thickness in the central coast of California and 30 ± 2 km thickness in southern California. Source: Mooney and Weaver, 1990.

differences in ground motion attenuation between these two regions. Specifically, for a given focal depth, the effect of critical reflections should occur at closer distances and be larger in northern California than in southern California.

DATA PRESENTATION

The large earthquakes whose strong ground motion recordings we have analyzed in this study include the 1952 Kern County, 1968 Borrego Mountain, 1971 San Fernando, 1983 Coalinga, 1986 North Palm Springs, 1987 Whittier Narrows, and 1989 Loma Prieta events. The data presentations that we prepared for each event include a map showing the locations of the epicenter and the strong motion recording stations; profiles of accelerograms in which accelerograms aligned in absolute time are displayed as a function of distance from the source; and plots of attenuation of peak acceleration with distance.

The profiles and attenuation plots were prepared for each of two components of motion. We have chosen to normalize the recorded motion to a fixed amplitude scale in these plots, to facilitate the correlation of waveforms. Use of an absolute ground motion scale would render illegible the waveforms of the more distant recordings, which are the main focus of this study. The absolute amplitudes are compared in the plots of peak acceleration versus distance. The two recorded horizontal components were rotated to the radial (horizontal component of SV) and tangential (SH) components in order to facilitate interpretation. Given the finiteness of the fault, these definitions of radial and tangential are approximations which are valid to the extent that the ground motions can be regarded as having originated from a point source at the hypocenter. For the distance range of most interest for critical reflections (50 to 150 km), and the size of most of the events being studied (fault dimensions of a few tens of km), this is a reasonable approximation.

Where there are sufficient data, separate profiles have been prepared for groups of stations along different azimuths from the source. Superimposed on the profiles of accelerograms from earthquakes in southern California are travel times for a crustal model for southern California developed by Helmberger *et al.* (1992, Model D). For the Coalinga earthquake, we used a crustal model derived by Eaton (1986), and for the 1987 Whittier Narrows earthquake we used a crustal

model derived by Magistrale (1990). The arrivals shown are the direct upgoing S wave and the S waves reflected from the Conrad, mafic, and Moho interfaces. In some profiles, the arrivals for P waves as well as S waves are shown.

For the older events, the strong motion recordings did not have absolute time, but we have prepared profiles in which the alignment of waveforms in time is inferred from the identification of direct S in velocity and displacement waveforms. This has been done to facilitate the identification of critical reflections in these strong motion recordings. In all profiles, the text and figure captions identify stations lacking absolute time but for which we have used this procedure to estimate trigger time.

DATA ANALYSIS

We now proceed to describe the data and their interpretation for each earthquake in turn. Our objective is to identify critically reflected phases in the profiles of strong motion recordings, and evaluate their influence on ground motion attenuation. For the later events, for which the strong motion recordings have absolute time, we have used synthetic seismograms to interpret the data.

1952 Kern County

The 1952 Kern County earthquake had a complex source process that lasted about 14 seconds (Wallace, 1988). None of the five strong motion recordings, whose locations are shown in Figure 6, had absolute trigger time. Using judgment, we aligned the time histories of four of the five recordings (HOLL and HOLC are co-located) to fit the travel-time curves from the Helmberger *et al.* (1992) crustal model (Figures 7 and 8). The long source duration makes it difficult to resolve the arrivals of the upgoing and diving energy. The attenuation of peak acceleration does not show a flattening trend (Figures 9 and 10). The path between the Kern County earthquake and the strong motion recording stations is quite complex since it crosses the San Andreas fault, and the Moho depth shallows from about 33 to 30 km. The lack of lateral continuity in crustal structure may have diminished the strength of critical reflections from the lower crust. Listed in Table 2 are the site conditions of the recordings analyzed.

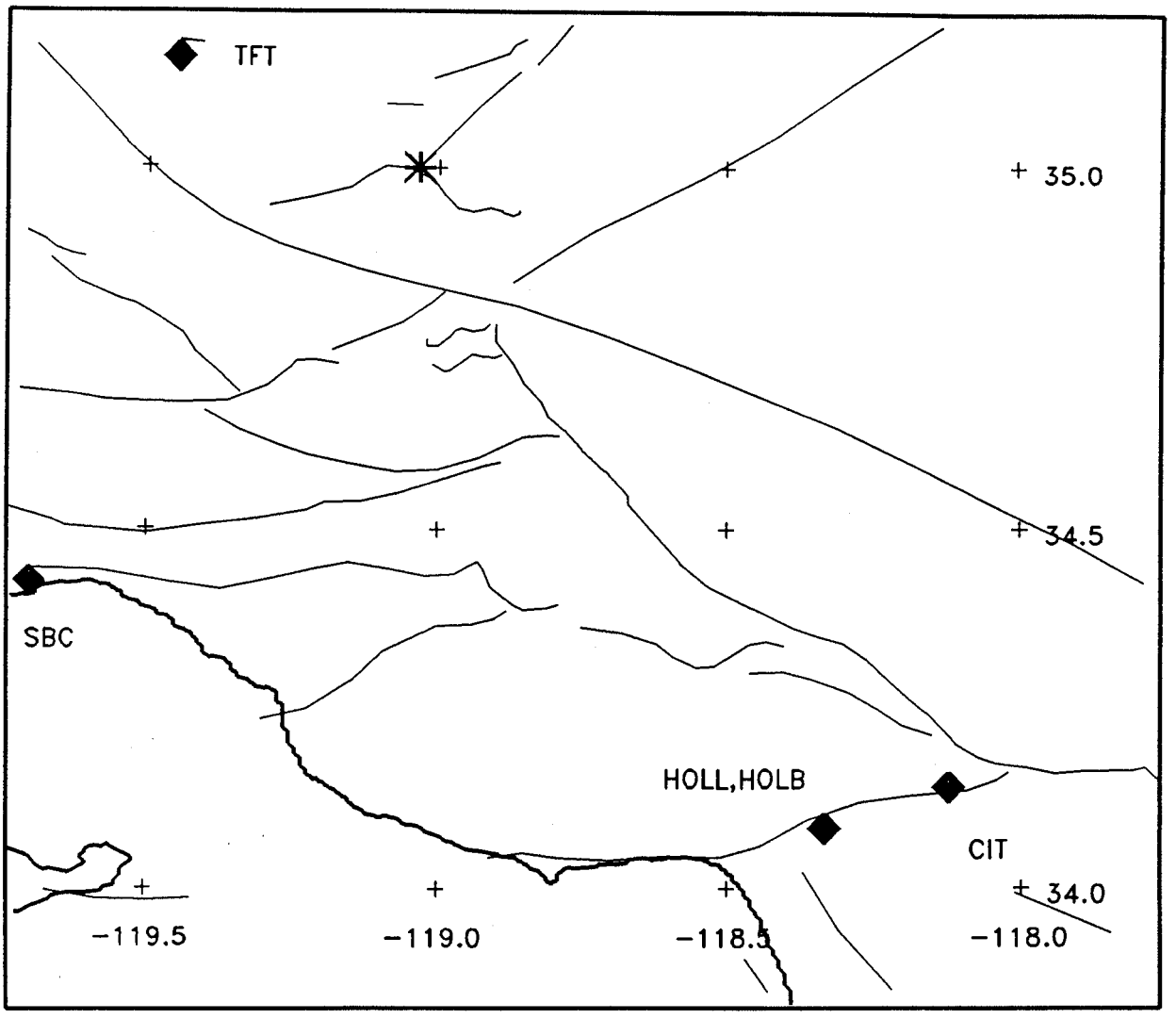

Figure 6. Map showing the location of the 1952 Kern County earthquake, and four strong motion instruments.

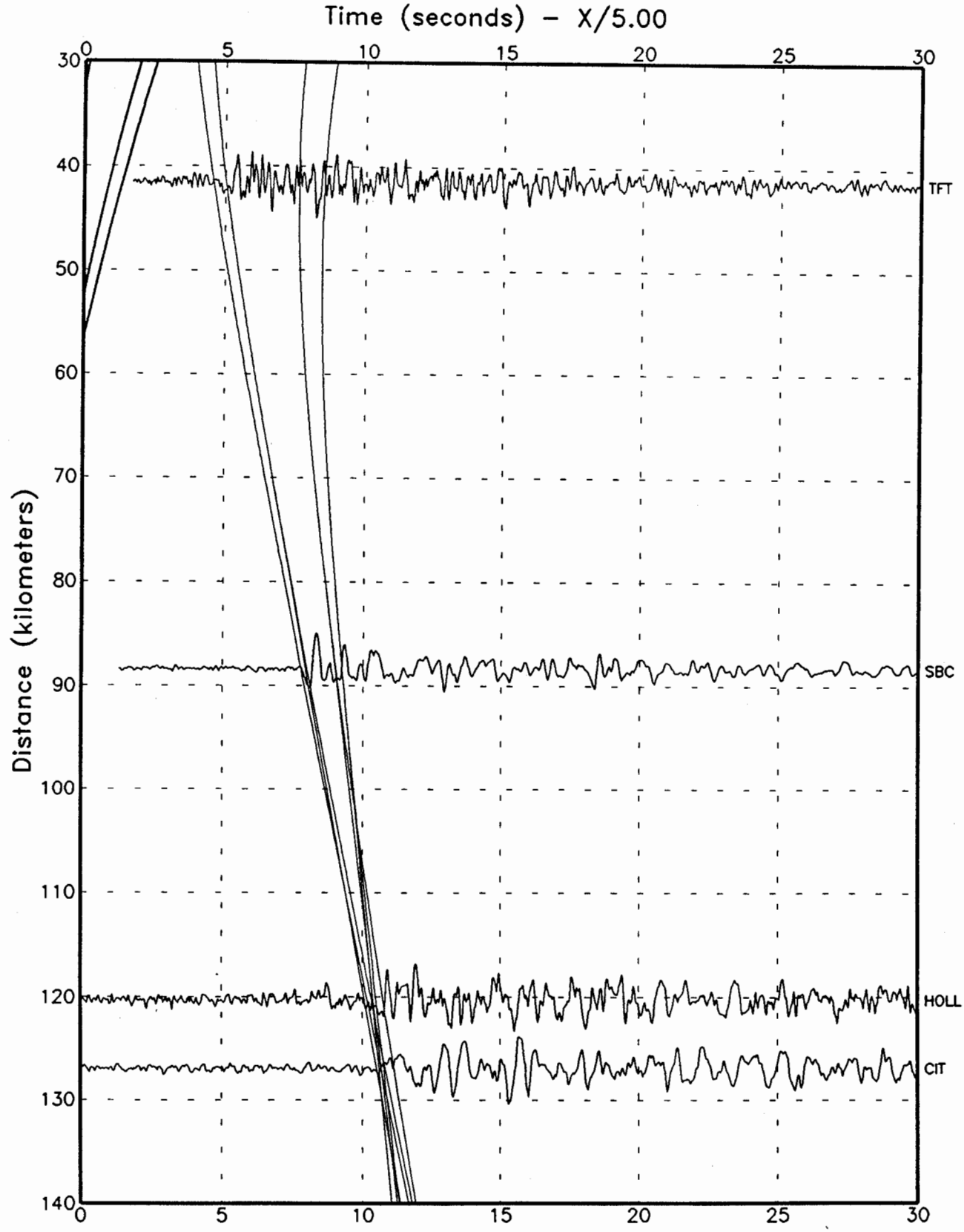

Figure 7. Tangential component accelerograms for the 1952 Kern County earthquake are plotted as a function of distance. These recordings did not have absolute timing. Travel times for the direct, Conrad reflected, mafic reflected and Moho reflected P and S waves determined from the Helmberger *et al.* (1992) crustal velocity model are also shown.

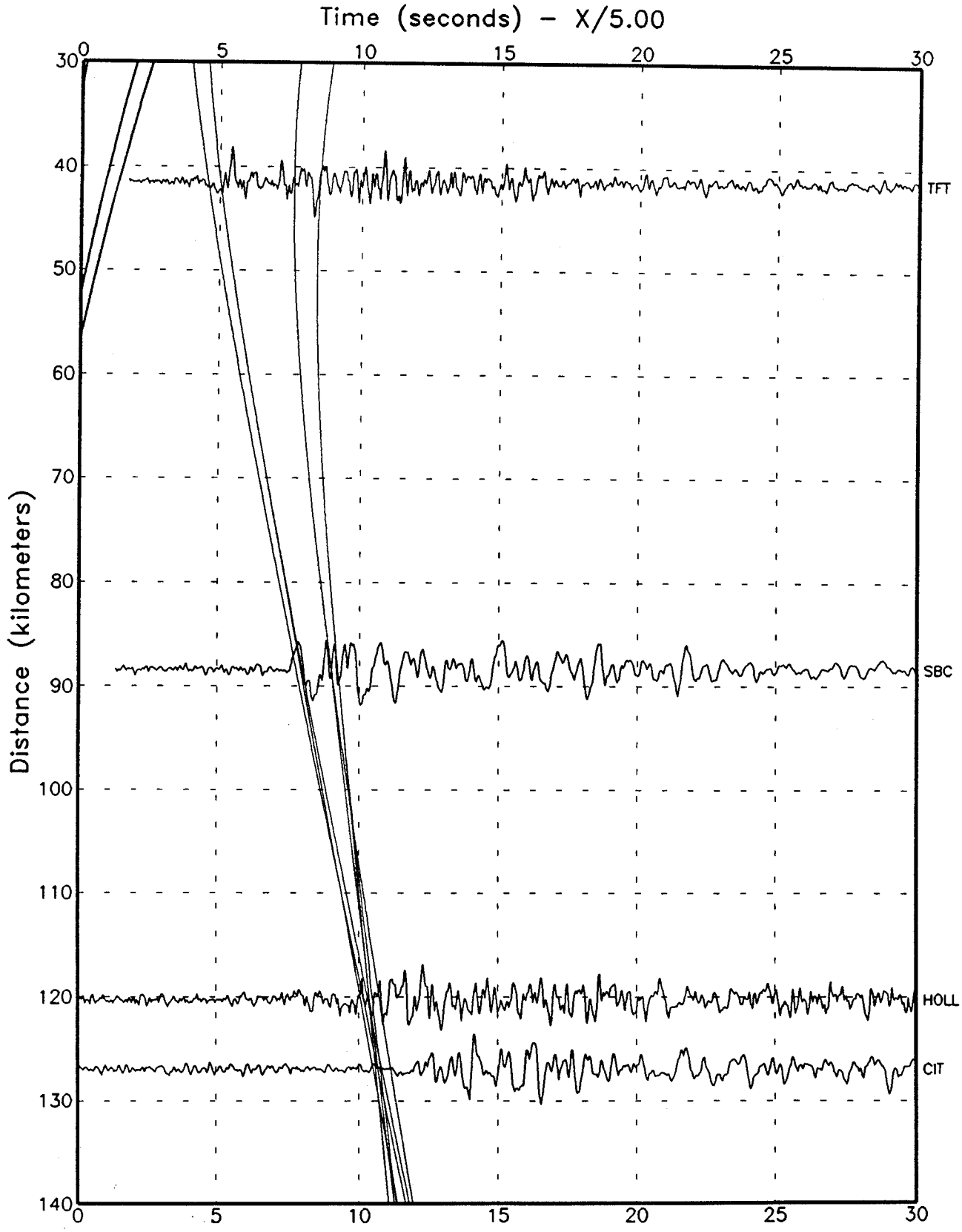

Figure 8. Radial component accelerograms for the 1952 Kern County earthquake are plotted as a function of distance. These recordings did not have absolute timing. Travel times for the direct, Conrad reflected, mafic reflected and Moho reflected P and S waves determined from the Helmberger *et al.* (1992) crustal velocity model are also shown.

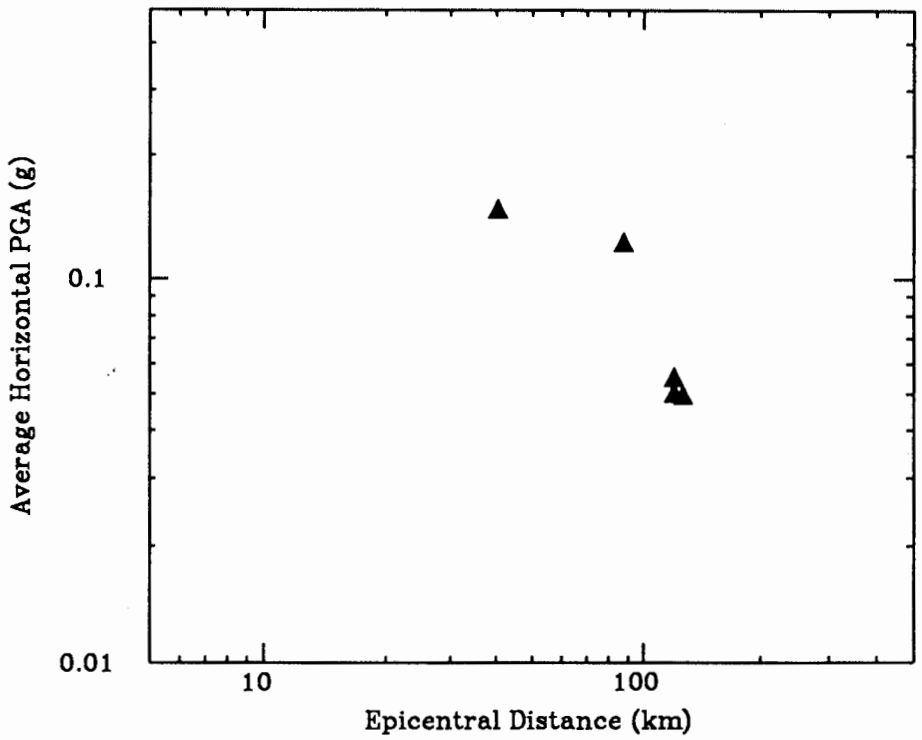

Figure 9. Peak tangential acceleration plotted as a function of distance from the 1952 Kern County event.

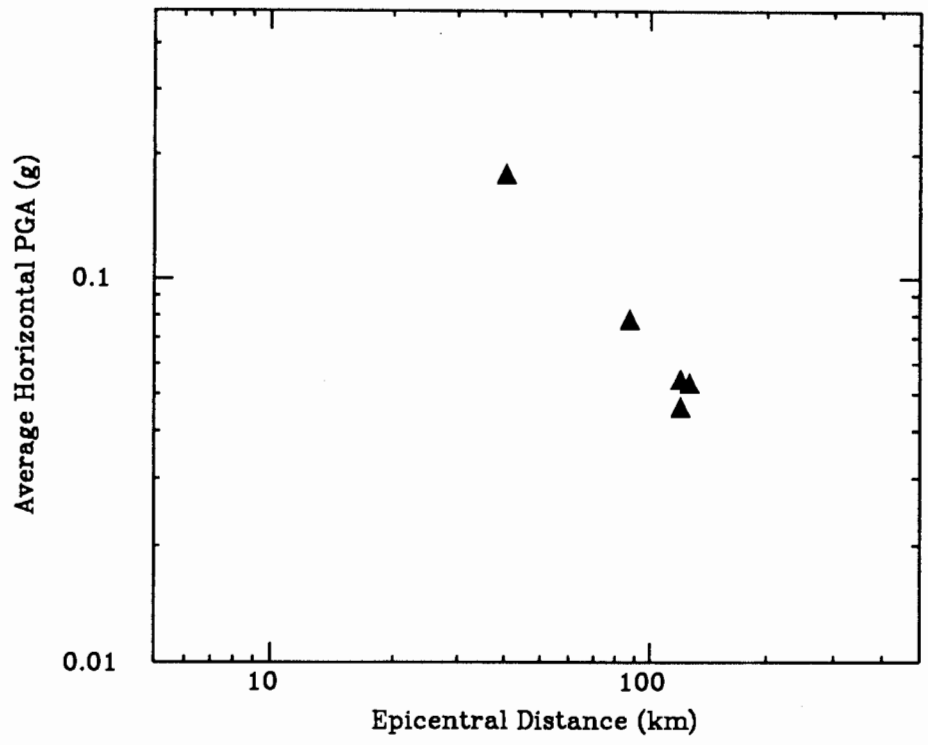

Figure 10. Peak radial acceleration plotted as a function of distance from the 1952 Kern County event.

Table 2. Locations, epicentral distances, and site characteristics for the stations used for the study of the July 21, 1952 Kern County Earthquake. The epicentral location used for determination of distances is 35.000N and 119.033W.

Station Identification	Latitude (North)	Longitude (West)	Epicentral Distance (km)	Site Geology
CIT (475) Cal Tech Athenaeum	34.139	118.121	127	Pleistocene deposits
HOLL (133) Hollywood Storage Basement	35.083	118.333	120	Recent alluvium
SBC (283) Santa Barbara Courthouse	34.424	119.701	88	Pleistocene deposits
TFT (095) Taft Lincoln School Tunnel	35.150	119.033	42	Recent alluvium

1968 Borrego Mountain

The 1968 Borrego Mountain earthquake had a source duration of 5 seconds as estimated from teleseismic body waves. It started with the massive rupture of a strong asperity (Burdick and Mellman, 1976). The recording stations of this earthquake are shown in Figure 11. None of the seven strong motion recordings had absolute trigger time. We aligned traces of five of the seven recordings with the travel time curves based on a pick of the direct S wave; the two other stations are at coincident distances.

In the resulting profiles (Figures 12 and 13), we can identify arrivals that correspond to the direct arrival and the critical reflections from the Conrad and the Moho. Support for this interpretation is provided by Ho-Liu and Helmberger (1989), who found that the largest ground motions recorded in the Los Angeles basin from the 1968 Borrego Mountain earthquake were due to critical reflections. These sharp pulses presumably correspond to the strong initiation of rupture of the earthquake inferred from teleseismic studies. Although the data are sparse, they do suggest a flattening of the attenuation relation in the distance range of 100 to 200 km (Figures 14 and 15). Listed in Table 3 are the site conditions of the recordings analyzed.

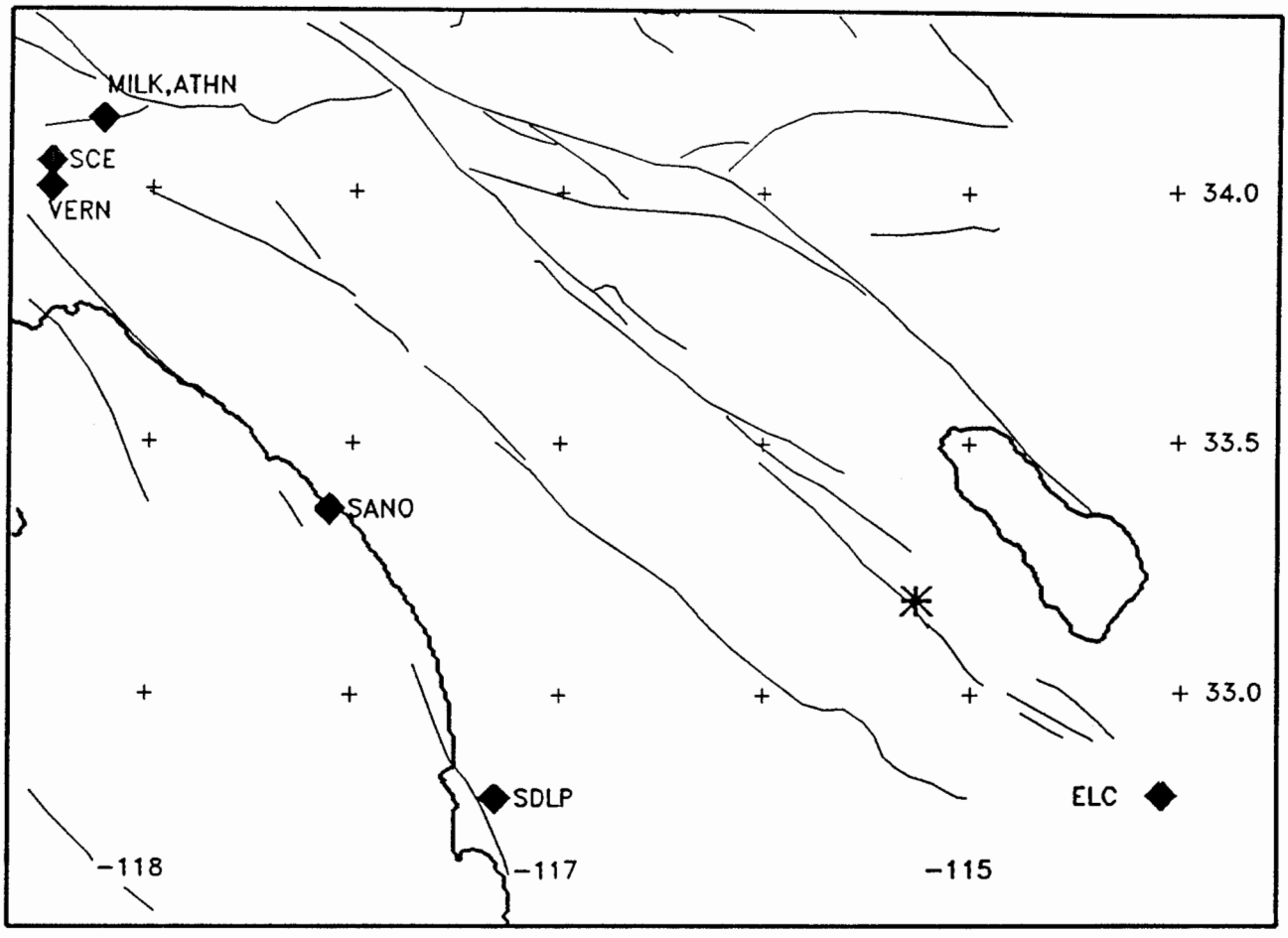

Figure 11. Map showing the location of the 1968 Borrego Mountain earthquake, and strong motion instruments.

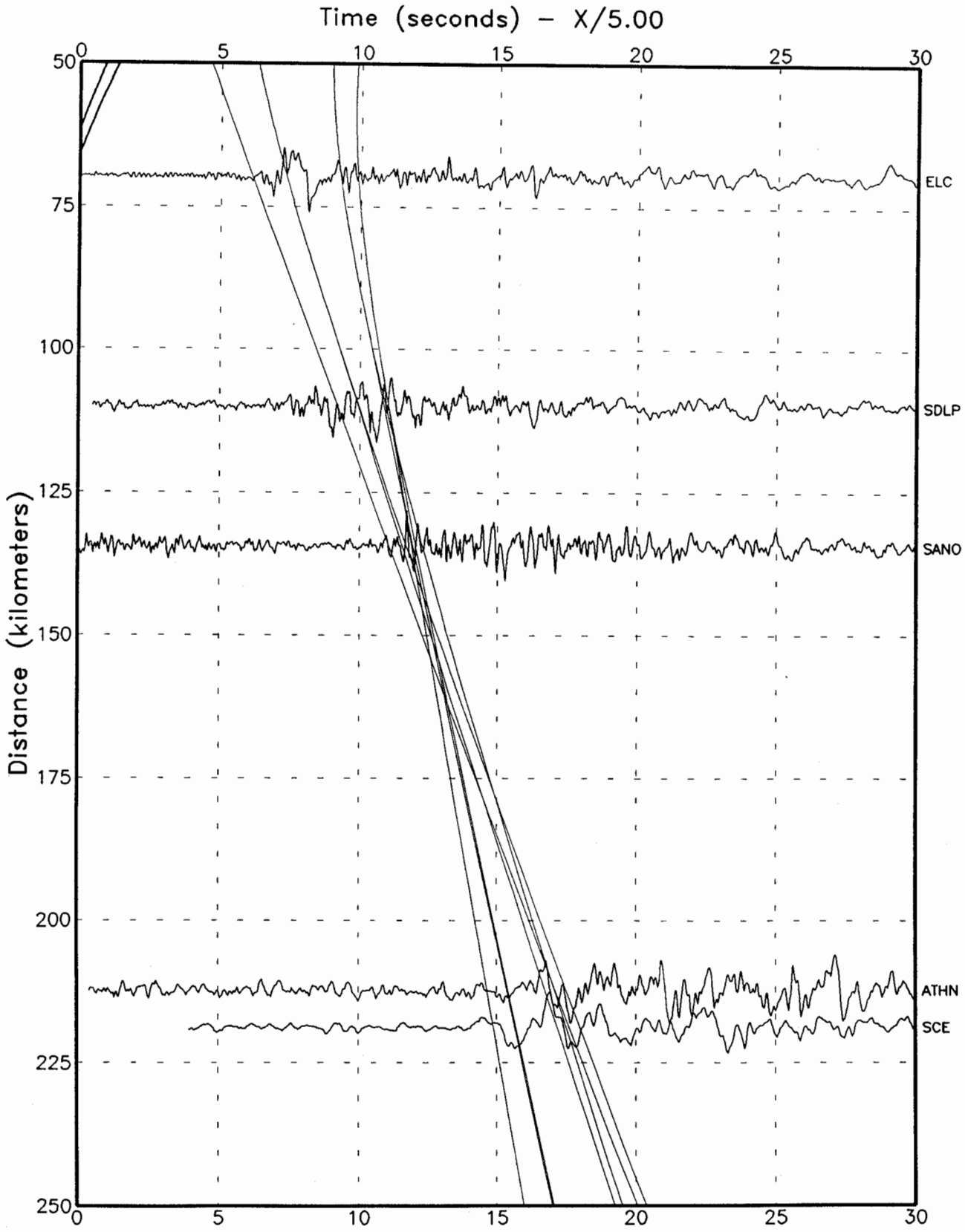

Figure 12. Tangential component accelerograms for the Borrego Mountain earthquake are plotted as a function of distance. These recordings did not have absolute timing. Travel times for the direct, Conrad reflected, mafic reflected and Moho reflected P and S waves determined from the Helmberger *et al.* (1992) crustal velocity model are also shown.

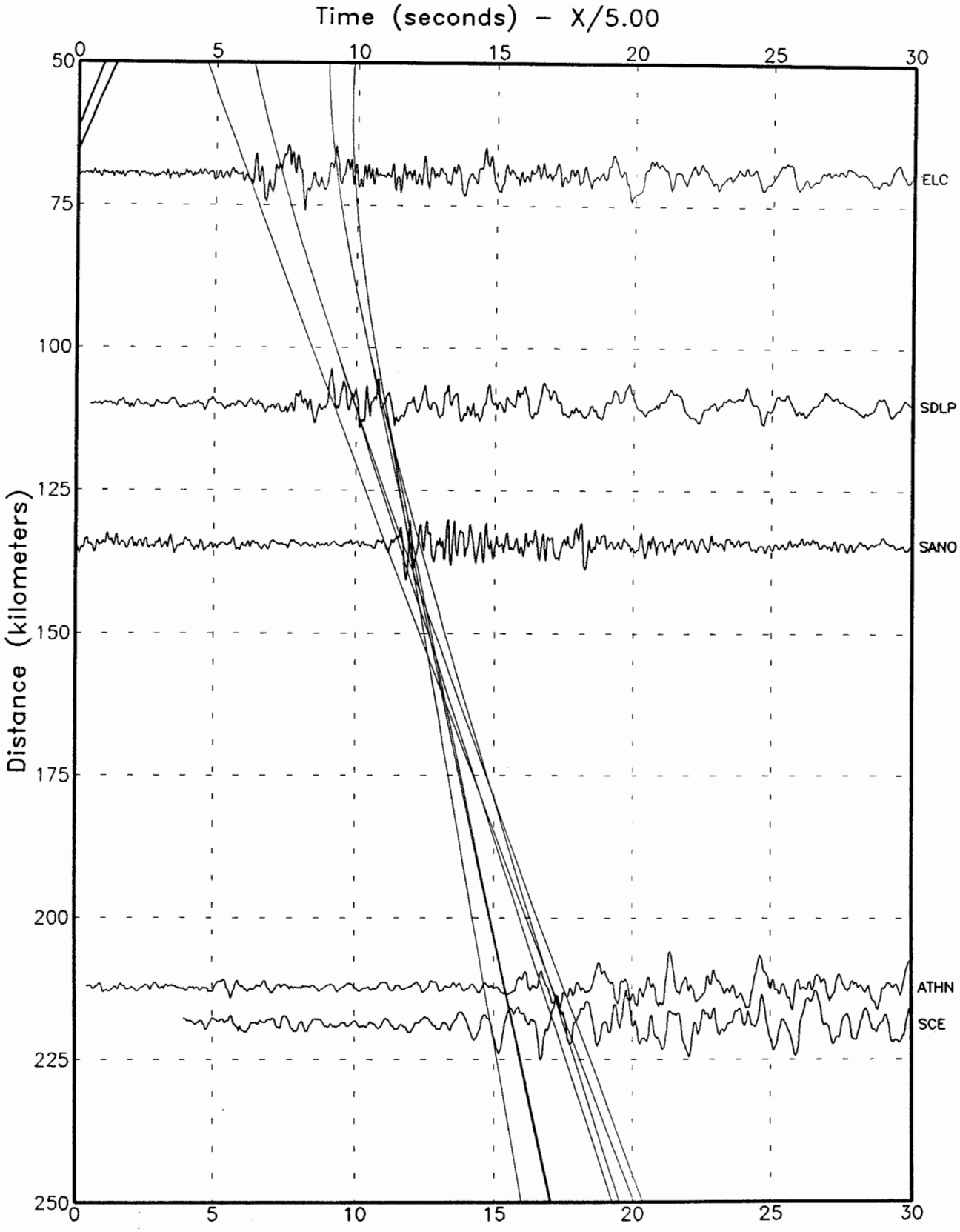

Figure 13. Radial component accelerograms for the Borrego Mountain earthquake are plotted as a function of distance. These recordings did not have absolute timing. Travel times for the direct, Conrad reflected, mafic reflected and Moho reflected P and S waves determined from the Helmberger *et al.* (1992) crustal velocity model are also shown.

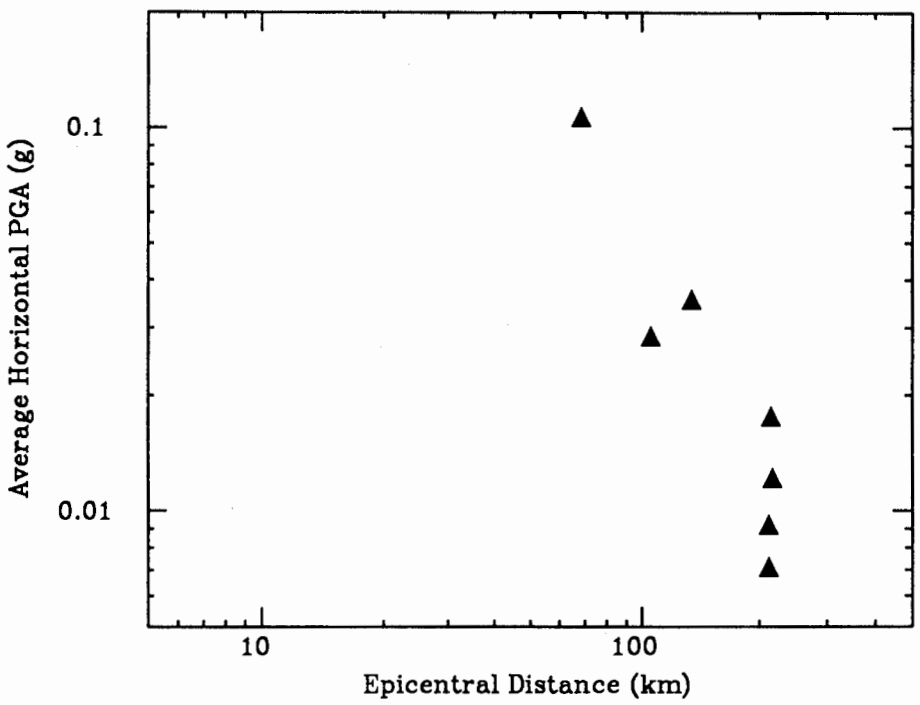

Figure 14. Peak tangential acceleration plotted as a function of distance from the Borrego Mountain event.

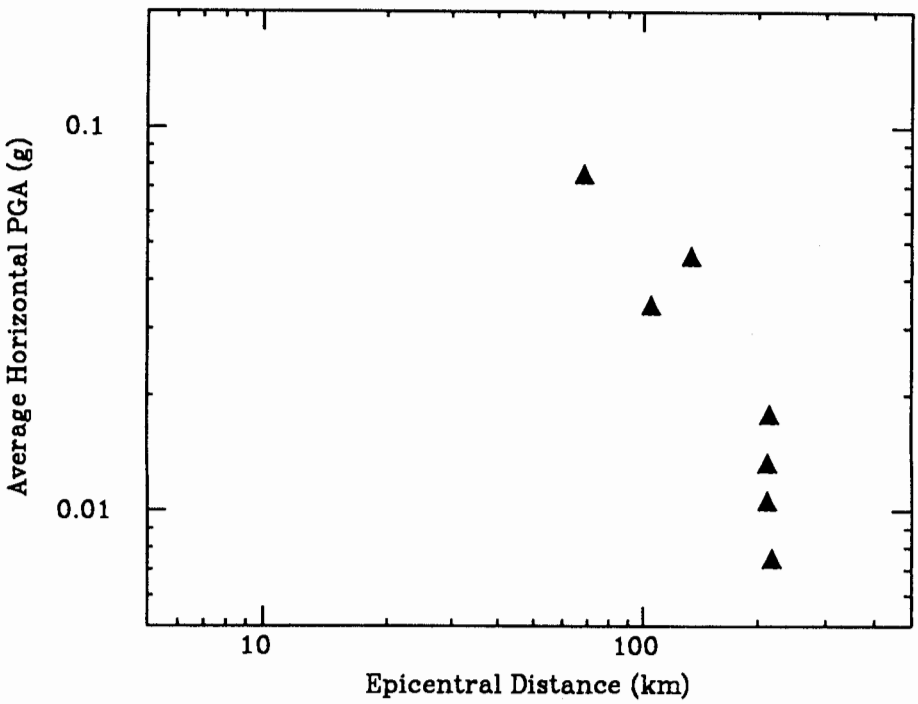

Figure 15. Peak radial acceleration plotted as a function of distance from the Borrego Mountain event.

Table 3. Locations, epicentral distances, and site characteristics for the stations used for the study of the April 9, 1968 Borrego Mountain Earthquake. The epicentral location used for determination of distances is 33.190N and 116.128W.

Station Identification	Latitude (North)	Longitude (West)	Epicentral Distance (km)	Site Geology
ATHN (253) Cal Tech Athenaeum	34.133	118.117	212	Pleistocene deposits
ELC (117) El Centro Site, Imperial Valley Irrigation District	32.795	115.549	70	Recent alluvium
MILK (264) Milikan Basement, Cal Tech	34.137	118.125	213	Pleistocene deposits
SANO (280) San Onofre SCE Power Plant	33.368	117.555	134	Lightly cemented sandstone
SCE (310) So. Cal Edison, 601 W. 5th St, Los Angeles	34.050	118.250	219	Shale
SDLP (277) San Diego Light & Power Bldg, 168 10th Street	33.707	117.155	110	Deep alluvium
VERN (288) CMD Bldg, Vernon	34.000	118.200	216	Recent alluvium

1971 San Fernando

The 1971 San Fernando earthquake is believed to have involved rupture of two fault planes, and it had a complex source process lasting about six seconds. None of the strong motion recordings have absolute trigger times. Accordingly, we have used judgment in aligning the accelerograms in constructing the profiles. We examine two profiles, one extending southeast of the epicenter through the basins to the coast of southern California, and the other extending east-southeast along the southwestern margins of the San Gabriel Mountains and the San Jacinto fault. A map showing these profiles of recording stations is given in Figure 16.

The long source duration makes it difficult to resolve between different arrivals in the strong motion records. However, in the southeast profile (Figures 17 and 18), there is a strong phase at the S_mS time at Fullerton at a distance of 75 km that may be a critical reflection. At the adjacent more distant stations

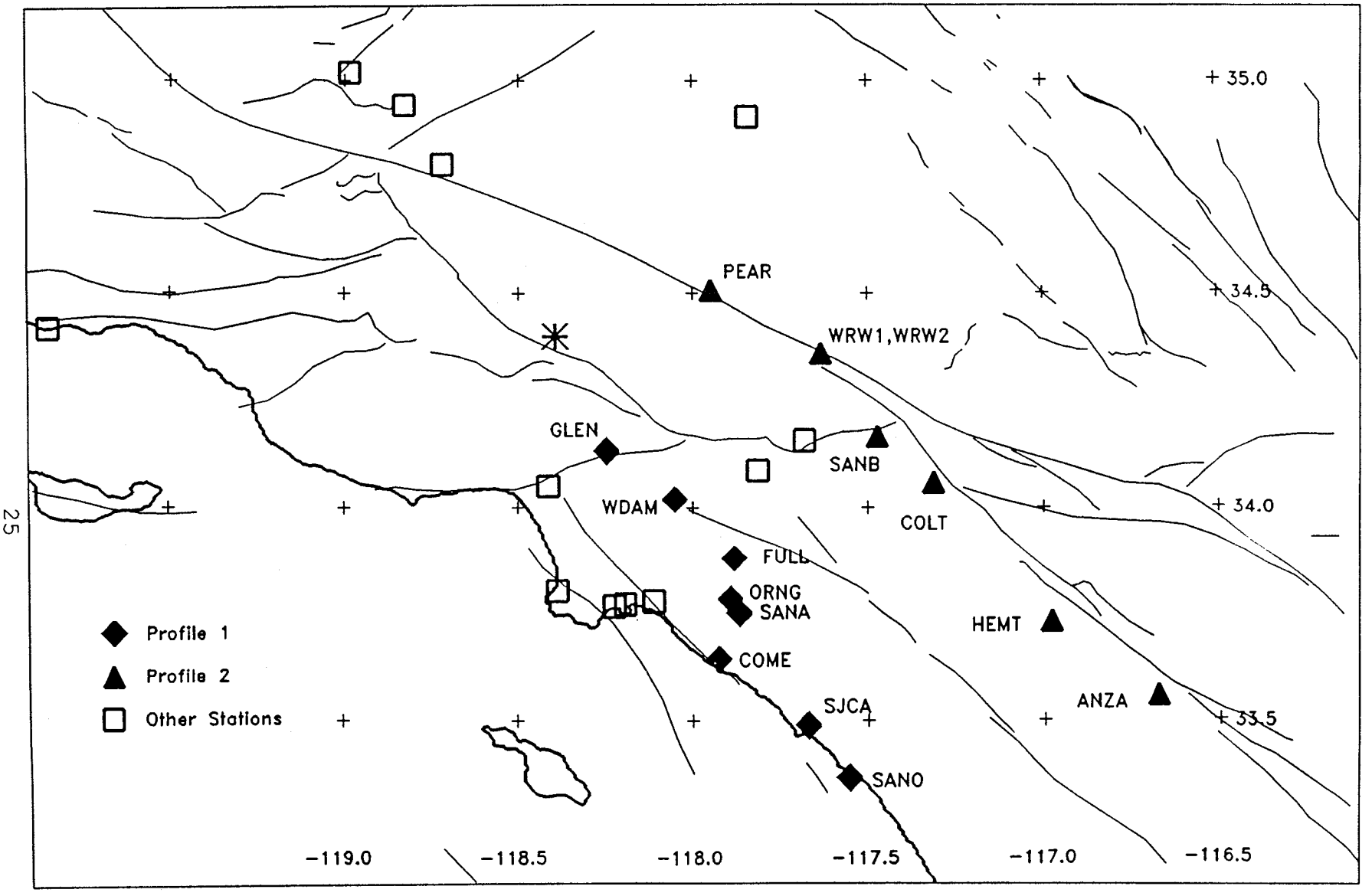

Figure 16. Map showing the location of the 1971 San Fernando earthquake, and strong motion instruments. The filled symbols show the locations of two profiles of instruments used in this study.

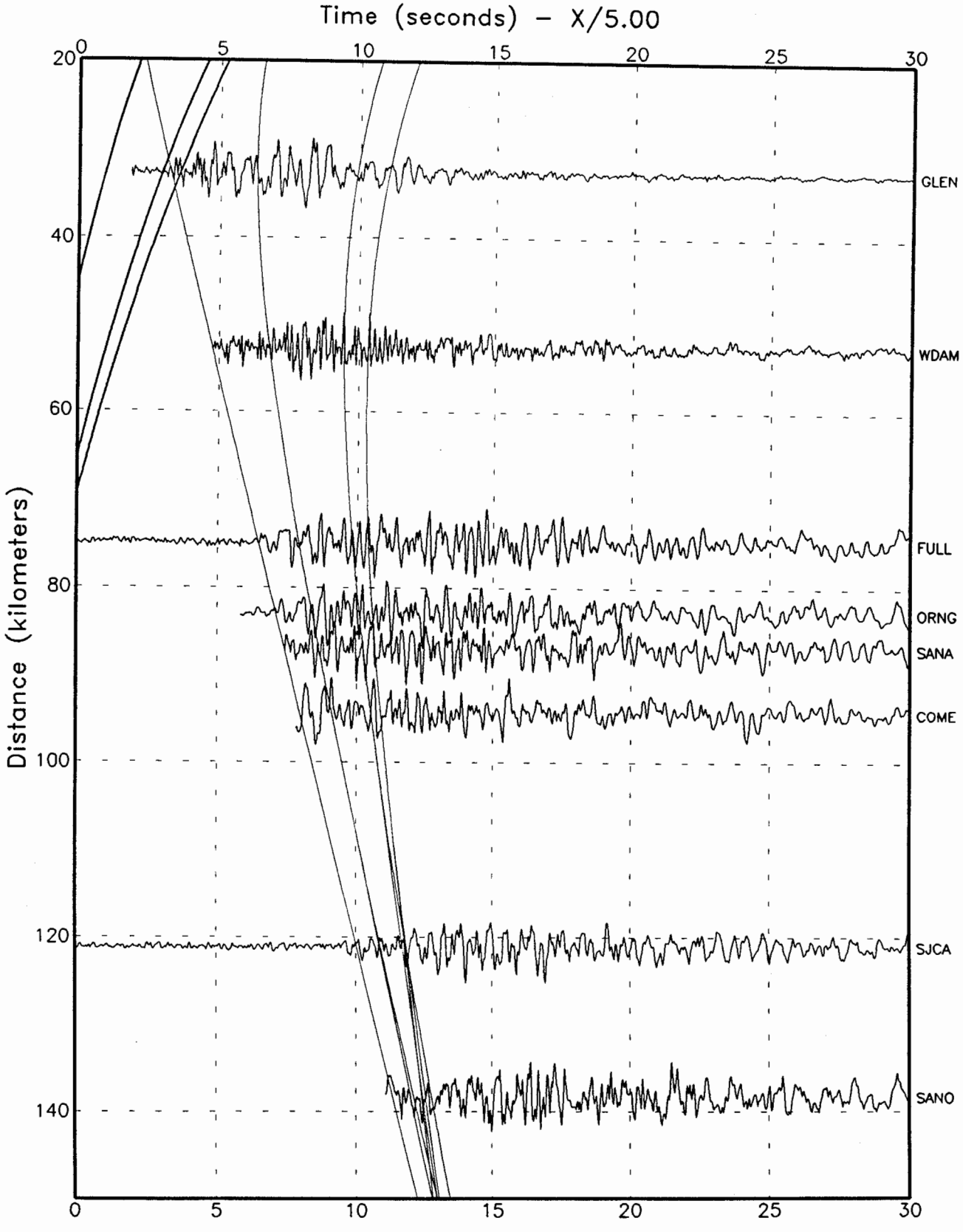

Figure 17. Tangential component accelerograms of the 1971 San Fernando earthquake recorded along Profile 1 are plotted as a function of distance. These recordings did not have absolute timing. Travel times for the direct, Conrad reflected, mafic reflected and Moho reflected P and S waves determined from the Helmberger *et al.* (1992) crustal velocity model are also shown.

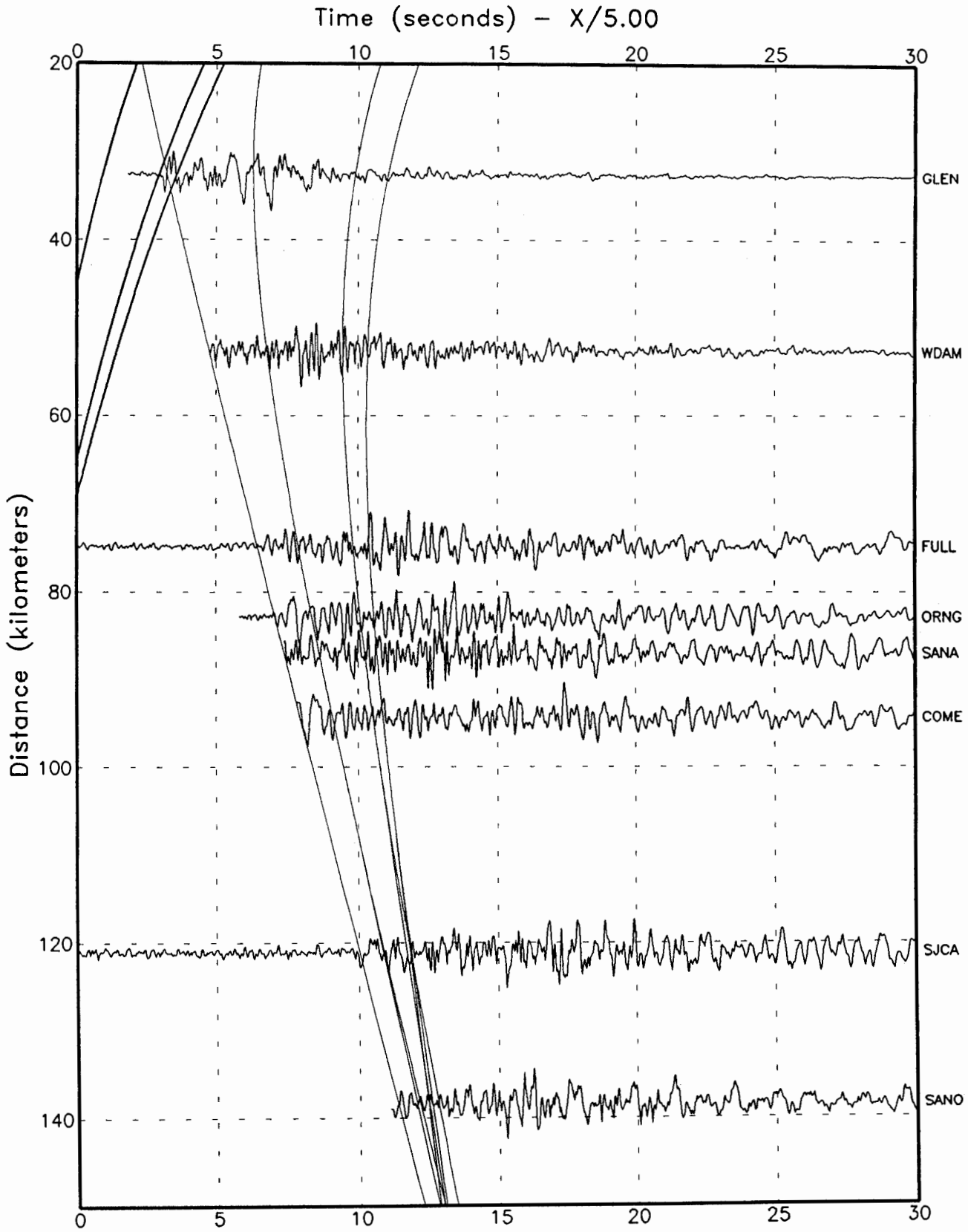

Figure 18. Radial component accelerograms of the 1971 San Fernando earthquake recorded along Profile 1 are plotted as a function of distance. These recordings did not have absolute timing. Travel times for the direct, Conrad reflected, mafic reflected and Moho reflected P and S waves determined from the Helmberger *et al.* (1992) crustal velocity model are also shown.

in Orange and Santa Ana, there are also large arrivals after the S_mS time. The attenuation of peak acceleration (Figures 19 and 20) shows a pronounced flattening in the distance range of 80 to 120 km, which is also compatible with these motions being critical reflections.

In the east-southeast profile (Figures 21 and 22), there is a strong phase at the S_mS time at Wrightwood at a distance of 70 km that may be a critical reflection. As in the case of the southeast profile, the attenuation of peak acceleration (Figures 23 and 24) shows a pronounced flattening that begins at about 70 km, but the flattening extends to the limit of the data at 180 km. This flattening is substantially more extensive that the flattening along the southeast profile, suggesting the presence of significant lateral heterogeneity in crustal structure. Listed in Table 4 are the site conditions of the recordings analyzed.

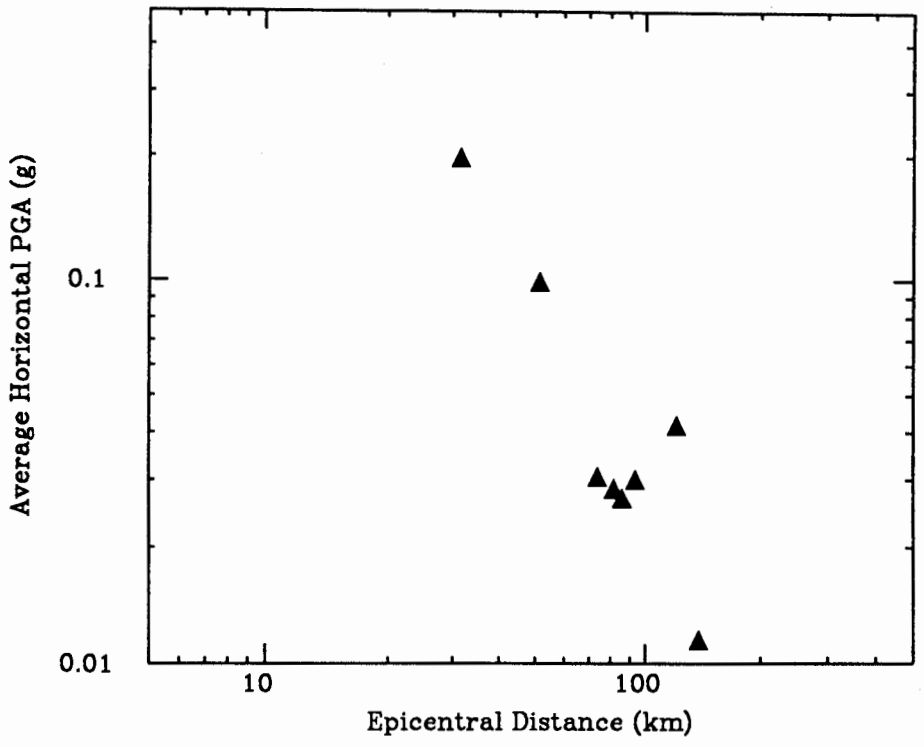

Figure 19. Peak tangential acceleration of the 1971 San Fernando earthquake plotted as a function of distance along Profile 1.

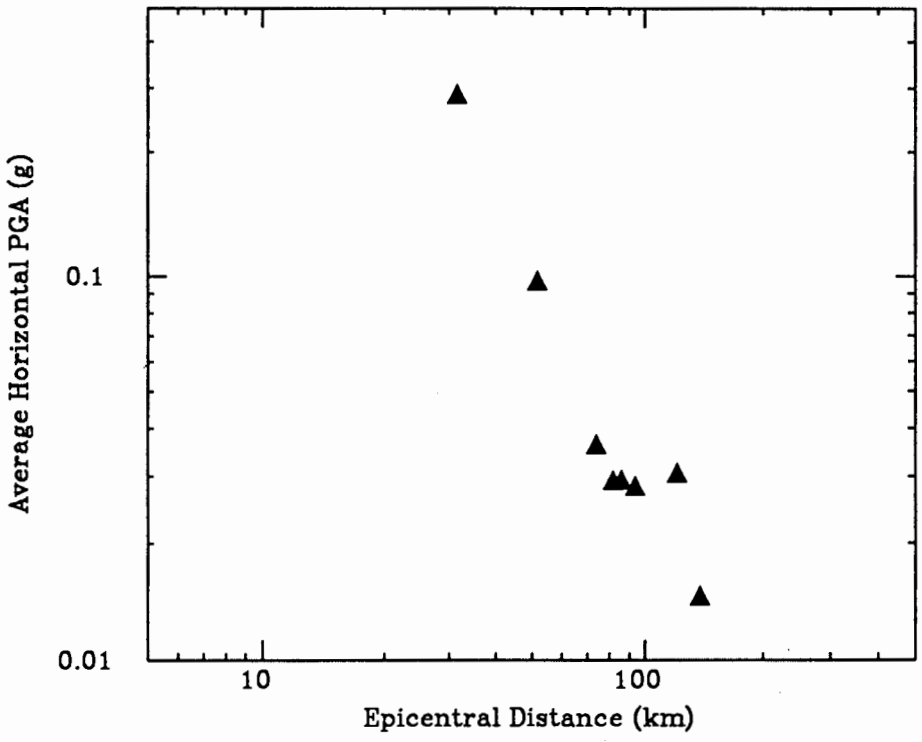

Figure 20. Peak radial acceleration of the 1971 San Fernando earthquake plotted as a function of distance along Profile 1.

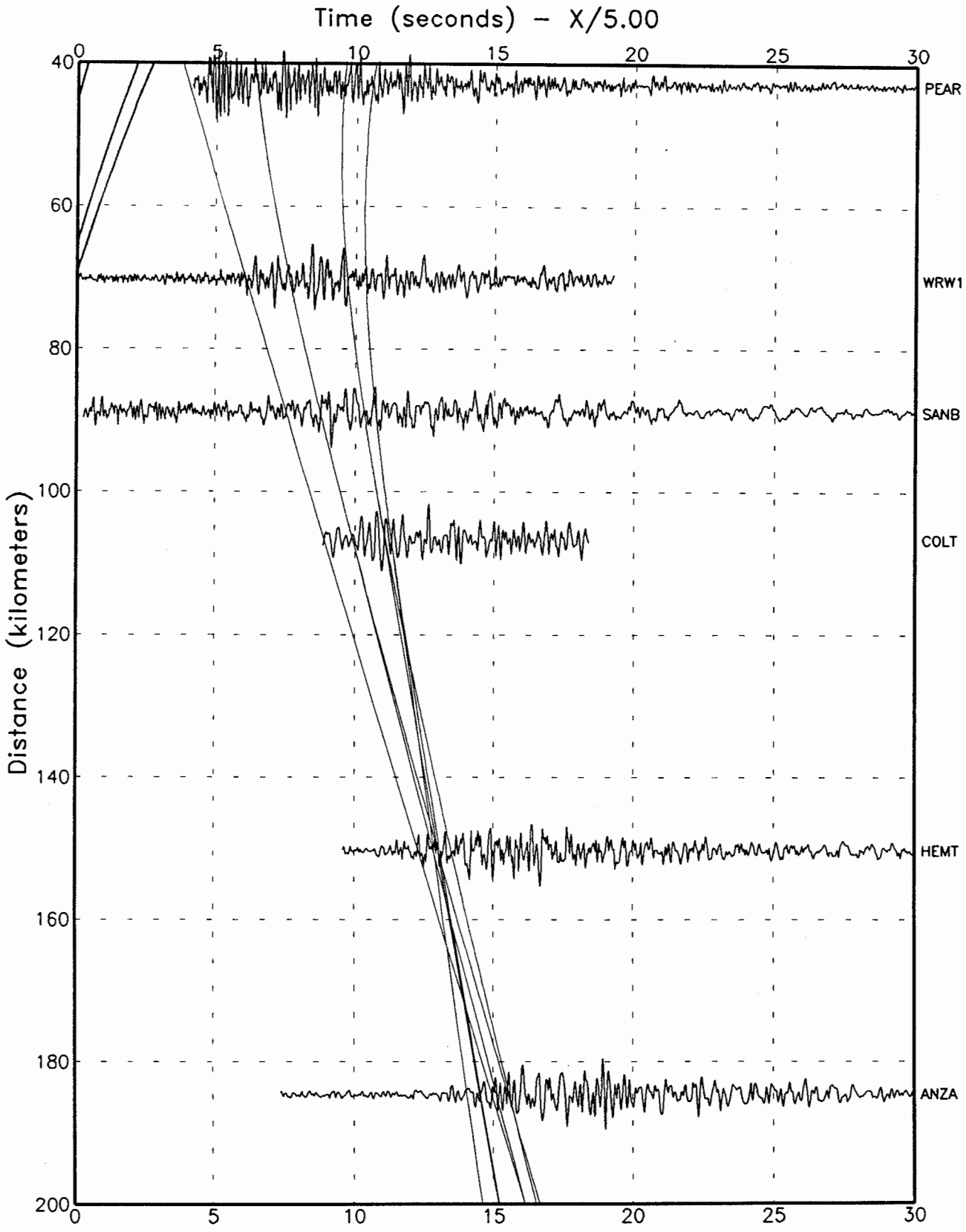

Figure 21. Tangential component accelerograms of the 1971 San Fernando earthquake recorded along Profile 2 are plotted as a function of distance. These recordings did not have absolute timing. Travel times for the direct, Conrad reflected, mafic reflected and Moho reflected P and S waves determined from the Helmberger *et al.* (1992) crustal velocity model are also shown.

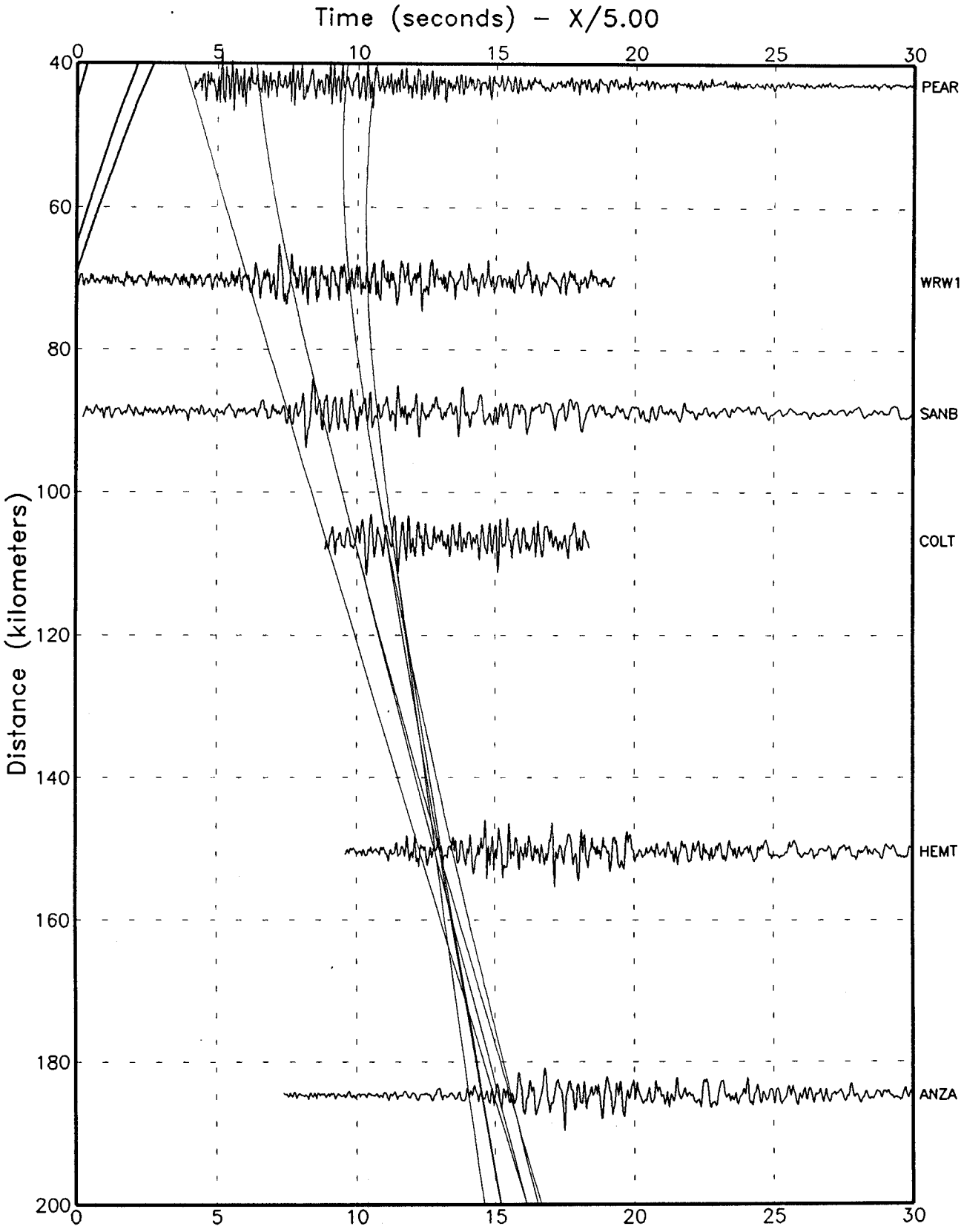

Figure 22. Radial component accelerograms of the 1971 San Fernando earthquake recorded along Profile 2 are plotted as a function of distance. These recordings did not have absolute timing. Travel times for the direct, Conrad reflected, mafic reflected and Moho reflected P and S waves determined from the Helmberger *et al.* (1992) crustal velocity model are also shown.

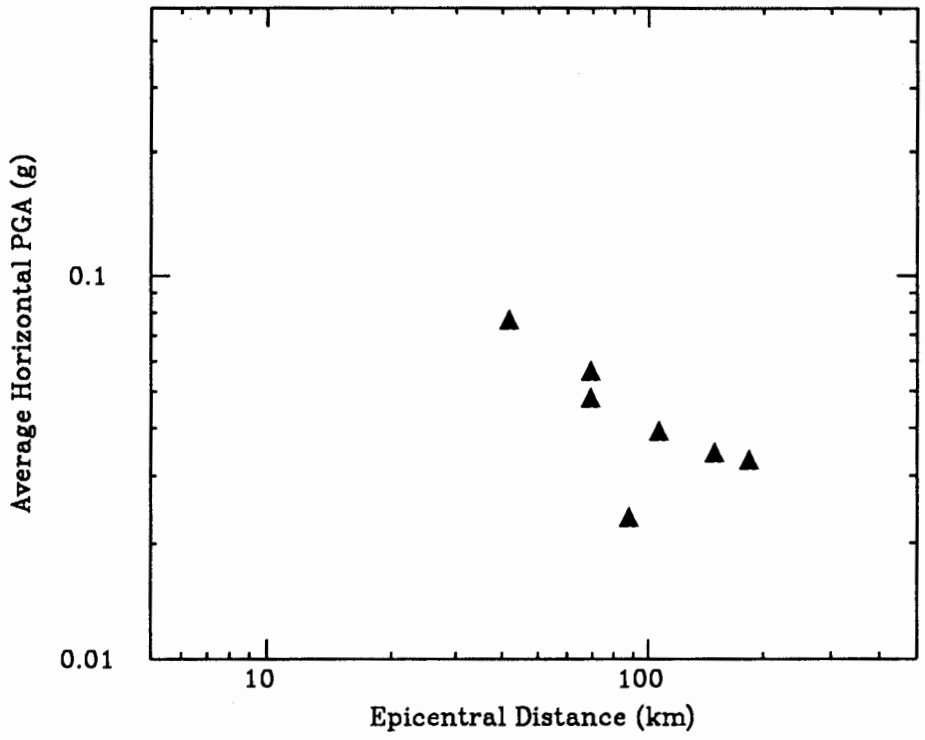

Figure 23. Peak tangential acceleration of the 1971 San Fernando earthquake plotted as a function of distance along Profile 2.

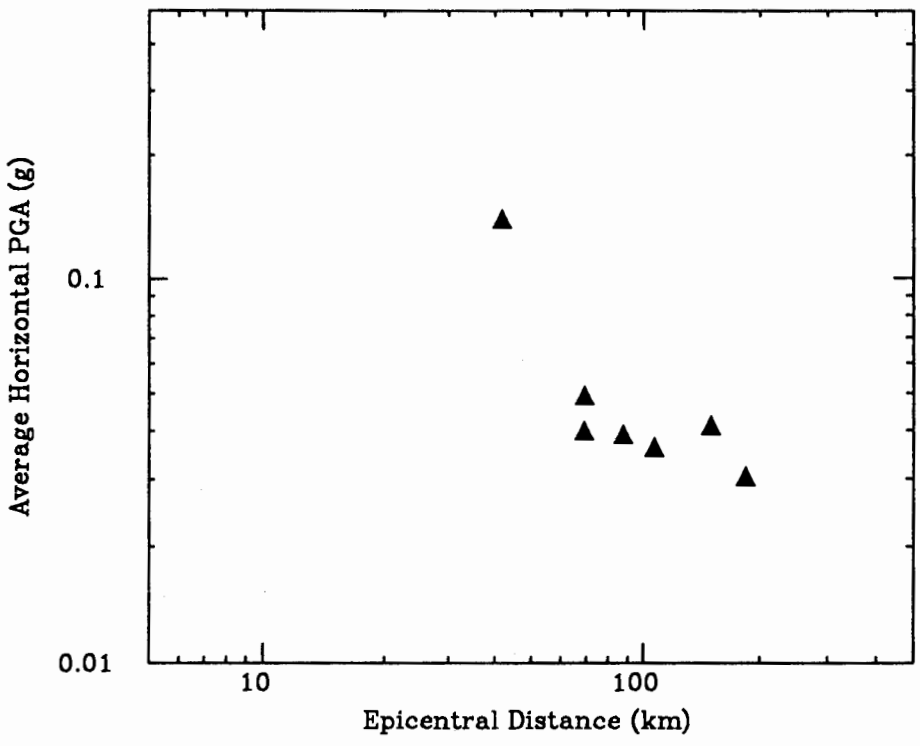

Figure 24. Peak radial acceleration of the 1971 San Fernando earthquake plotted as a function of distance along Profile 2.

Table 4. Locations, epicentral distances, and site characteristics for the stations used for the study of the February 9, 1971 San Fernando Earthquake. The epicentral location used for determination of distances is 34.400N and 118.395W.

Station Identification	Latitude (North)	Longitude (West)	Epicentral Distance (km)	Site Geology
COME (114) Costa Mesa, 666 W. 19th St, Ground Floor	33.644	117.926	94	20-25 feet fine sand over shale
FULL (476) 2600 Nutwood Ave., Fullerton Basement	33.878	117.881	75	Alluvium, > 20m
GLEN (122) 633 E. Broadway, Municipal Srvs Bldg, Glendale	34.133	118.247	33	Alluvium, > 8m
ORNG (472) 4000 W Chapman Ave, Basement, Orange	33.781	117.895	83	> 90m alluvium over shale
SANA (281) Engineering Bldg, Santa Ana	33.750	117.867	87	Alluvium
SANO (280) So Cal Edison Nuclear Power Plant, San Onofre, CA	33.368	117.555	138	Lightly cemented sandstone
SJCA (465) San Juan Capistrano	33.489	117.671	121	Sand-siltstone and conglomerate
WDAM (289) Whittier Narrows Dam	34.020	118.053	53	Alluvium, > 45m
ANZA (103) Anza Post Office Storage Room	33.560	116.674	185	Alluvium
COLT (113) Edison Co, Colton	34.059	117.313	107	Deep alluvium
HEMT (123) Hemet Fire Station, Hemet, Hose Storage Room	33.730	116.979	150	Deep alluvium
PEAR (269) Pumping Plant, Pear Blossom	34.508	117.922		Shallow soil
SANB (274) Hall of Records, San Bernardino	34.106	117.284	89	Recent alluvium
WRW1 (290) Wrightwood, 6074 Park Dr, Ground Level	34.361	117.633		Shallow soil
WRW2 (290) Wrightwood, 6074 Park Dr, Ground Level	34.361	117.633		Shallow soil

1983 Coalinga

As seen teleseismically, the Coalinga earthquake had a complex source function, starting with a small event followed two seconds later by a larger event having a duration of 5 seconds (Hartzell and Heaton, 1986). This small precursory event is clearly seen in strong motion recordings in the Parkfield region. Of the many stations, we have chosen to show those of the Chalome array (Figure 25). About half of the stations have absolute trigger times, as denoted on the profiles (Figures 26 and 27). The correlation of waveforms across the array is quite high, leaving little uncertainty in how to align the remaining traces using judgment. The first arrivals are small, followed two seconds later by larger arrivals that we interpret as the direct arrivals from the main rupture. These are followed two seconds later by further large arrivals, whose times are compatible with them being S_mS from the main rupture. Beyond about 60 km, these are the largest arrivals. The data for this earthquake span a narrow distance range, and thus do not provide good definition of the attenuation relation (Figures 28 and 29). Listed in Table 5 are the site conditions of the recordings analyzed.

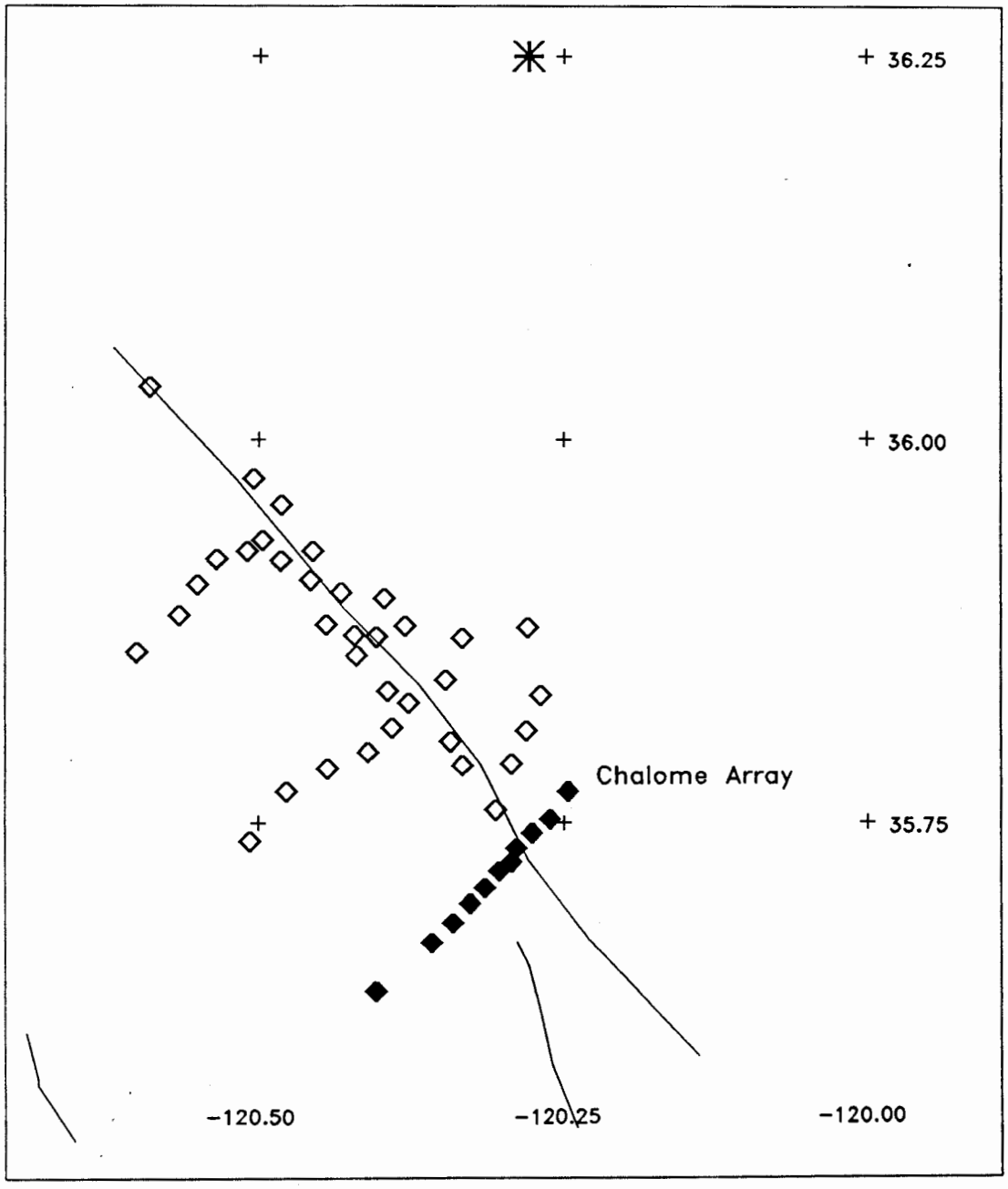

Figure 25. Map showing the location of the 1985 Coalinga earthquake, and strong motion instruments of the Parkfield array. The filled symbols show the locations of instruments used in this study.

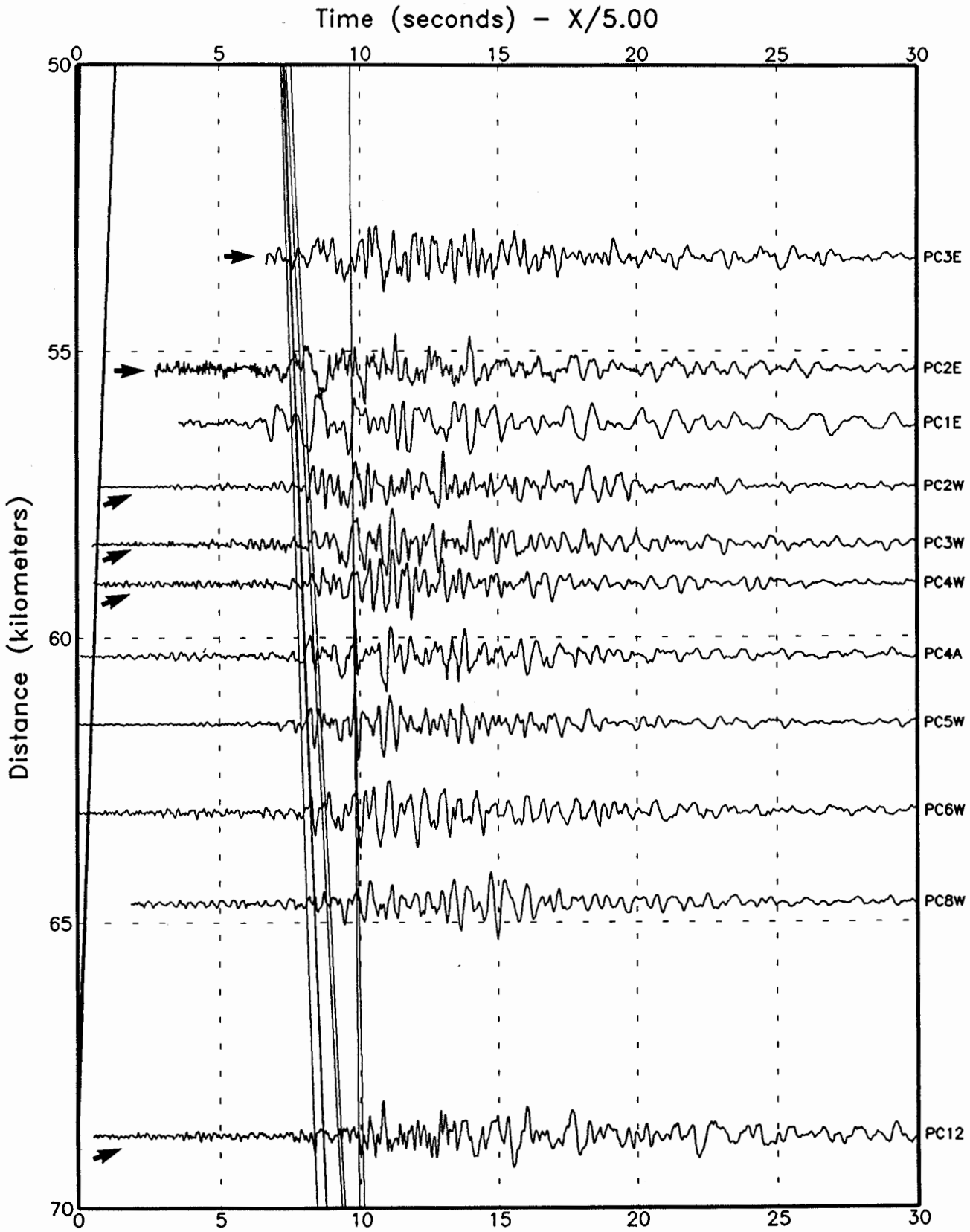

Figure 26. Tangential component accelerograms for the 1985 Coalinga earthquake are plotted as a function of distance. The recordings marked by arrows indicate stations with known trigger times. Travel times for the direct, Conrad reflected, mafic reflected and Moho reflected P and S waves calculated from a crustal model developed by Eaton (1986) are also shown.

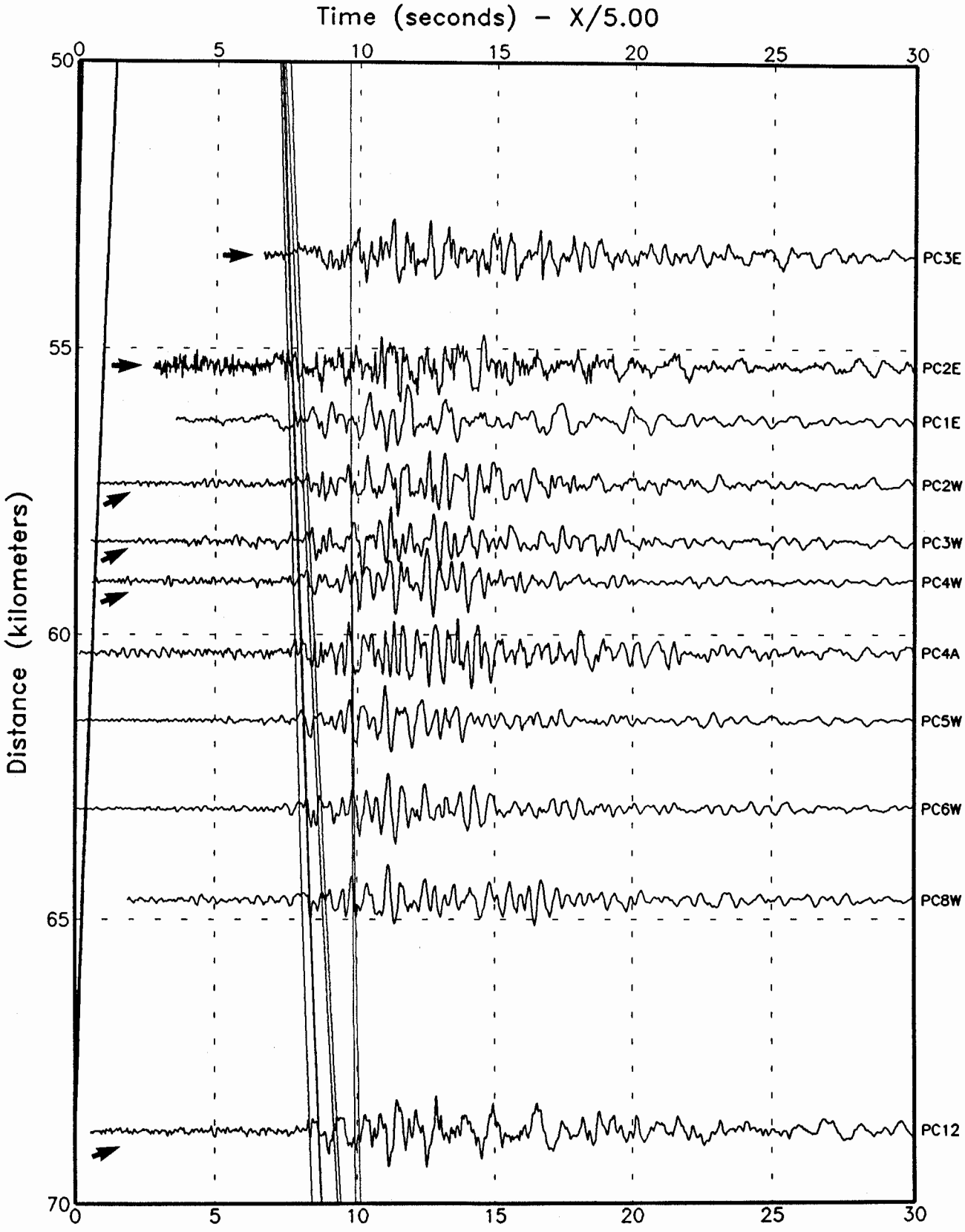

Figure 27. Radial component accelerograms for the 1985 Coalinga earthquake are plotted as a function of distance. The recordings marked by arrows indicate stations with known trigger times. Travel times for the direct, Conrad reflected, mafic reflected and Moho reflected P and S waves calculated from a crustal model developed by Eaton (1986) are also shown.

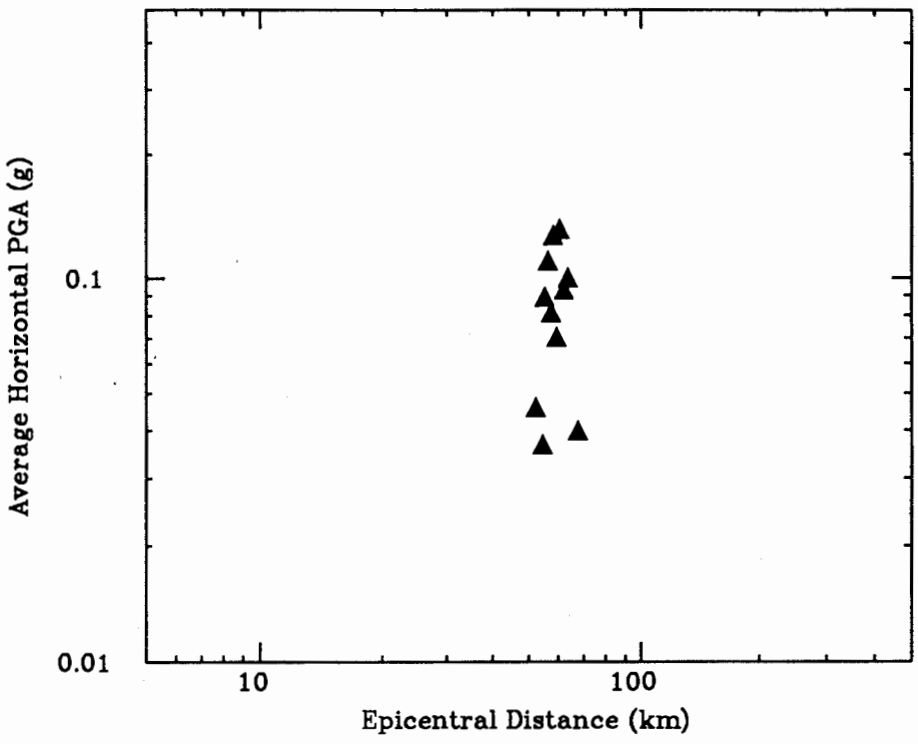

Figure 28. Peak tangential acceleration of the 1985 Coalinga earthquake plotted as a function of distance.

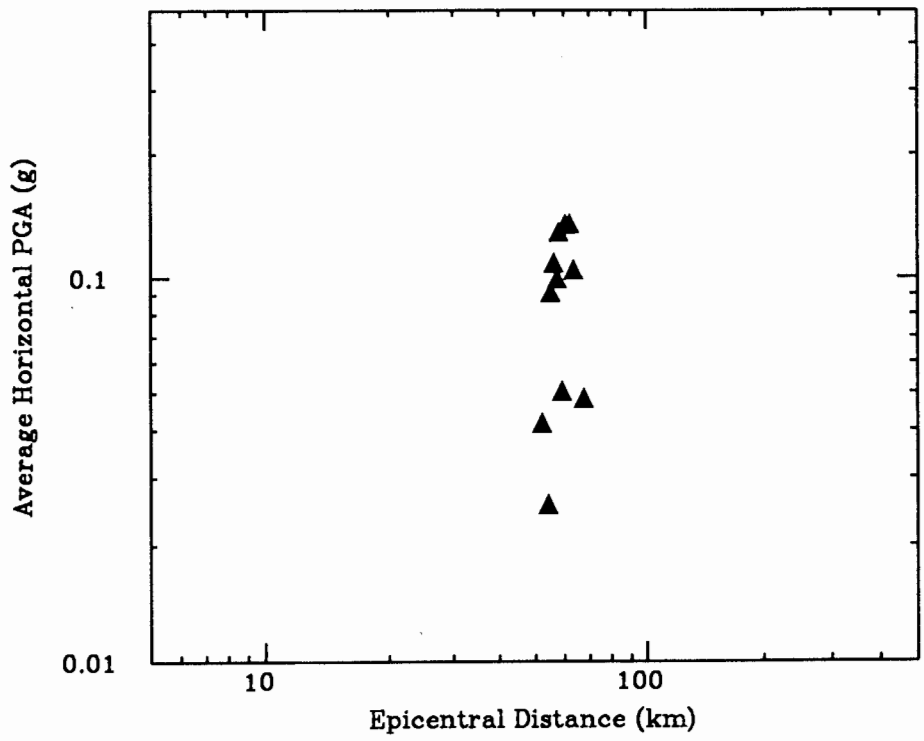

Figure 29. Peak radial acceleration of the 1985 Coalinga earthquake plotted as a function of distance.

Table 5. Locations, epicentral distances, and site characteristics for the stations used for the study of the May 2, 1983 Coalinga Earthquake. The epicentral location used for determination of distances is 36.250N and 120.280W.

Station Identification	Latitude (North)	Longitude (West)	Epicentral Distance (km)	Site Geology
PC1E (36452) Chalome 01 East	35.743	120.277	56.3	Alluvium, sandstone (?)
PC2E (36230) Chalome 02 East	35.752	120.262	55.4	Soil, sandstone
PC3E (36450) Chalome 03 East	35.770	120.247	53.5	Soil, sandstone
PC2W (36228) Chalome 02 West	35.733	120.290	57.4	Alluvium, sandstone (?)
PC3W (36410) Chalome 03 West	35.724	120.294	58.4	Alluvium, sandstone
PC4W (36411) Chalome 04 West	35.718	120.304	59.0	Thin alluvium, sandstone
PC4A (36412) Chalome 04A West	35.707	120.316	60.3	Alluvium, sandstone
PC5W (36227) Chalome 05 West	35.697	120.328	61.4	Alluvium, sandstone
PC6W (36451) Chalome 06 West	35.684	120.342	62.9	Alluvium, sandstone
PC8W (36266) Chalome 08 West	35.671	120.359	64.5	Alluvium, sandstone
PC12 (36229) Chalome 12 West	35.639	120.404	68.4	Alluvium, sandstone

1986 North Palm Springs

We analysed a closely and fairly evenly spaced array of CDMG stations of the Hemet Array extending southwest from the epicenter in the distance range of 30 to 75 km (Figure 30). From the analysis of near-source and teleseismic data, Hartzell estimated that the source duration of the earthquake was approximately 5 seconds. This duration is comparable to the expected difference in travel-time between direct S and S_mS at a distance of 50 km, and makes it difficult to separate source effects from the wave propagation effects that we are investigating.

There is not much waveform coherence across the array (Figures 31 and 32), even in the displacement profiles, but we can discern the arrival time trends of wave packets. Within 70 km, the largest motions on the tangential component

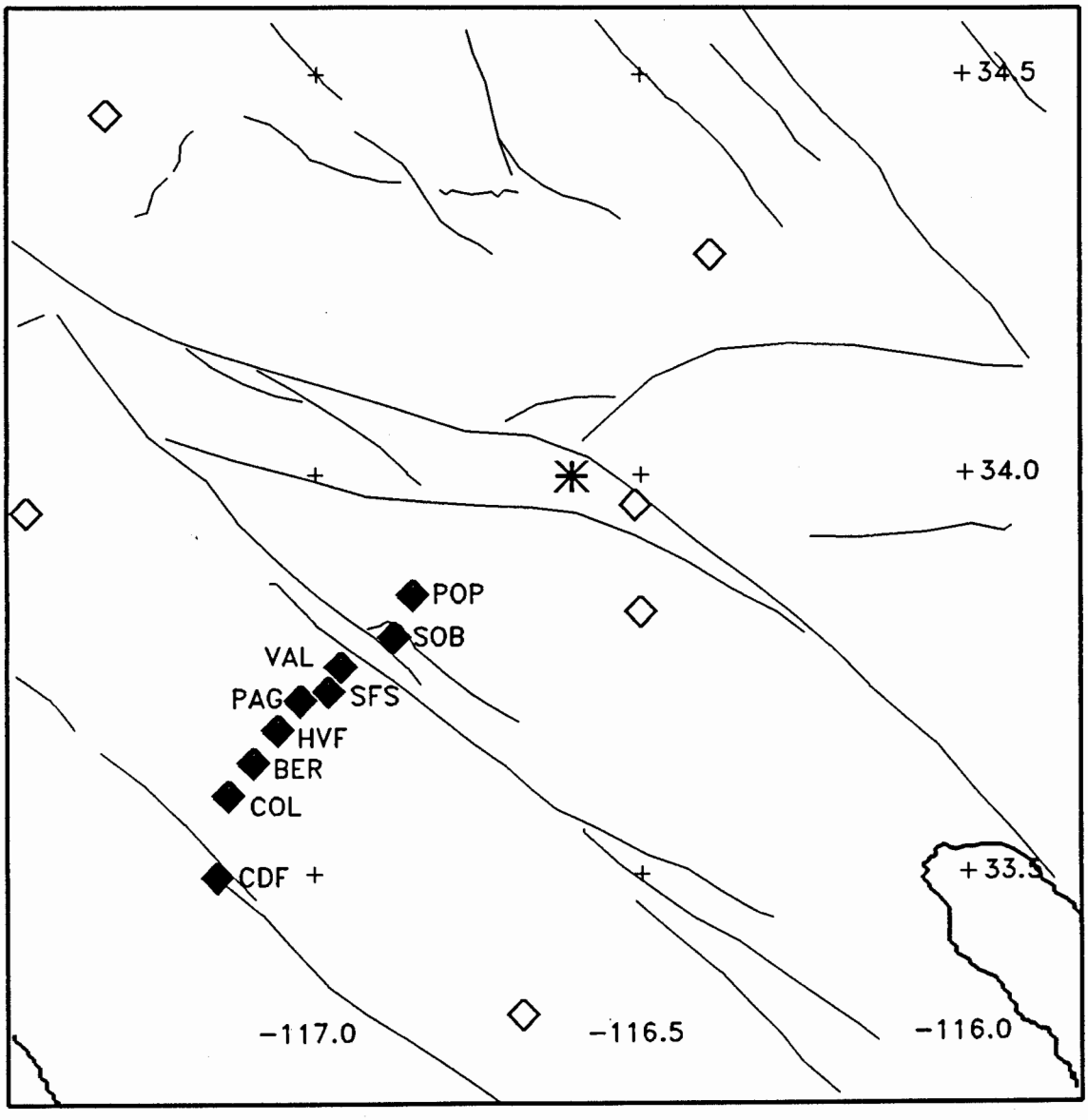

Figure 30. Map showing the location of the 1986 North Palm Springs earthquake. The filled symbols show the locations of instruments of the Hemet array used in this study.

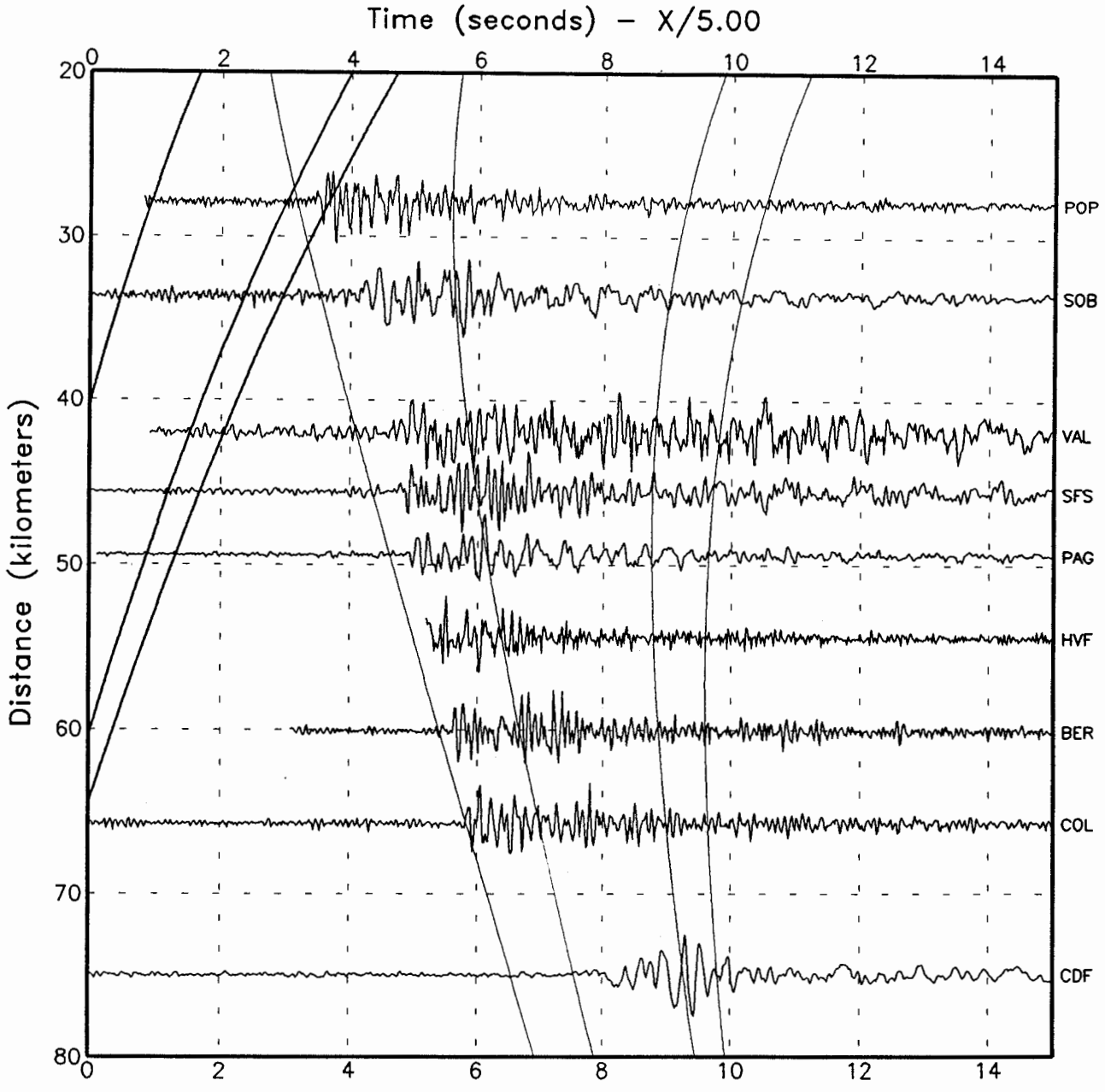

Figure 31. Tangential component accelerograms for the 1986 North Palm Springs earthquake plotted as a function of distance. All of the stations have known trigger times. Travel times for the direct, Conrad reflected, mafic reflected and Moho reflected P and S waves calculated from the Helmberger *et al.* (1992) crustal model are also shown.

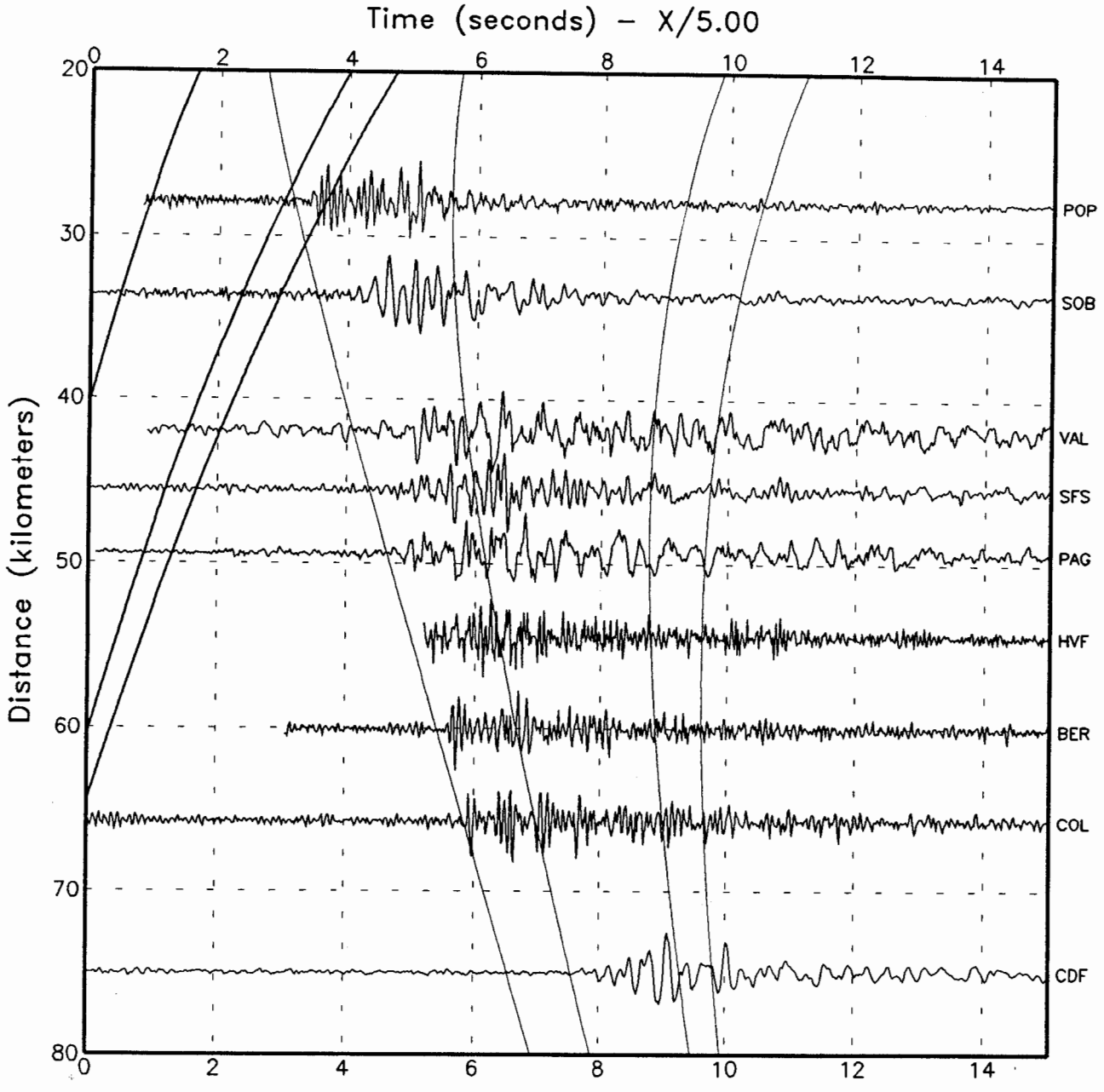

Figure 32. Radial component accelerograms for the 1986 North Palm Springs earthquake plotted as a function of distance. All of the stations have known trigger times. Travel times for the direct, Conrad reflected, mafic reflected and Moho reflected P and S waves calculated from the Helmberger *et al.* (1992) crustal model are also shown.

generally are associated with the direct S wave. However, on the vertical and radial components, the Conrad reflection appears to be responsible for the largest motions. Critical reflections from the mafic and Moho layers are not evident in the data.

The most distant station has waveforms and arrival times that are quite different from those of the other stations. This station is in Temecula on the west side of the Elsinore fault. The arrival time at this station is at least one second slower than that at Puerta La Cruz, which is at the same epicentral distance (75 km) but on the east side of the Elsinore fault. For this reason, it is doubtful that the largest arrivals on the Temecula record are critical reflections from the lower crust, as a literal interpretation of the travel time would indicate. The attenuation of peak acceleration (Figures 33 and 34) shows a large degree of scatter and no flattening trend in the distance range of 30 to 75 km. Listed in Table 6 are the site conditions of the recordings analyzed.

The seismograms recorded at Pasadena, at a distance of 145 km from the North Palm Springs earthquake, show clear evidence of critical reflections from the Moho. The upper trace of Figure 35 shows the tangential component of the 1986 mainshock recorded on the Wood-Anderson short-period seismograph. Below is shown a synthetic seismogram computed using the reflectivity method. The generalized ray calculations shown in Figure 4 were used to identify specific phases in this synthetic seismogram. The largest arrival in both the recorded and synthetic seismograms is the phase S_mS.

A later earthquake of M_L= 4.8 on December 16, 1988 near North Palm Springs was recorded on the very broad band Streckeisen seismograph at Pasadena at a distance of 140 km. The recorded displacement seismograms and synthetic seismograms computed using the reflectivity method are shown in Figure 36. As for the 1986 event, the largest high frequency motions in both the recorded and synthetic seismograms are due to the phase S_mS.

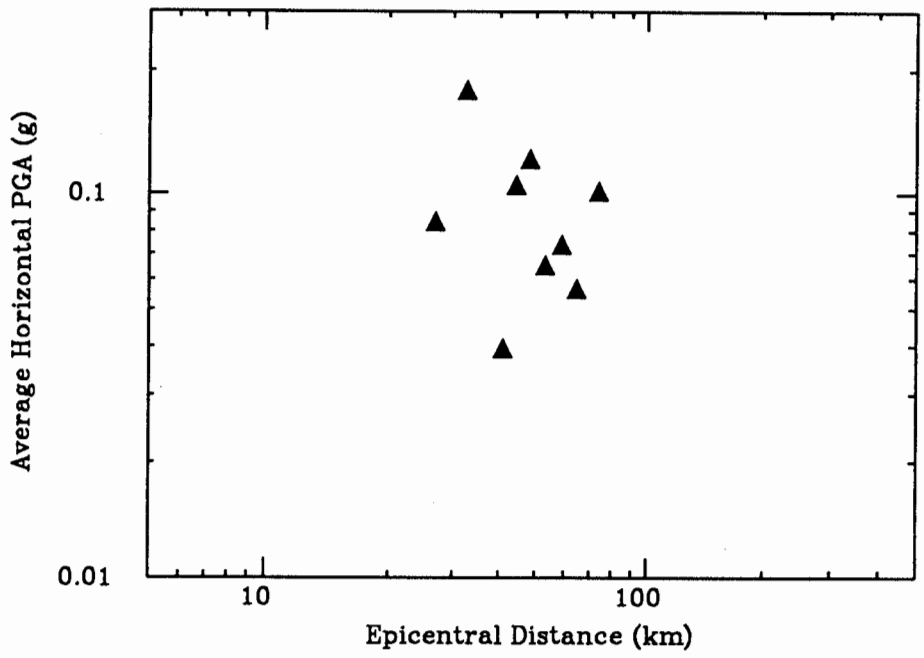

Figure 33. Peak tangential acceleration plotted as a function of distance from 1986 the North Palm Springs event.

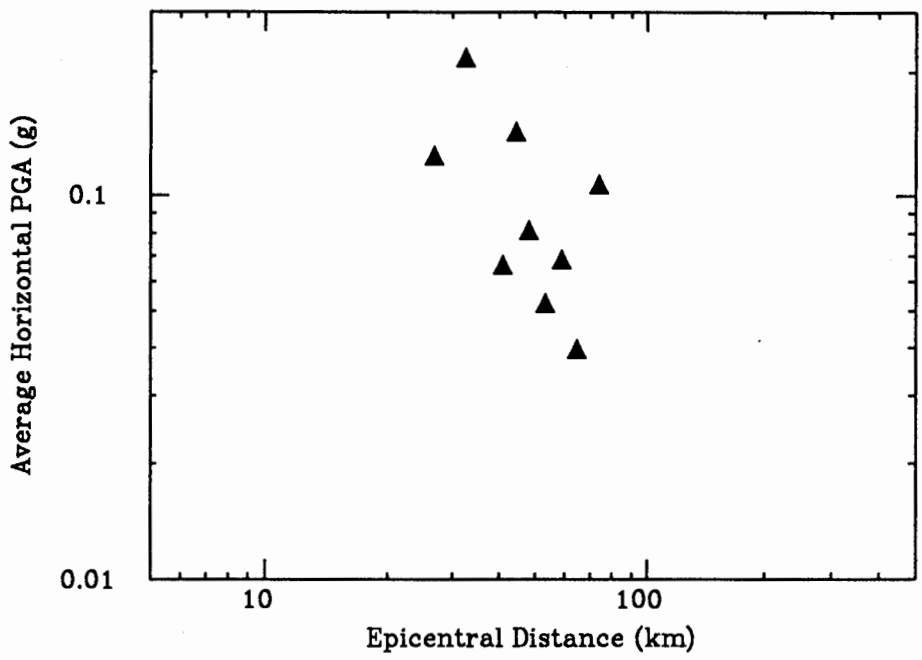

Figure 34. Peak radial acceleration plotted as a function of distance from the 1986 North Palm Springs event.

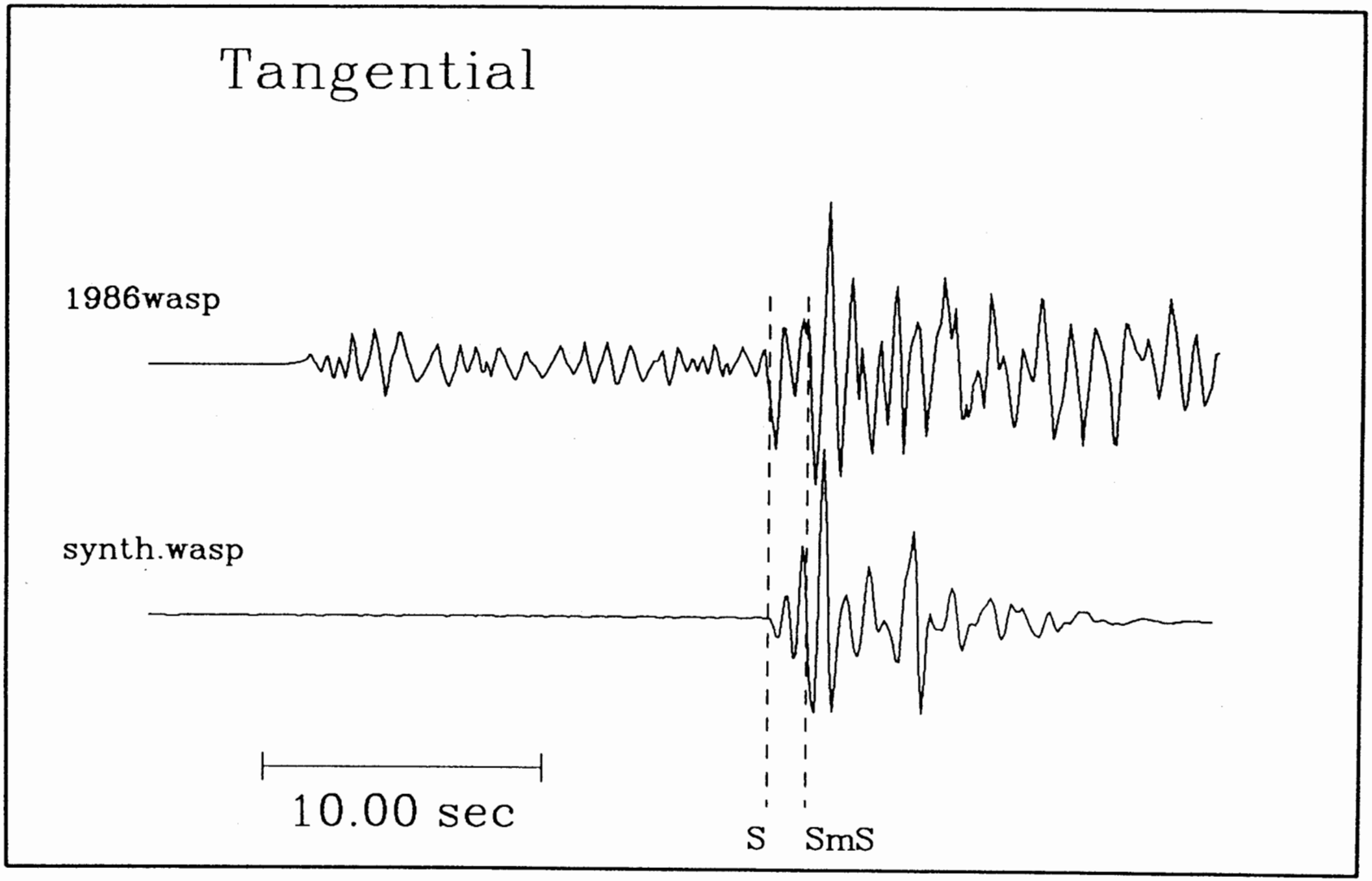

Figure 35. Recorded (above) and synthetic (below) short-period Wood-Anderson seismograms of the 1986 North Palm Springs earthquake.

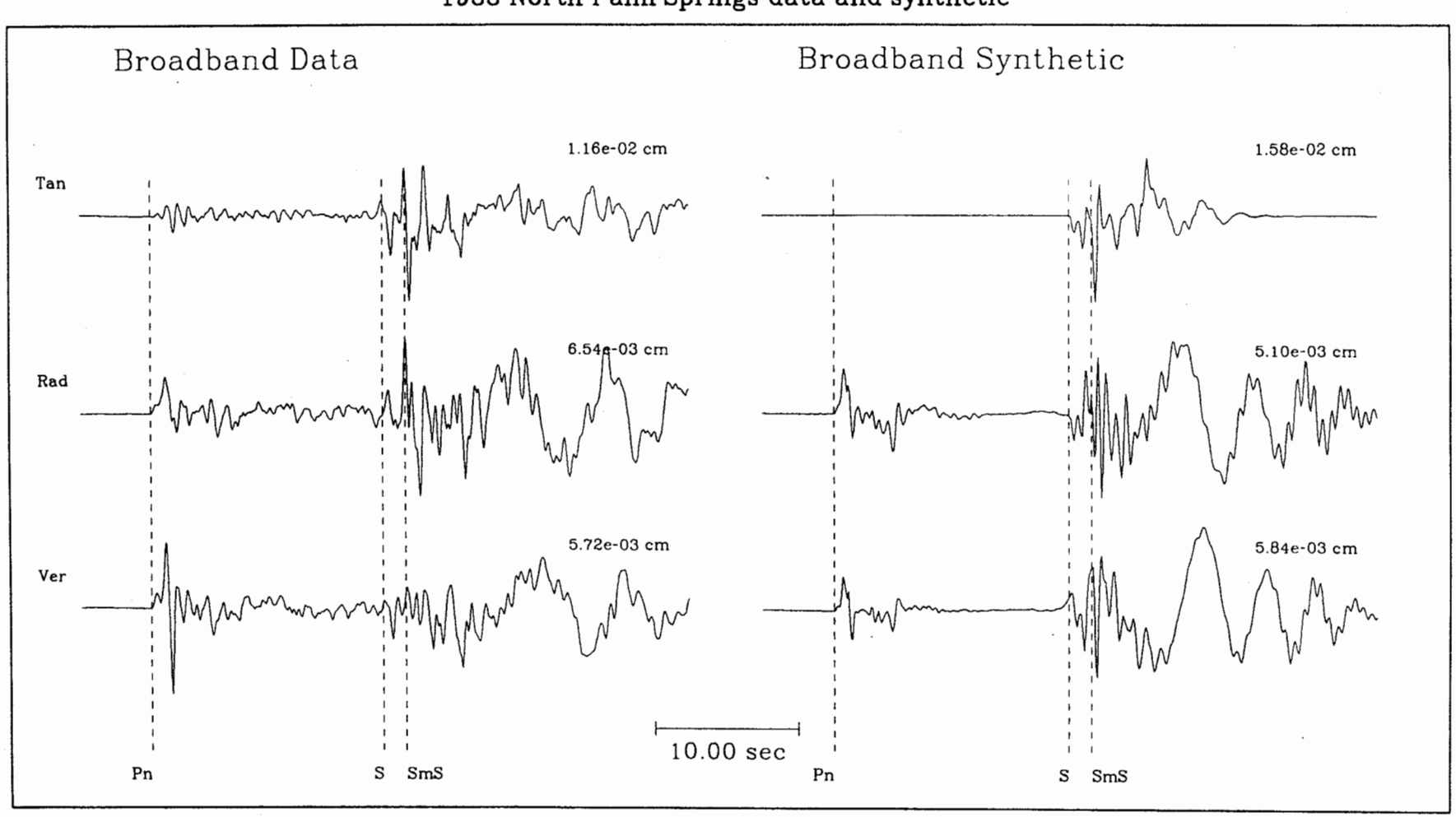

Figure 36. Recorded (left) and synthetic (right) very broad band displacement seismograms of the 1988 North Palm Springs earthquake.

Table 6. Locations, epicentral distances, and site characteristics for the stations used for the study of the July 8, 1976 Palm Springs Earthquake. The epicentral location used for determination of distances is 33.998N and 1116.606W.

Station Identification	Latitude (North)	Longitude (West)	Epicentral Distance (km)	Site Geology
BER (13199) Winchester, Bergman Ranch	33.640	117.094	60	Weathered granite
CDF (13172) Temecula, CDF Fire Station	33.496	117.149	75	Alluvium
COL (13198) Murieta Hot Springs Collins Ranch	35.599	117.132	66	Thin soil (1m) over weathered granite
HVF (13200) Winchester, Hidden Valley Farms	33.681	117.056	55	Thin soil (1m) over schist & granite
PAG (13201) Winchester, Page Brothers Farm	33.718	117.022	50	Deep (200m?) alluvium
POP (12206) Silent Valley, Poppet Flat	33.851	116.852	28	Weathered granite
SFS (12331) Hemet, Stetson Ave Fire Station	33.729	116.979	46	Deep alluvium
SOB (12204) San Jacinto, Soboba	33.797	116.880	34	Alluvium
VAL (12202) San Jacinto, Valley Cemetery	33.760	116.960	42	Alluvium

1987 Whittier Narrows

We have analysed a profile of 10 recordings (LEO5 and LEO6 are co-located) extending north from the epicenter past Lancaster to Rosamond, shown in Figure 37. In the distance range of zero to 55 km, the peak acceleration is associated with the time of the direct S arrival, as seen in Figures 38 and 39 for the radial and tangential components respectively. However, beyond about 55 km, the largest arrivals occur at times corresponding to reflections from the lower crust (the mafic and Moho layers). This is most clearly seen at Lancaster (at 70 km) and Rosamond (at 90 km), where the small direct arrival is followed by a larger mafic layer reflection and an even larger Moho reflection. These critically

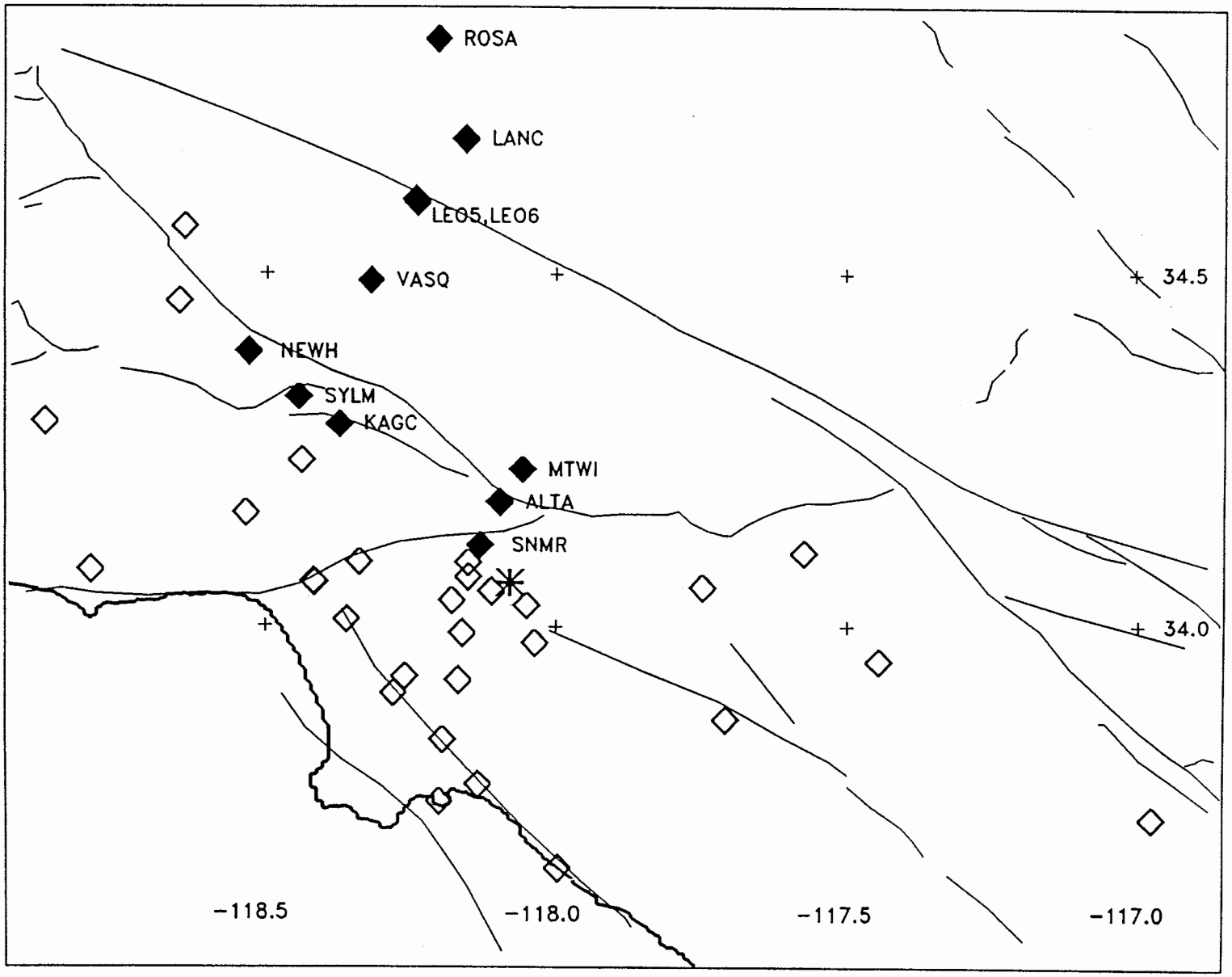

Figure 37. Map showing the location of the 1987 Whittier Narrows earthquake. The filled symbols show the locations of instruments used in the study.

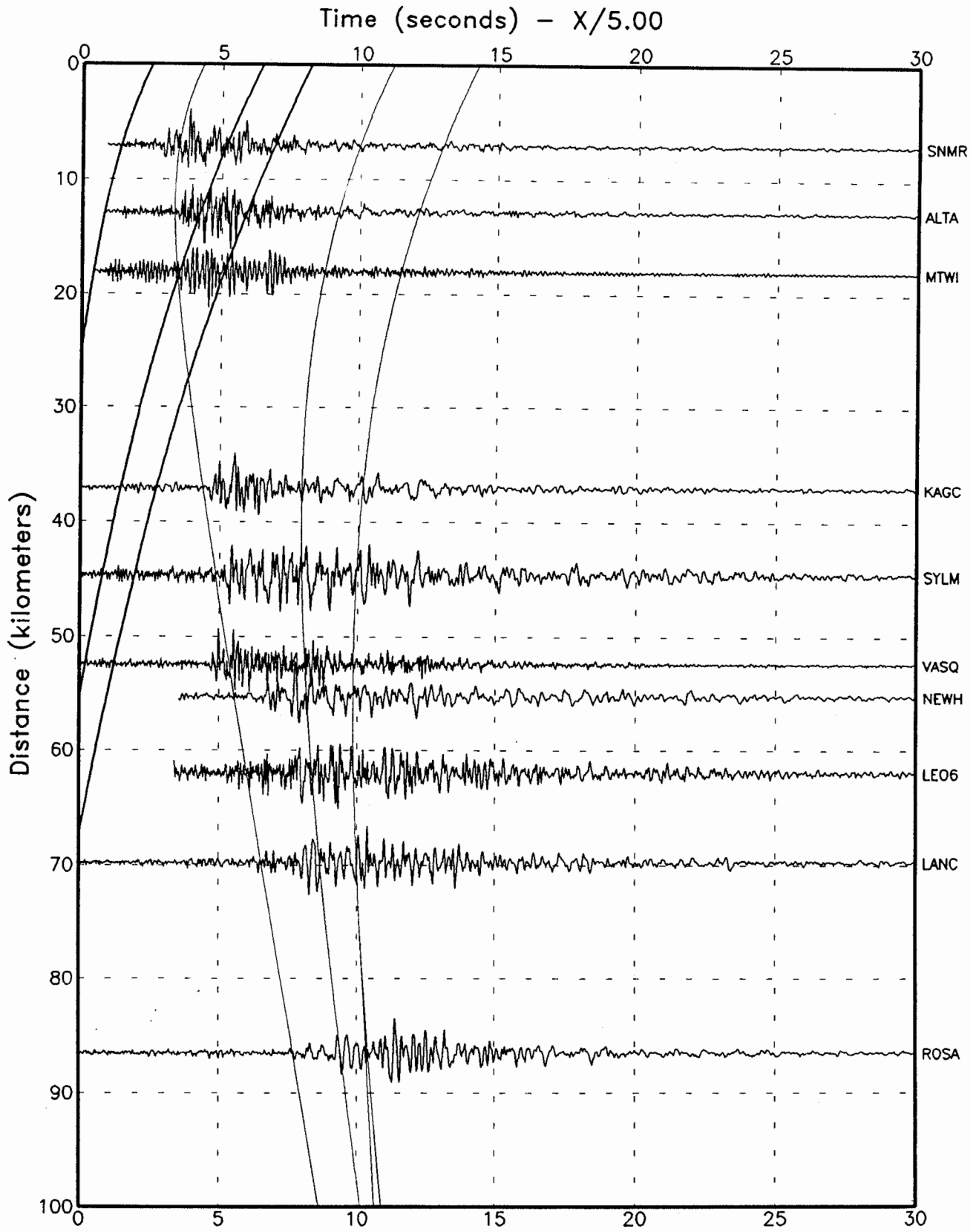

Figure 38. Tangential component accelerograms for the 1987 Whittier Narrows earthquake along a profile extending north from the epicenter. All of the stations have known trigger times. Travel times for the direct, Conrad reflected, mafic reflected and Moho reflected P and S waves calculated from the Magistrale (1990) crustal model are also shown.

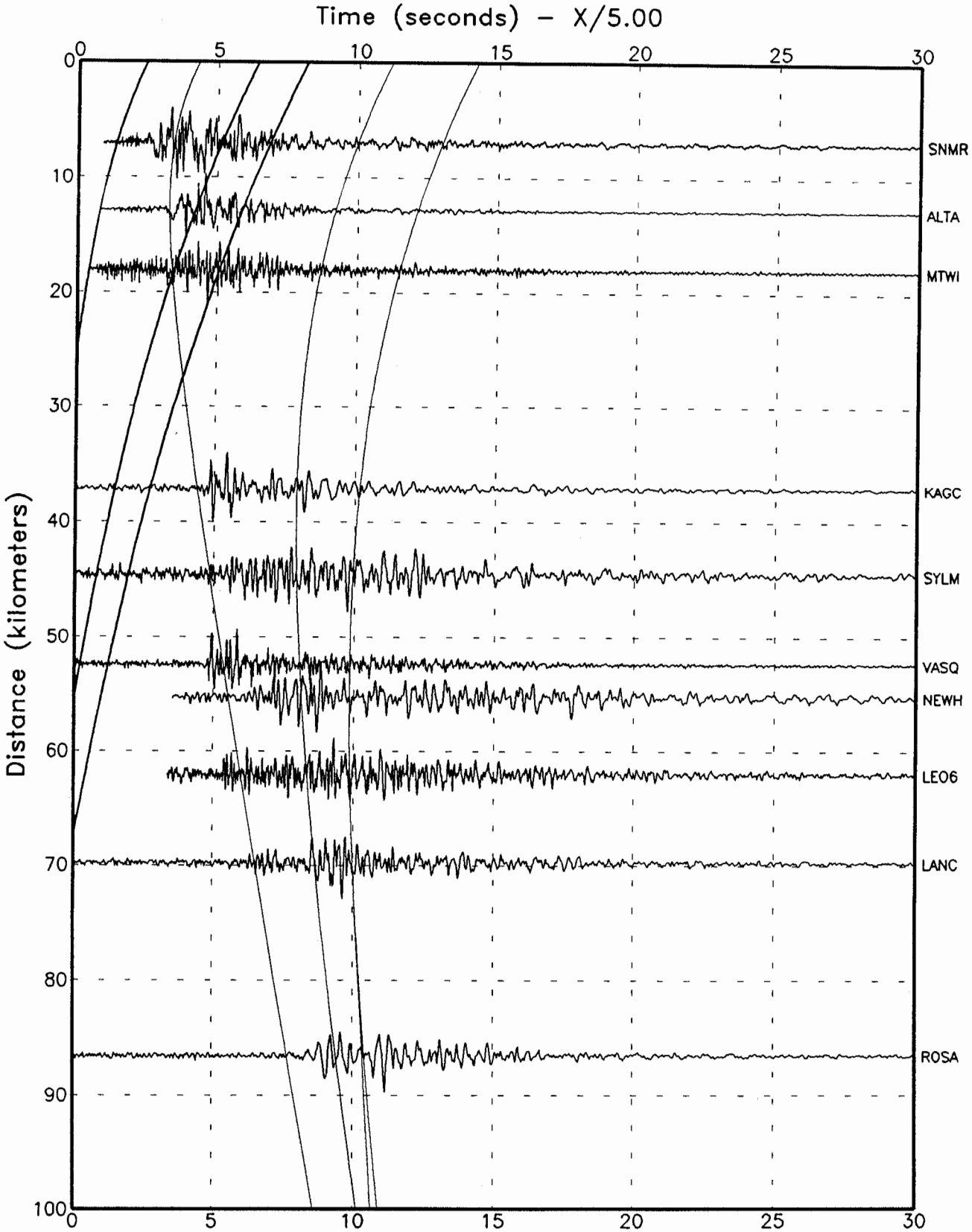

Figure 39. Radial component accelerograms for the 1987 Whittier Narrows earthquake along a profile extending north from the epicenter. All of the stations have known trigger times. Travel times for the direct, Conrad reflected, mafic reflected and Moho reflected P and S waves calculated from the Magistrale (1990) crustal model are also shown.

reflected waves have large amplitudes, and cause the peak acceleration to show almost no attenuation in the distance range of 50 to 90 km, as shown in Figures 40 and 41.

Using teleseismic waveforms, Bent and Helmberger (1989) modeled the Whittier Narrows event as a double source, where the second source is lagged 1 second after the first and has a seismic moment 5 times larger than that of the first source. Figure 42 shows tangential velocity synthetic seismograms incorporating this source model. At Lancaster and Rosamond (70 and 90 km), the large later arrivals in the recorded data are matched in the synthetic seismograms by critically reflected waves from the mafic and Moho layers.

Synthetic velocity profiles for tangential strike-slip and dip-slip mechanisms respectively, calculated using a reflectivity method (to 10 Hz) and a velocity model for the Los Angeles region are compared in Figure 43. The critically reflected phases have significantly larger relative amplitudes for the dip-slip mechanism. Thus in addition to the dependence of the amplitudes of critical reflections on source depth, crustal thickness and velocity profile, the focal mechanism may also contribute to the strength of critically reflected arrivals. Earthquakes with significant dip-slip components are expected to generate large critically reflected Moho phases in the distance range of 70 to 100 km. Listed in Table 7 are the site conditions of the recordings analyzed.

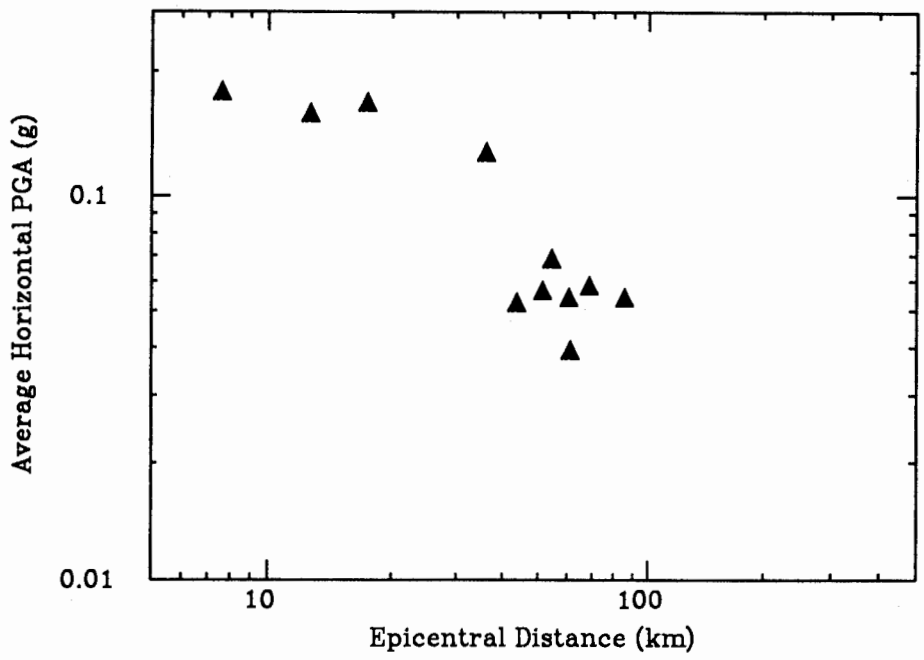

Figure 40. Peak tangential acceleration plotted as a function of distance from the Whittier Narrows event.

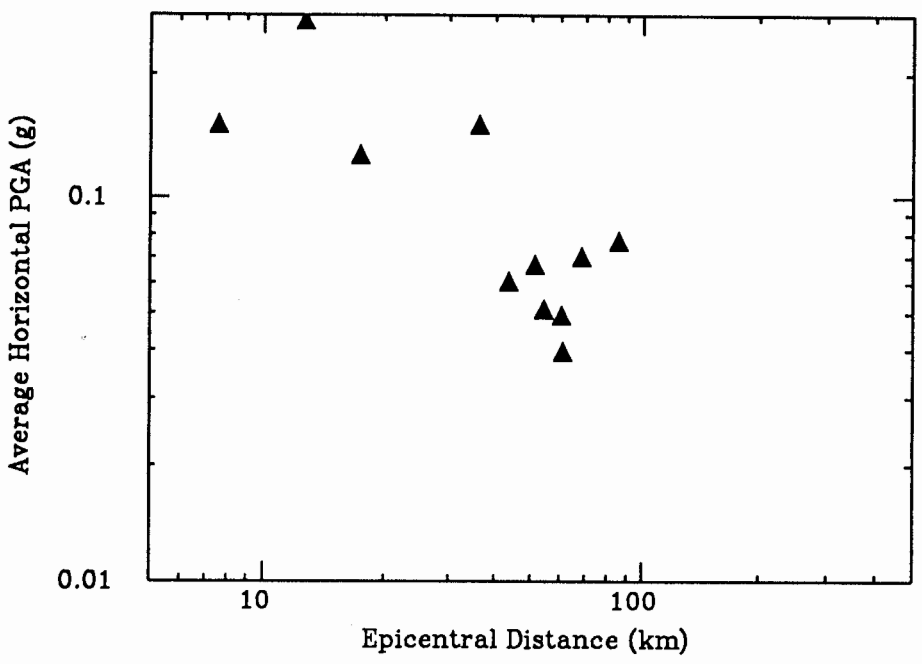

Figure 41. Peak radial acceleration plotted as a function of distance from the Whittier Narrows event.

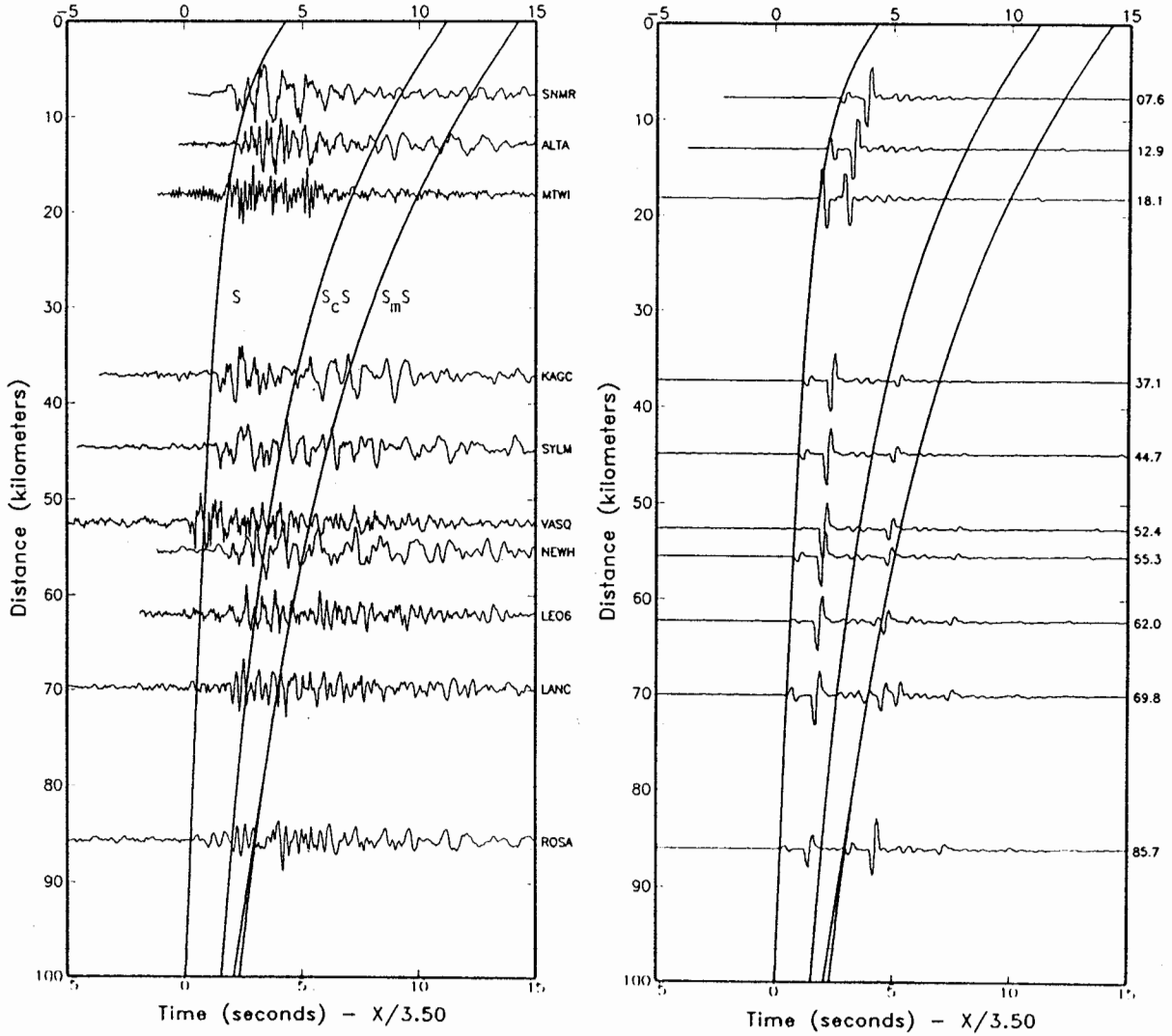

Figure 42. Recorded (left) and synthetic (right) tangential velocity seismograms of the 1987 Whittier Narrows earthquake along a profile extending north from the epicenter. The synthetic seismograms were computed using a reflectivity method (to 10 Hz) and the Los Angeles Basin velocity model of Magistrale (1990). A triangular source time function with a duration of 0.36 seconds was used.

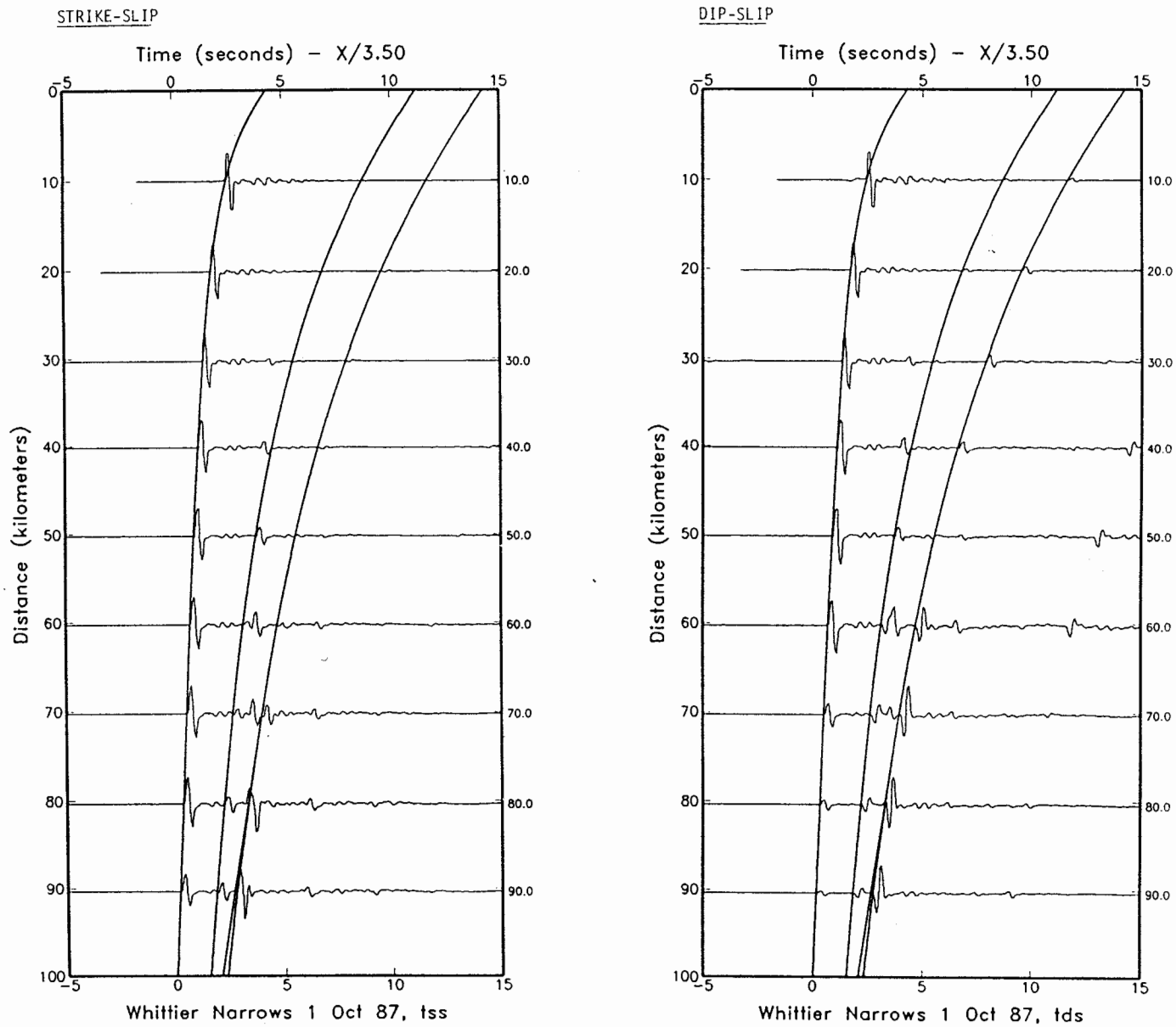

Figure 43. Synthetic tangential velocity seismograms for strike-slip (left) and dip-slip (right) fault models, using the depth and crustal model of Figure 42.

Table 7. Locations, epicentral distances, and site characteristics for the stations used for the study of the October 1, 1987 Whittier Earthquake. The epicentral location used for determination of distances is 34.062N and 118.078W.

Station Identification	Latitude (North)	Longitude (West)	Epicentral Distance (km)	Site Geology
ALTA (24402) Altadena, Eaton Canyon Park	34.177	118.096	13	Alluvium
KAGC (24088) Pacoima, Kagel Canyon	34.288	118.375	38	Sandstone
LANC (24526) Lancaster, Medical Office Bldg, FF	34.688	118.156	70	Alluvium
LEO5 (24055) Leona Valley #5, Ritter Ranch	34.600	118.241	62	Alluvium
LEO6 (24309) Leona Valley #6	34.604	118.244	62	
MTWI (24399) Mt. Wilson, CalTech Seismic Station	34.224	118.057	19	Quartz diorite
NEWH (24279) Newhall, LA County Fire Station	34.390	118.530	56	Alluvium
ROSA (24274) Rosamond, Godde Ranch	34.827	118.265	87	Alluvium
SNMR (24401) San Marino, Southwestern Academy	34.115	118.120	8	Alluvium
SYLM (24514) Sylmar, Olive View Medical Center, FF	34.326	118.444	45	
VASQ (24047) Vasquez Rocks Park	34.490	118.320	50	Shallow alluvium over sandstone

1989 Loma Prieta

The influence of critical reflections on the attenuation of strong ground motion from the Loma Prieta earthquake was analysed by Somerville and Smith (1991). A map of recording stations is shown in Figure 44. A record section of accelerograms of the Loma Prieta earthquake (Figure 45, left side) was compiled using all accelerograms to the north of the epicenter (i.e. in the San Francsico Bay region) that have known trigger time. The recordings are from a variety of site conditions, as annotated in the Figure and discussed further below. Arrival time curves for three principal waves are shown in Figure 45: the direct shear wave (S), the shear wave reflected from the Conrad layer at a depth of 19 km

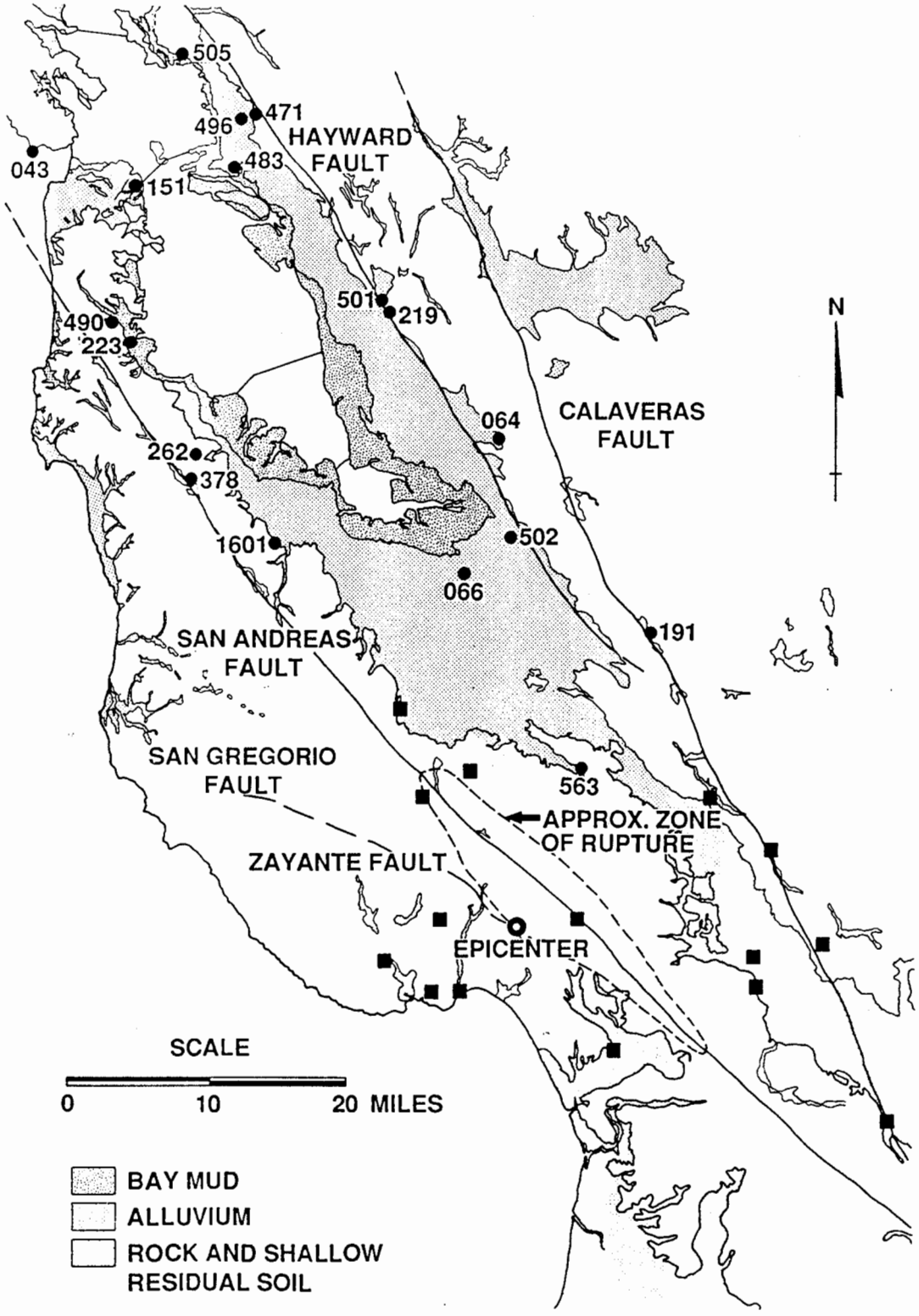

Figure 44. Map showing the location of the 1989 Loma Prieta event and the locations of recording stations analyzed in Figures 45 and 46.

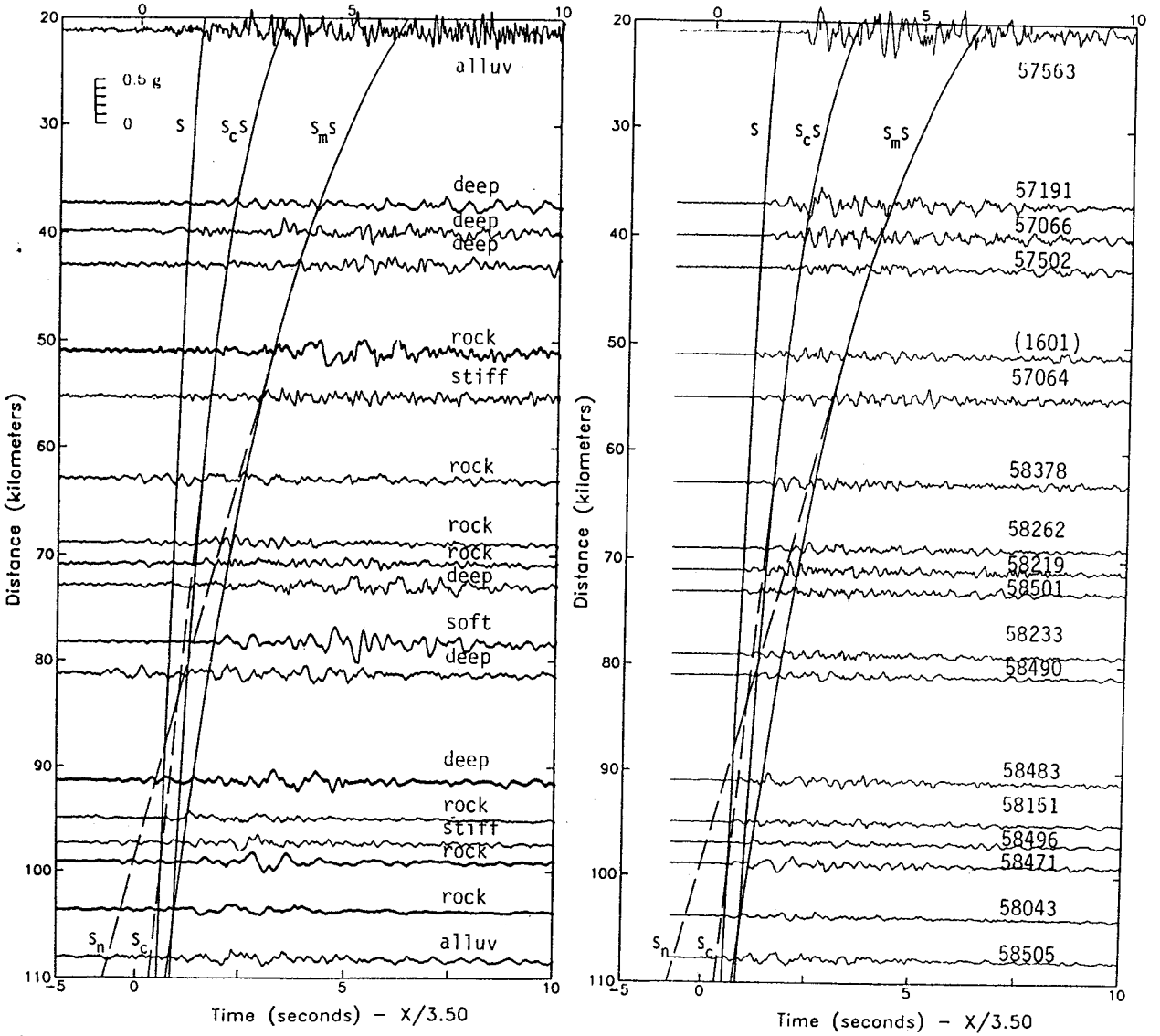

Figure 45. Profiles of recorded (left) and simulated (right) accelerograms of the 1989 Loma Prieta earthquake, compiled using epicentral distance and a travel time reduction of 3.5 km/sec. All of the stations have known trigger times. Soil conditions are annotated on recorded accelerograms, and CSMIP (and USGS in parentheses) station numbers are annotated on simulated accelerograms.

(S_cS), and the shear wave reflected from the Moho at a depth of 25 km (S_mS). The smaller, lower frequency refracted arrivals S_c and S_n are shown by dashed lines. The curves were computed using the crustal structure model of Dietz and Ellsworth (1990), using a focal depth of 12 km to represent the center of energy release (Nabelek, 1990; Kanamori and Satake, 1990; Wald *et al.*, 1991). To facilitate the interpretation of the strong motion data using these point source travel time curves, the accelerograms are plotted in the profile at their epicentral distances rather than at their closest distance to the fault.

The onset of the largest accelerations at each station coincides with the arrival time of the critical Moho reflection S_mS at distances beyond about 50 km. The moveout of this onset with distance follows the S_mS arrival time curve and not that of direct S, as shown in Figure 46. The duration of strong motion following the S_mS arrival time curve is about 5 seconds, which is compatible with the 6-second duration of the source observed teleseismically (Nabelek, 1990; Kanamori and Satake, 1990). We see a similar pattern in a profile of simulated accelerograms on the right side of Figure 45. The simulated accelerograms have large S_mS waves whose onset coincides with the S_mS arrival time curve and whose moveout is that of the S_mS arrival and not that of direct S. The duration of strong motion of the simulated S_mS waves is about 5 sec. In all of these respects, the simulated accelerograms resemble the recorded accelerograms, and support the interpretation of the recorded accelerograms given above. The simulated accelerograms were generated using a crustal structure model having a surface shear wave velocity of 1 km/sec, appropriate for soft rock or stiff soil conditions.

The peak accelerations of the simulated accelerograms show a trend similar to that of the recorded accelerograms, as shown in Figure 47. In this figure, the northerly profile of stations of Figure 44 has been augmented by stations that lie within 30 km of the epicenter. The peak accelerations attenuate normally to about 40 km, but then do not attenuate further until reaching an epicentral distance of 80 km. In the distance range of 60 to 100 km, the largest simulated motions at a given station are due to critical reflections, and we infer this to be also true of the recorded motions based on the similarity in arrival times

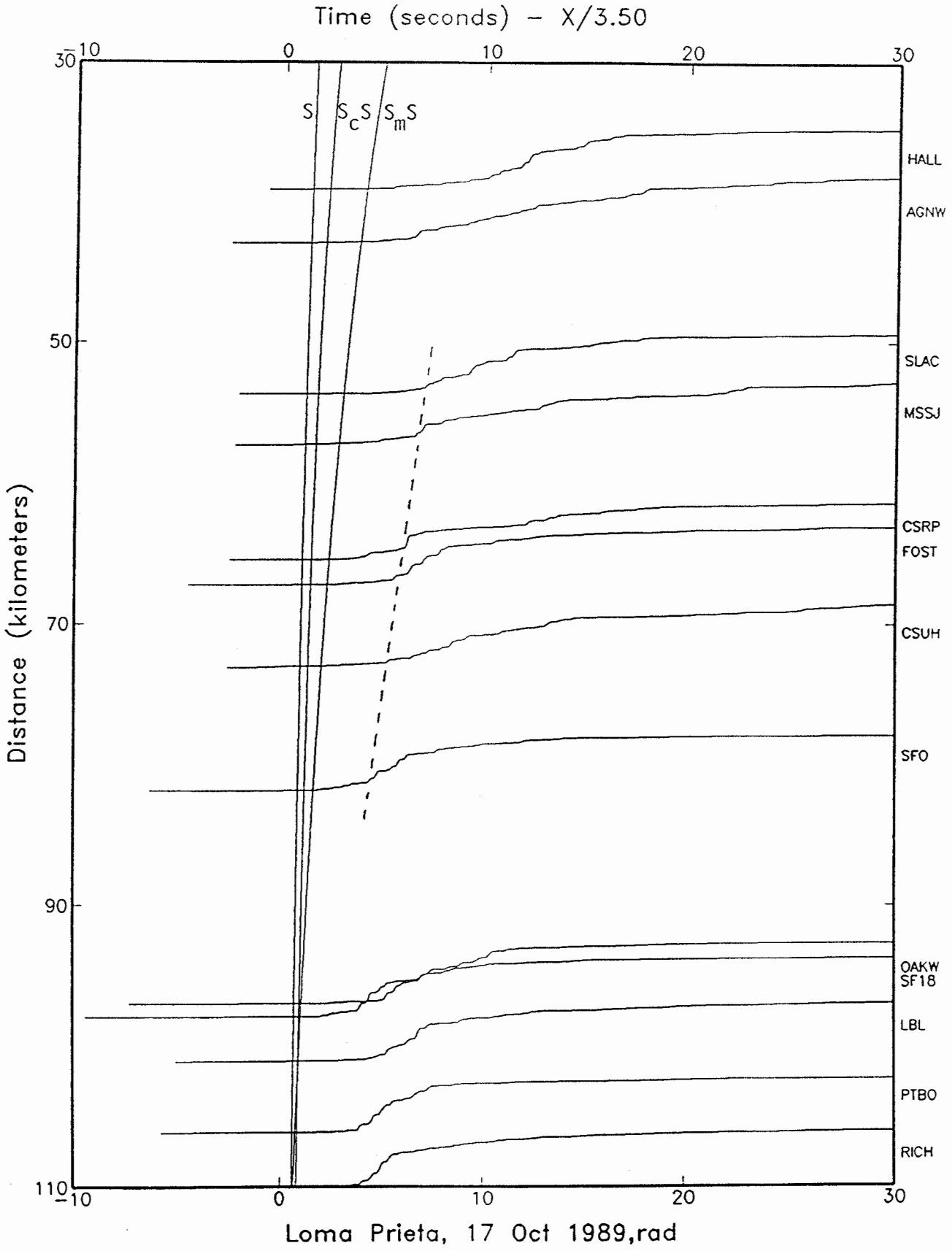

Figure 46. Integrated squared radial acceleration from the Loma Prieta earthquake along the northwest profile shown in Figure 43. A strong arrival whose phase velocity is at least as fast as S_mS is seen at distances beyond 50 km.

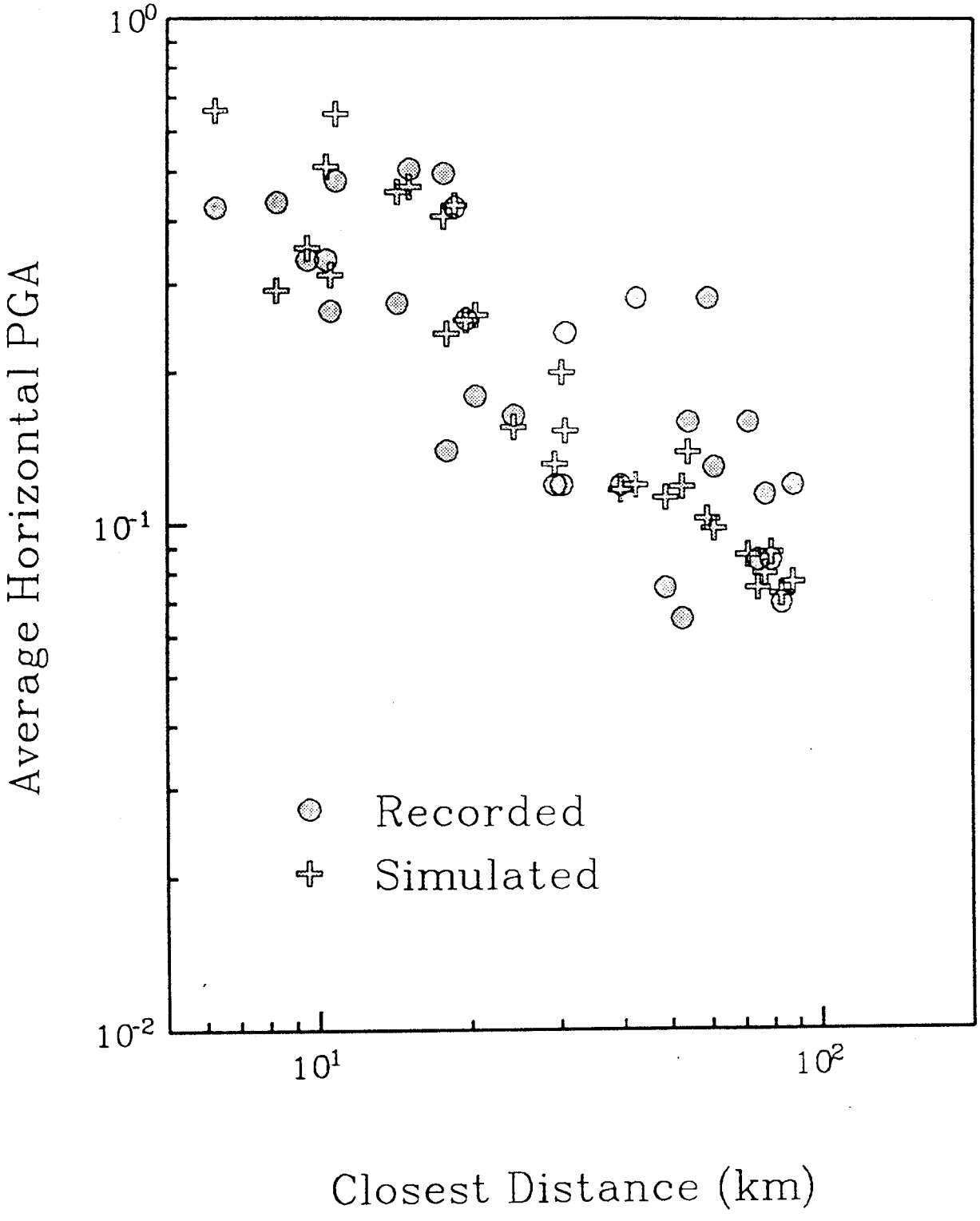

Figure 47. Comparison of recorded (solid triangles) and simulated (open circles) peak horizontal acceleration of the 1989 Loma Prieta earthquake as a function of closest distance for sites within 30 km and for Bay Area sites having known trigger times.

and phase velocity described above. While site conditions are presumably responsible for the larger amount of scatter in recorded peak accelerations (compared with the simulated ones) at a given distance, it does not appear that site conditions explain the overall lack of attenuation between 40 and 80 km in both the recorded and simulated values. Listed in Table 8 are the site conditions of the recordings analyzed.

The relatively long source duration of the Loma Prieta earthquake makes the unambiguous identification of specific seismic phases such as S_mS difficult, notwithstanding the evidence based on travel time and phase velocity described above. To obtain better resolution of seismic phases, we have examined recordings of aftershocks of the Loma Prieta earthquake. In Figure 48 we show a profile of the east component of acceleration recorded at stations northwest of the 1:30 am aftershock of November 5, 1989. The data are described by Mueller and Glassmoyer (1990); all of the recordings have absolute times, allowing them to be aligned in time with a travel time reduction of 3.5 km/sec. Superimposed on the profile are travel times for the direct S, Conrad critical reflection (S_cS), and Moho critical reflection (S_mS). Except at the closest station, the direct arrival has a small amplitude relative to later arrivals, and the first conspicuous phase has the arrival time of the critical Conrad reflection S_cS. The largest phase at all stations except the closest station occurs soon after the expected arrival time of the critical Moho reflection S_mS. These aftershock recordings clearly indicate that at distances beyond about 50 km, the recorded peak ground motion amplitudes are controlled, not by the direct S wave, but by the wave that is critically reflected from the Moho.

Further confirmation of this conclusion is provided by the results of a series of explosions that were detonated in the Loma Prieta region and near the north end of the Golden Gate Bridge in Marin County during the summer of 1991. Preliminary examination of the data show large wide-angle reflections in the Northern San Francisco Bay region (in the distance range of 90 to 110 km) from the Loma Prieta shots, and in the Loma Prieta area from the Marin County shots

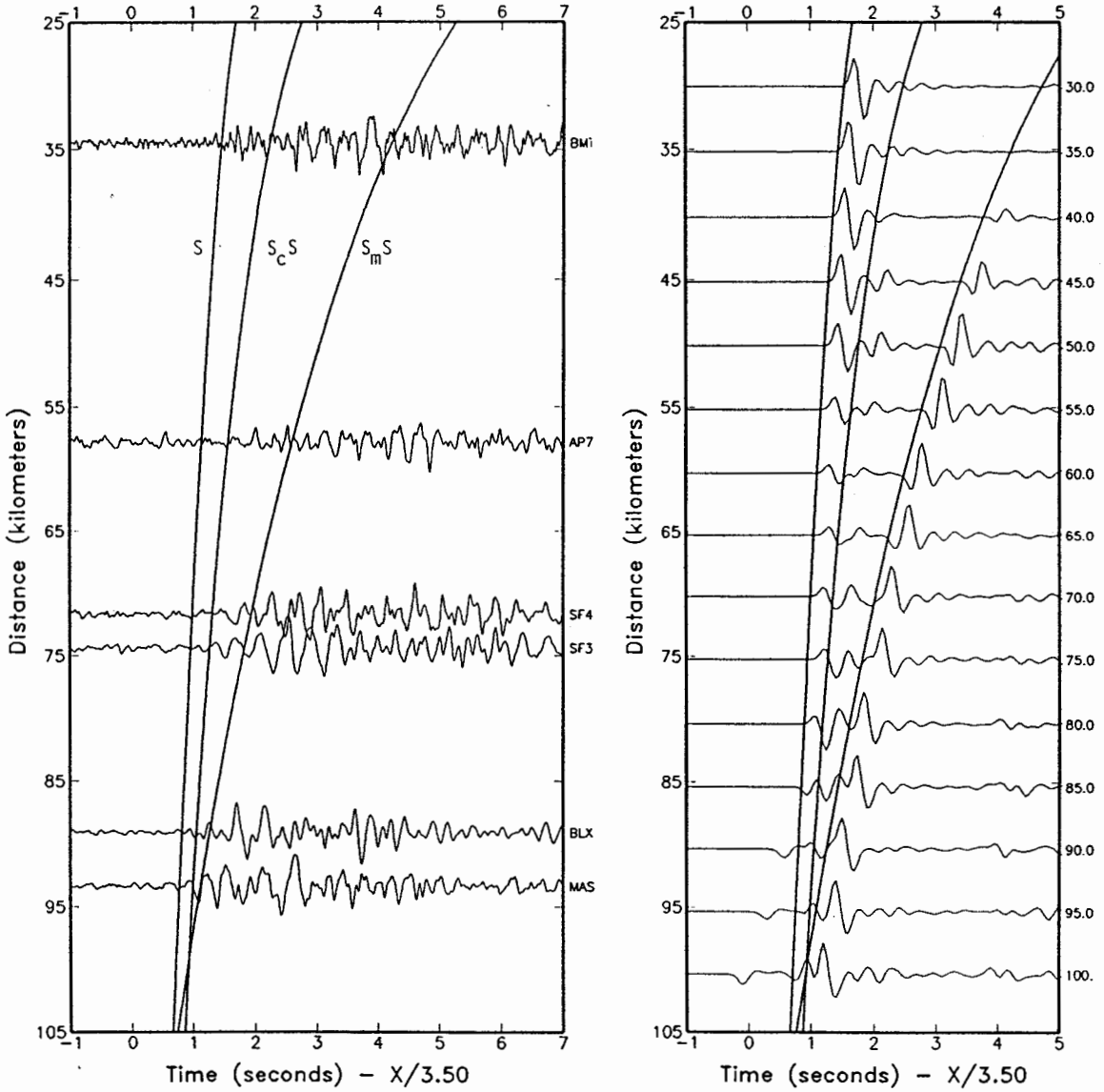

Figure 48. Profile of recorded accelerograms of the 1:30 am, November 5 aftershock of the 1989 Loma Prieta earthquake, compiled using epicentral distance and a travel time reduction of 3.5 km/sec. Travel time curves are explained in the text. USGS station abbreviations are annotated on right side of traces.

(Rufus Catchings, personal communication, 1991). The critical distance for surface explosions is larger than for a deep earthquake source, consistent with the large amplitudes being observed closer to the Loma Prieta earthquake.

To generate the synthetic accelerograms shown in Figure 45, we used a simulation method developed by Hadley, Helmberger and Orcutt (1982) and refined by Wald *et al.* (1988). For crustal earthquakes, the ground motions of the large event are obtained by summing contributions from fault elements having dimensions of about 3 km. Strong ground motion recordings very close to the source of a magnitude 5 earthquake, scaled back to the source, are used to represent the source functions of the fault elements. Green's functions including the direct S wave and primary reflections from interfaces, calculated from the regional structure model, are used to represent the propagation path. The contributions from each fault element are lagged, scaled and summed in such a way as to simulate the propagation of rupture over the fault surface. Asperities are modeled by weighting the contributions of the fault elements. The decrease in coherence of the radiation pattern that is observed to occur as frequencies increase is represented empirically using a suite of empirical source functions. The reliability of this simulation procedure was demonstrated using recorded strong ground motions of the 1979 Imperial Valley, 1985 Nahanni, and 1987 Whittier Narrows earthquakes (Abrahamson *et al.*, 1990), and has been further demonstrated using the near-source recordings of the Loma Prieta earthquake.

We used a rupture model of the Loma Prieta earthquake derived by Wald *et al.* (1991) from the inversion of near-source strong motion data. The rupture surface is 40 km long and 15 km wide, and rupture spreads circularly from the 18 km-deep hypocenter at an average speed of 2.7 km/sec that is independant of depth. Slip occurs in thee time windows each having 0.7 sec duration and 0.1 sec overlap. The seismic moment is 2.9×10^{26} dyne-cm, and the strike and dip of 128 and 70 degrees respectively of Kanamori and Satake (1990) were used. The rake varies on the fault plane. A near-source, range-independent component of anelastic absorption was represented empirically by that contained in the empirical source functions.

Table 8. Locations, epicentral distances, and site characteristics for the stations used for the study of the October 17, 1989 Loma Prieta Earthquake. The epicentral location used for determination of distances is 37.037N and 121.883W.

Station Identification	Latitude (North)	Longitude (West)	Epicentral Distance (km)	Site Geology
AGNW (57066) Agnews State Hospital	37.397	121.952	40	Alluvium
BHOS (58496) Berkeley, 2 story hospital	37.855	122.256	97	Alluvium
CSUH (58219) CSUH Stadium Grounds	37.657	122.061	71	Franciscan green stone
HALL 57191) Halls Velley, Graut Park	37.338	121.714	37	Alluvium
HBRT (58501) Hayward, Bart Elevated Station	37.671	122.087	73	Alluvium
LBL (58471) Lawrence Berkeley Lab	37.876	122.249	99	Thin alluvium on shale, siltstone
LCSD (58233) Lower Crystal Springs Dam	37.529	122.361	69	Franciscan grey-wacke
MILP (57502) Milpitas, 2 story Bldg	37.430	121.897	43	Alluvium
MSSJ (57064) Fremont, Mission San Jose	37.530	121.919	55	Alluvium
O24B (58483) Oakland 24 Story Bldg	37.798	122.257	91	Alluvium
PULG (58378) Upper Crystal Springs Reservoir, Pulgas Temple	37.490	122.310	63	Sandstone
PTBA (58043) Point Bonita	37.820	122.520	104	Broken rock & soil (2m), sandstone
RICH (58505) Richmond, City Hall Parking Lot	37.935	122.342	108	Alluvium
SB6 (58490) San Bruno, 6 Story Bldg	37.628	122.424	81	Alluvium
SFO (58223) San Francisco Airport	37.622	122.398	79	Deep alluvium
SFRH (58151) San Francisco, Rincon Hill	37.790	122.390	95	Franciscan sand-stone, shale
SLAC (1601) Stanford Univ. Linear Accelerator	37.419	122.205	51	Alluvium
STH (57563) San Jose, Santa Teresa Hills	37.210	121.803	21	Alluvium over Ser-pentine

Effects of Lateral Variation in Seismic Velocity Structure

Simple layered crustal models were used to generate the synthetic seismograms described above. These synthetic seismograms (and the attenuation relations derived from them) prominently show the effects of critical reflections from the lower crust, and these effects are also apparent in the recorded strong motion data. However, as we saw in the case of the San Fernando earthquake, the attenuation of ground motion seems to be different along different azimuths, suggesting lateral variations in seismic velocity. The simple synthetic seismograms described above lack the effects of laterally varying structure, and we wish to determine whether the presence of lateral heterogeneities like those shown in Figure 49 may reduce the influence of reflected phases and introduce other, more pronounced effects (Helmberger *et al.*, 1992).

In Figure 50 we compare profiles of synthetic seismograms generated for laterally homogeneous and laterally heterogeneous crustal models. The latter model (Figure 49) has random variations of 20% in seismic velocities in the upper crust using the model of Frankel and Clayton (1984), and is intended to represent a more realistic crustal model than the laterally homogeneous one. The source is at a depth of 10 km. The effect of the laterally heterogeneous upper crust is to prolong the duration of the high frequency energy, but it does not significantly affect the amplitudes or timing of the critically reflected phases, which contribute the two strongest phases (S_mS and sS_mS) at the beginning of the shear wave arrival. In the comparison of attenuation relations for these two profiles (Figure 51), we see that the influence of the critically reflected phases is not significantly affected by the presence of the laterally heterogeneous structure in the upper crust; in both cases, a bump at about 120 km due to critical reflections is present. If the entire crust is made strongly laterally heterogeneous, then the coherence of this bump is destroyed but the elevation of ground motion amplitudes by critical reflections is still evident. The shoulder in the attenuation relation at 60 km is due to the phase sS, and would occur at a closer distance for a source shallower than the 10 km depth used here.

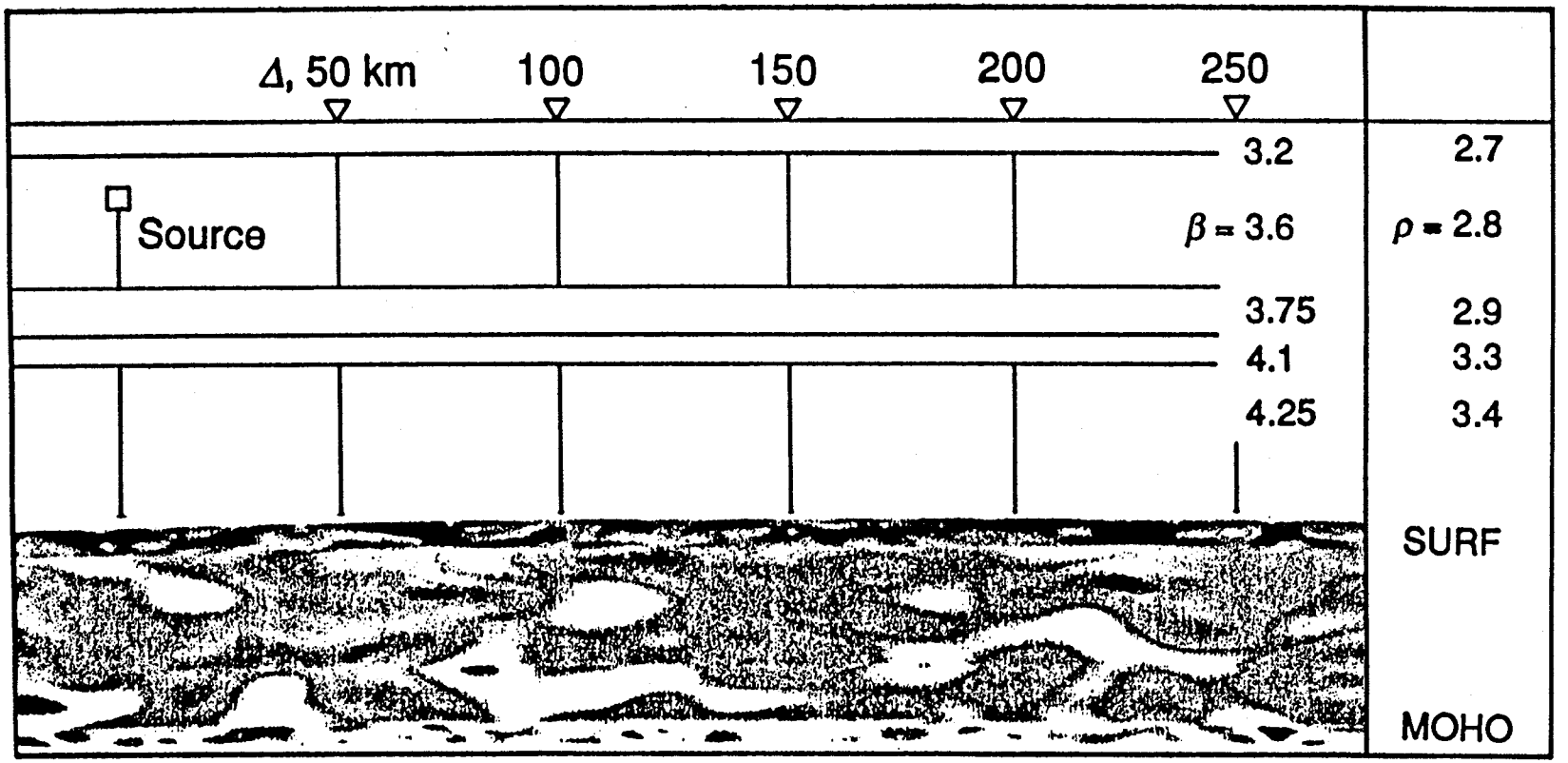

Figure 49. Model of heterogeneous velocity in a layered crustal model. Source: Helmberger *et al.*, 1992.

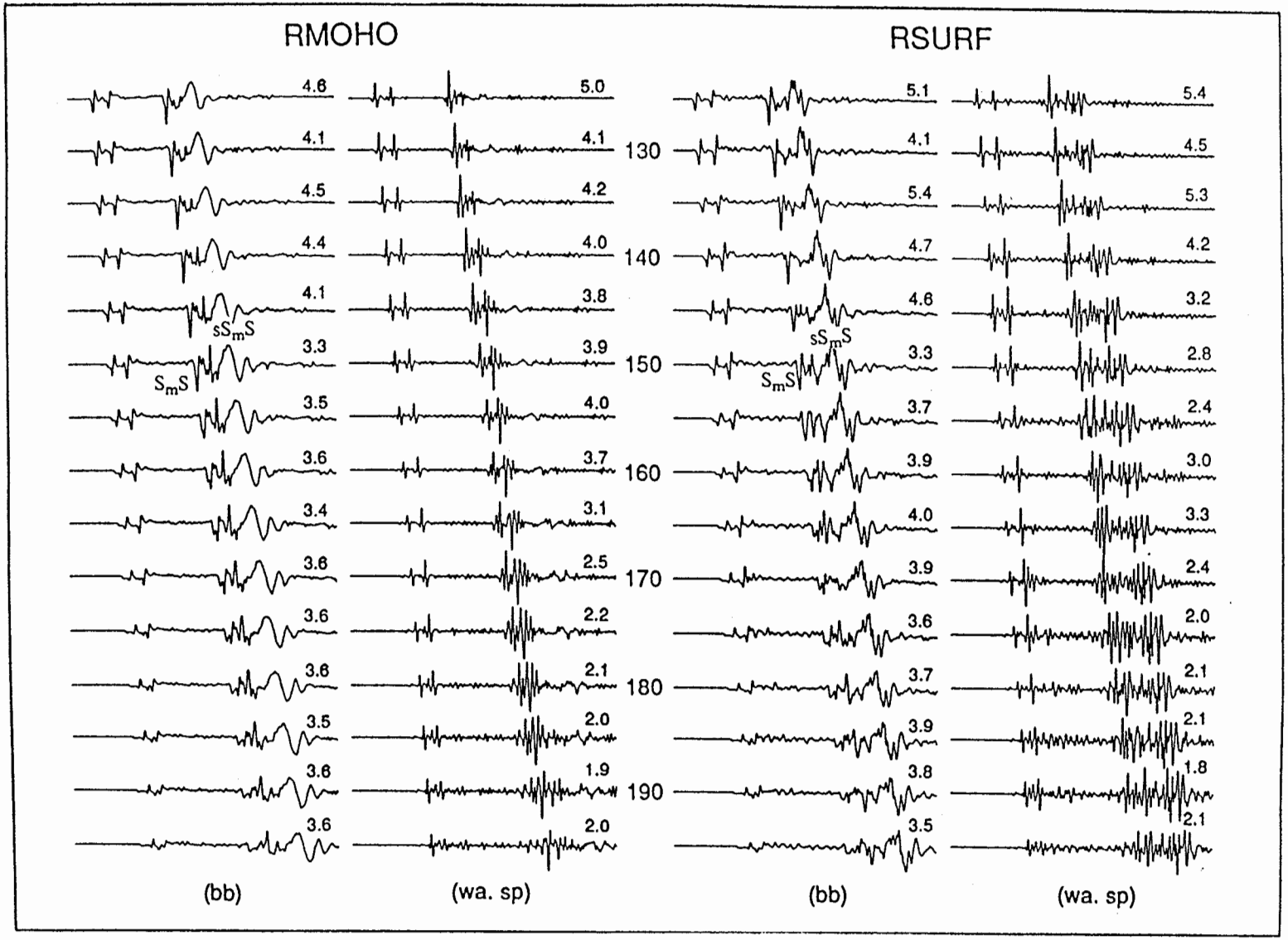

Figure 50. Comparison of synthetic seismograms for the case when only the velocity below the Moho is heterogeneous (RMOHO) with the case when the surface layer is heterogeneous (RSURF). The synthetic seismograms are for both broadband and Wood-Anderson instruments. Strong Moho reflections (S_mS and sS_mS) are apparent in both sets of seismograms. Source: Helmberger *et al.*, 1992.

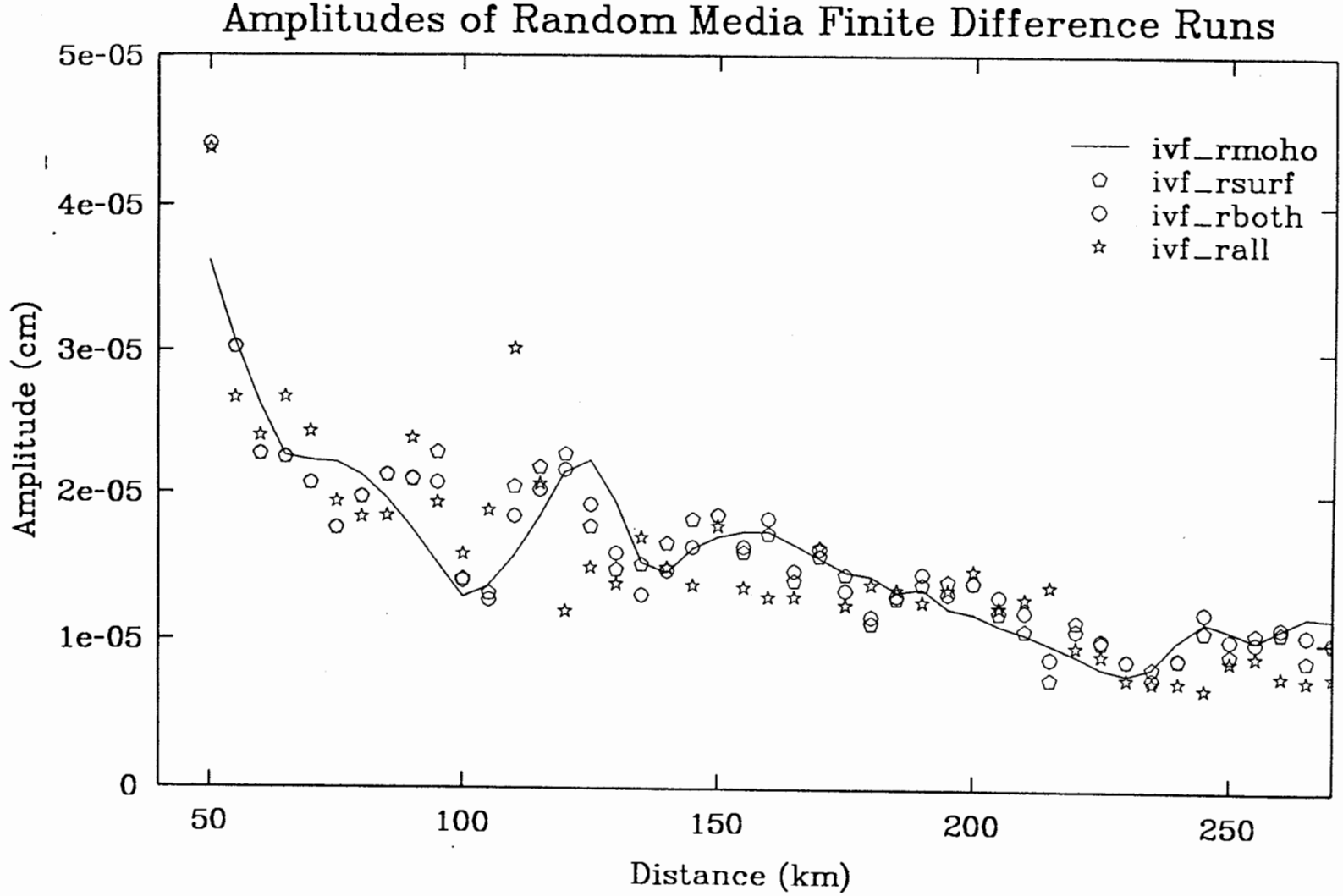

Figure 51. Comparison of attenuation curves for the case when only the velocity below the Moho is heterogeneous (RMOHO) with the case when the surface layer is heterogeneous (RSURF). Both have a bump at about 120 km due to Moho reflections. Attenuation for the cases when both the surface layer and the mantle are heterogeneous (RBOTH), and when the whole medium is heterogeneous (RALL), are also shown. Source: Helmberger *et al.*, 1992.

DISCUSSION

The results of our analysis of seven large California earthquakes are summarized in Table 1. Evidence for the presence of critical reflections consists of large phases that arrive near the time predicted for critical reflections from lower crustal layers such as the Conrad and Moho. The only event among the seven studied for which this kind of evidence is not present is the 1952 Kern County earthquake, for which we have only four recordings that lack absolute times, and whose estimated source process time of 14 seconds makes the resolution of phases difficult. For the Loma Prieta mainshock, whose estimated source process time is six seconds, the identification of reflected phases is ambiguous, but it is unambiguous for aftershock recordings on GEOS instruments. The North Palm Springs earthquake did not trigger strong motion instruments beyond 100 km, but reflected phases are evident on Wood-Anderson recordings at Pasadena at a distance of 145 km. We conclude that critical reflections are generally present in strong motions recorded beyond the critical distance in large California earthquakes.

We next wish to assess the influence of these critical reflections on the attenuation of strong ground motion. We expect that the effect of these reflections to be a flattening in the slope of the attenuation curve beginning at the critical distance and extending over the distance range for which the reflections have large amplitudes. The amount of flattening and the distance range over which it occurs should depend of the earthquake source depth and the thickness and structure of the crust. The critical distance decreases with increasing source depth and decreasing crustal thickness. For average source depths (about 8 km), crustal thickness (30 km) and shear wave velocity profiles (3.5 km/sec at the source and 4.5 km/sec below the Moho) in California, the critical distance is about 65 km. Variations in source depth, crustal thickness and crustal structure from event to event would produce variations in the critical distance.

As seen in Table 1, we see evidence of flattening in the attenuation relations for five of the seven events analyzed. The flattening is most clearly seen for events in which the recorded data provide a good sampling of distances out to

100 km or more: these include the San Fernando, Whittier Narrows and Loma Prieta earthquakes. For the Coalinga earthquake, the sampled distance range (53-69 km) is too narrow to define the shape of the attenuation curve. For the North Palm Springs earthquake, the distance range of triggered strong motion instruments (30-75 km) may not extend far enough to include critical reflections. The number of recordings of the Kern County and Borrego Mountain earthquakes is not large enough to clearly define the attenuation pattern. We conclude that the recorded data support the expectation that, for a given earthquake, critical reflections may cause a flattening in the attenuation relation.

The averaging of a large amount of strong motion data in the derivation of attenuation relations using regression techniques should yield attenuation relations that contain an averaged effect of critical reflections. However, most attenuation relations have a smoothly decreasing shape, and do not contain an inflection of the kind that would be needed to describe the effects of critical reflections. Thus if we examine the residuals of a specific earthquake from an average attenuation relation, or even from an attenuation relation derived from the specific event itself, we might expect to see this inflection.

In Figure 52, we show evidence of these inflections in the shape of attenuation relations. Residuals of peak ground accelerations at deep soil sites (top panel) and rock sites (middle panel) with respect to the attenuation relation derived from the deep soil recordings of the 1987 Whittier Narrows earthquake are shown. For both data sets, the residuals are predominantly negative in the distance range of 30 to 60 km, become zero on average at about 70 km, and are positive between 80 and 110 km. This indicates that the functional form used to model the attenuation of the Whittier Narrows data does not fit the data. The derived attenuation relation overpredicts the data by about one to two standard deviations in the distance range of 30 to 60 km, and underpredicts the data by a similar amount in the distance range of 80 to 110 km. This is consistent with the expected effect of critical reflections on the attenuation of strong ground motion.

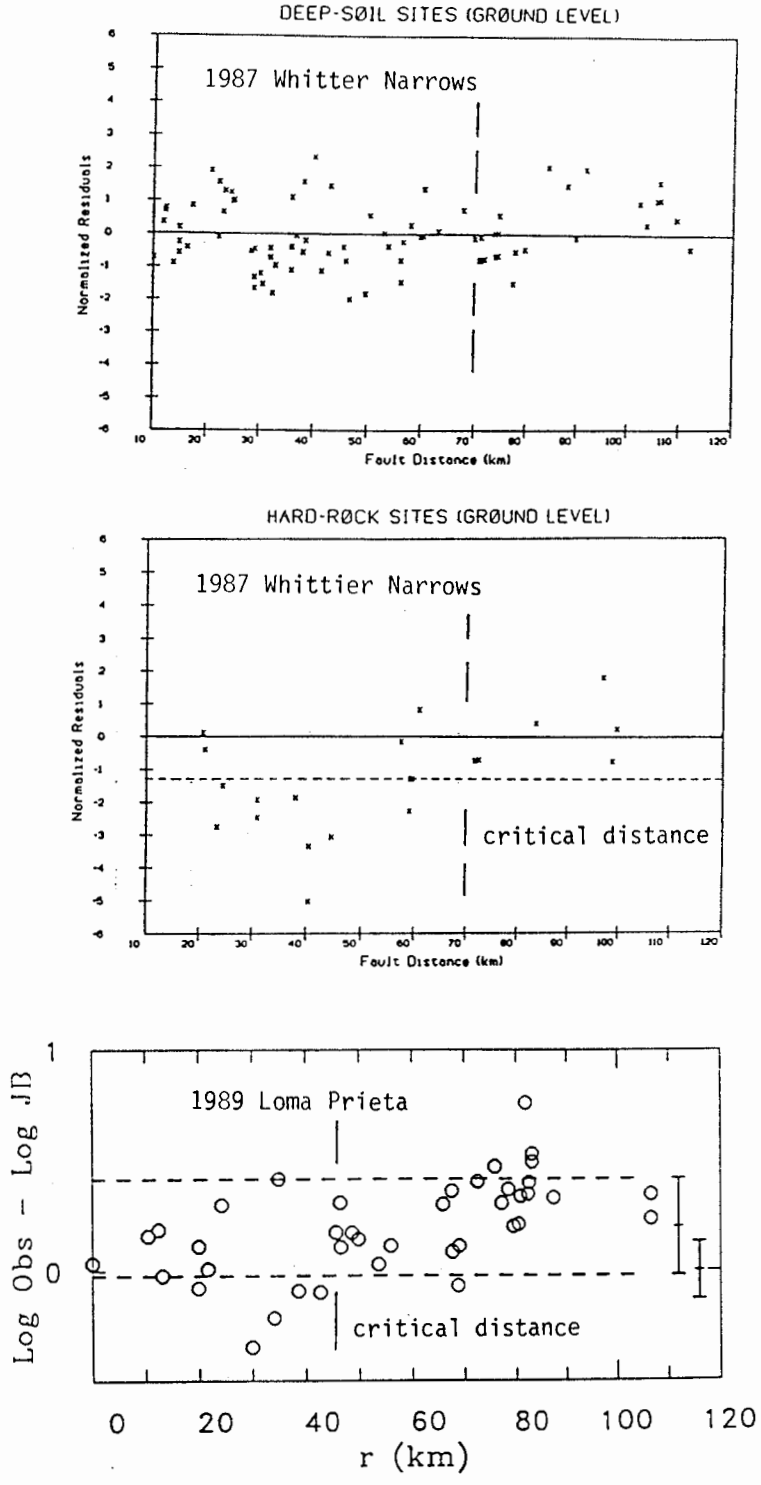

Figure 52. Top and Center: Residuals of recorded peak acceleration from the regression relations derived from deep soil and hard rock recordings of the 1987 Whittier Narrows earthquake, after Campbell (1988). Bottom: Residuals of peak acceleration from the regression relation of Joyner and Boore (1988) for rock site recordings of the 1989 Loma Prieta earthquake, after Boore *et al.* (1989).

A similar pattern of residuals was obtained for rock site recordings of the 1989 Loma Prieta earthquake (Boore *et al.*, 1989), as shown in the lower panel of Figure 52. Here, the crossover from negative to positive residuals occurs at a closer distance (about 45 km compared with 70 km). This is what we would expect from the shallower depth of the Moho beneath the Loma Prieta earthquake (25 km) compared with the Whittier Narrows earthquake (32 km), and the deeper depth of the Loma Prieta earthquake. In both cases, the crossover distance corresponds to the critical distance for the Moho reflection.

In his analysis of the attenuation of the 1989 Loma Prieta earthquake, Campbell (1991) allowed the attenuation curve to have inflections in slope. The attenuation relation that he derived from the 71 strong motion recordings on alluvial sites is shown in Figure 53. There is no attenuation in the distance range of 50 to 80 km. Campbell examined the azimuthal distribution of residuals of the Loma Prieta data, and found evidence for directivity effects producing an enhancement of ground motions to the northwest of the source region of about 20% above the average observed ground motion. This effect does not explain the flattening of the attenuation relation shown in Figure 53. Using the simulation procedure described above, we have modeled directivity effects, and find that we are able to explain the observed directivity in addition to the flattening of the attenuation relation.

Finally, we wish to address the potential influence of surface waves on strong ground motions within two hundred km of the source. To see these surface waves clearly, we need to look at very broadband recordings such as those on a Streckeisen seismograph. In Figure 36, we analyze data from an earthquake of M_L= 4.8 on December 16, 1988 near North Palm Springs recorded on the very broad band Streckeisen seismograph on rock at Pasadena at a distance of 140 km. The recorded displacement seismograms are compared with synthetic seismograms computed using the reflectivity method. This method generates all body wave and surface wave phases for a flat layered crustal model. The largest high frequency displacements in both the recorded and synthetic seismograms are due to the phase S_mS. The surface waves follow the arrival of the phase S_mS, and have a much

ATTENUATION RELATIONSHIPS
LOMA PRIETA EARTHQUAKE

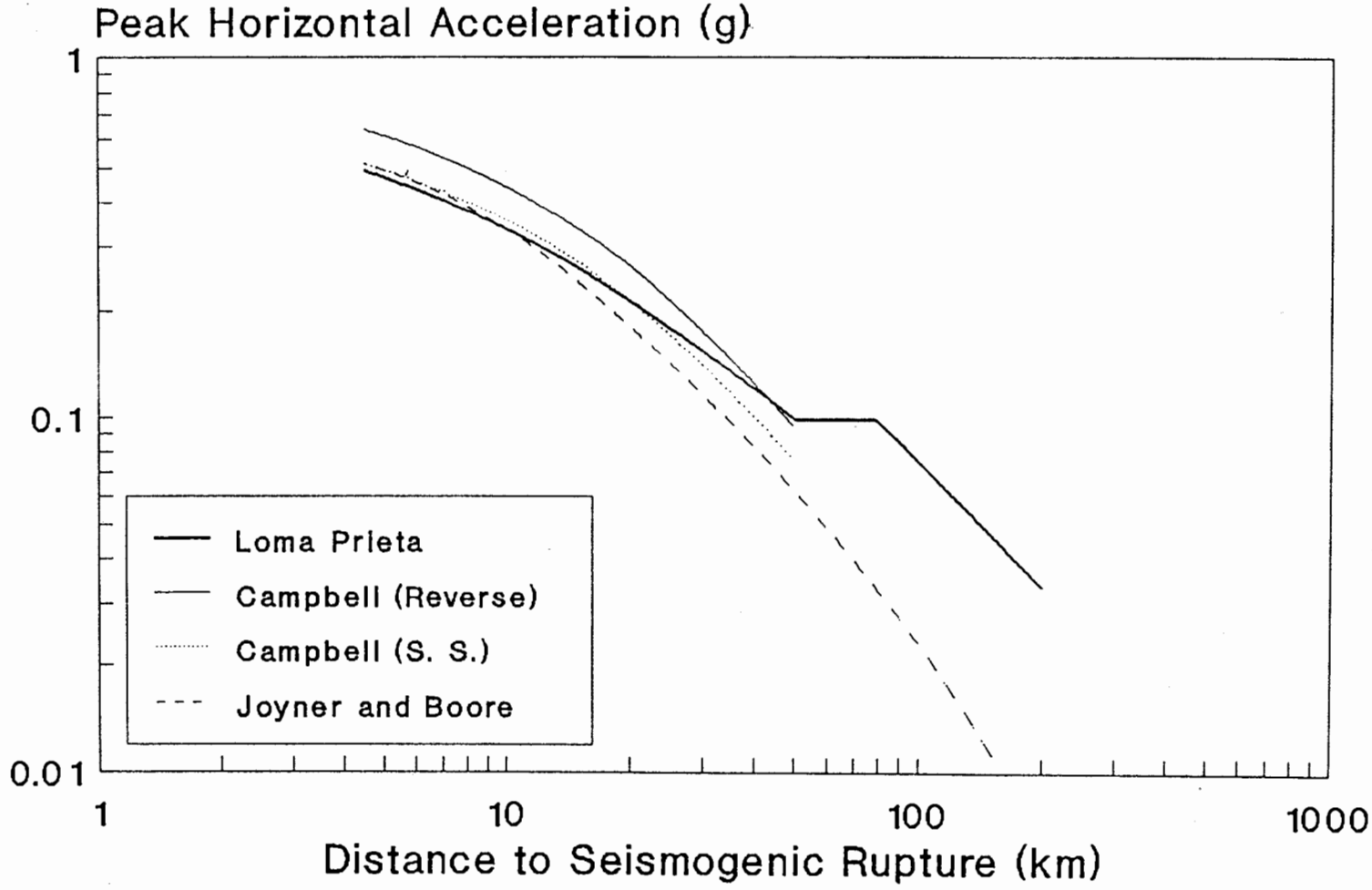

FIGURE 2

Figure 53. Empirical attenuation relation for alluvium site recordings of the Loma Prieta earthquake. Source: Campbell, 1991.

longer period than the S_mS phase. This indicates that, at least for a rock site on a plane-layered crustal structure at this distance, the S_mS phase and the surface waves can be distinguished on the basis of both arrival time and frequency content, and that accelerations due to the S_mS phase will be much larger than those due to surface waves.

When large surface waves having relatively short periods are present in strong motion recordings, it is because they have been locally generated by the interaction of body waves with shallow non-planar geological structure (Vidale and Helmberger, 1987; 1988). In this case, the surface waves will arrive soon after the body waves, and more elaborate analyses (such as analyses of polarization and phase velocity) may be required to separate the body waves from the surface waves. There is the possibility that surface waves generated by the direct body wave could be misidentified as the S_mS phase at a single station. However, by plotting profiles of recordings at a range of distances, as we have done for each event, we see apparent phase velocities that are compatible with that expected for S_mS, and incompatible with the much lower apparent phase velocity that surface waves would have. This suggests that it is unlikely that surface waves locally generated by the direct S wave are being misinterpreted as the S_mS phase. It is possible that part of the phase that we identify as S_mS is due to surface waves generated by the S_mS body wave, but we have not attempted to separate these phases because both are due in a broad sense to the phenomenon of critical reflections from the lower crust.

CONCLUSIONS

We have analyzed profiles of accelerograms from seven large California earthquakes and several aftershocks. For the older events, the strong motion recordings did not have absolute time, and so it was difficult to identify critical reflections in these recordings. Also, for the larger events, the source duration was sufficiently long that it obscured the individual phases that we would like to identify. Nevertheless, we generally found evidence of critical reflections in large, late wave arrivals that may be S_mS, and these arrivals were associated with a flattening of the empirical attenuation curve. The only event among the seven studied for which this kind of evidence is not present is the 1952 Kern County earthquake, for which we have only four recordings that lack absolute times, and whose estimated source process time of 14 seconds makes the resolution of phases difficult.

These results suggest that critical reflections influence the attenuation of strong ground motion throughout California, and are already included to an extent in standard attenuation relations. However, the smoothly decaying functional form of most attenuation relations, while fitting observed strong motion data when averaged over many events, may not accurately describe the attenuation that is observed in a single event. The attenuation relation of the Loma Prieta earthquake, shown in Figure 53, is the most prominent demonstration of this. Since we do not expect crustal earthquakes in California to occur much deeper than 18 km, or the crustal thickness to be much less than 25 km, the Loma Prieta case may approximately represent an upper bound on the departure of the attenuation relation of an individual event from that of the larger strong motion data set in California.

A contour map of crustal thickness in California is shown in Figure 5 (Mooney and Weaver, 1990). In the region of the San Andreas fault system extending from north of the Transverse Ranges to north of the San Francisco Bay area, the depth to the Moho is 25 ± 1 km. In the region south of the Transverse Ranges, including almost all of southern California, the crustal thickness is 30 ± 2 km. The

relatively uniform crustal thickness in each of these regions, and the significant contrast in crustal thickness between them, suggests that there could be differences in ground motion attenuation between these two regions. Specifically, for a given focal depth, the effect of critical reflections should occur at closer distances and be larger in northern California than in southern California, as suggested by the residuals for the Loma Prieta and Whittier Narrows earthquakes discussed above. As a rule of thumb, we expect that the distance at which the attenuation curve for a given earthquake begins to flatten can be estimated from the critical distance of the S_mS phase, which can easily be calculated from the crustal structure and the focal depth of the earthquake.

REFERENCES

Abrahamson, N.A., P.G. Somerville, and C. Allin Cornell (1990). Uncertainty in numerical strong motion predictions, *Proc. 4th U.S. National Conference on Earthquake Engineering*, **1**, 407-416.

Bent, A. and Helmberger (1989). Source complexity of the October 1, 1987 Whittier Narrows earthquake, *J. Geophys. Res.*, **94**, 9548-9556.

Boore, D.M., L. Seekins and W. Joyner (1989). Peak accelerations from the 17 October 1989 Loma Prieta earthquake, *Seismological Research Letters* **60**, 151-166.

Burger, R.W., P.G. Somerville, J.S. Barker, R.B. Herrmann, and D.V. Helmberger (1987). The effect of crustal structure on strong ground motion attenuation relations in eastern North America, *Bull. Seism. Soc. Am.* **77**, 420-439.

Campbell, K. (1988). The Whittier Narrows, California earthquake of October 1, 1997 - preliminary analysis of peak horizontal acceleration, *Earthquake Spectra* **4**, 115-137.

Campbell, K. (1991). An empirical analysis of peak horizontal acceleration from the 18 October 1989 Loma Prieta Earthquake, *Bull. Seism. Soc. Am.*, **81**, 1838-1858.

Dietz, L.D. and W. L. Ellsworth, "The October 17, 1989 Loma Prieta, California Earthquake and its Aftershocks: Geometry of the Sequence from High-Resolution Locations," *Geophysical Research Letters* 17 (1990): 1417-1420.

Eaton, J., R. Cockerham, and F. Lester (1983). Study of the May 2, 1983 Coalinga earthquake and its aftershocks, based on the USGS Seismic Network in Northern California; in *The 1983 Coalinga, California earthquakes:* California Division of Mines and Geology Special Publication 66, 261-273.

Frankel, A. and R.W. Clayton (1984). A finite difference simulation of wave propagation in two-dimensional random media, *Bull. Seism. Soc. Am.*, **74**, 2167-2186.

Ho-Liu, P. and D.V. Helmberger (1989). Modeling regional Love waves: Imperial Valley to Pasadena, *Bull. Seism. Soc. Am.* **79**, 1194-1209.

Hadley, D.M., D.V. Helmberger and J.A. Orcutt (1982). Peak acceleration scaling studies, *Bull. Seism. Soc. Am.* **72**, 959-979.

Hartzell, S.H. and T.H. Heaton (1983). Teleseismic mechanism of the May 2 Coalinga, California earthquake from long-period body waves, in in *The 1983 Coalinga, California earthquakes:* California Division of Mines and Geology Special Publication 66, 241-246.

Helmberger, D.V., D. Dreger, R. Stead, and H. Kanamori (1992). Impact of broadband seismology on strong motion attenuation, Manuscript submitted for publication.

Kanamori, H. and K. Satake (1990). Broadband Study of the 1989 Loma Prieta Earthquake, *Geophysical Research Letters, 17*, 1179-1182.

Magistrale, H.W. (1990). Three dimensional velocity structure of southern California, Ph.D Thesis, Part II, 294 pp. California Institute of Technology, February.

Mooney, W. and C.S. Weaver (1990). Regional crustal structure and tectonics of the Pacific Coastal States; California, Oregon and Washington. in *Geophysical Framework of the Continental United States,* Geological Society of America Memoir 172, 129 - 162.

Mueller, C. and G. Glassmoyer (1990). Digital recordings of aftershocks of the 17 October 1989 Loma Prieta, California earthquake, U.S.G.S. Open File Report 90-503.

Nabelek, J. (1990). Rupture Process of the October 18, 1989 Loma Prieta Earthquake from Broadband Teleseismic Body Waves, *Seismological Research Letters, 61*, 46.

Somerville. P.G. and N.F. Smith (1991). Source, path and site effects on Loma Prieta strong motions, *Proceedings of the Fourth International Conference on Seismic Zonation,* **III**, 335-342.

Somerville, P.G., J.P. McLaren, C.K. Saikia, and D.V. Helmberger (1990). The November 25, 1988 Saguenay, Quebec earthquake: source parameters and the attenuation of strong ground motion. *Bull. Seism. Soc. Am.*, **80**, 1118-1143.

Vidale, J.E. and D.V. Helmberger (1987). Path effects in strong motion seismology, in *Seismic Strong Motion Synthetics*, Bruce Bolt (ed.), Academic Press, Orlando, Florida, pp. 267-319.

Vidale, J.E. and D.V. Helmberger (1988). Elastic finite-difference modeling of the 1971 San Fernando earthquake, *Bull. Seism. Soc. Am.* **78**, 122-141.

Wald, D.J., L.J. Burdick and P.G. Somerville (1988). Simulation of acceleration time histories close to large earthquakes. *Earthquake Engineering and Soil Dynamics II - Recent Advances in Ground Motion Evaluation*, Geotechnical Special Publication 20, J. Lawrence Von Thun, ed., 430-444.

Wald, D.J., D.V. Helmberger, and T.H. Heaton (1991). Rupture model of the 1989 Loma Prieta earthquake from the inversion of strong motion and broadband seismic data, *Bull. Seism. Soc. Am.*, **81**, 1540-1572.

Wallace, T.C. (1988). The seismic source process of the 1952 Kern County, California, earthquake. *Seismological Research Letters* **59**, 20 (abstract).